# DIFFUSION BARRIERS
# FOR
# VLSI APPLICATIONS

Thesis by

Frank Cheung Tao So

In Partial Fulfillment of the Requirements
for the Degree of
Doctor of Philosophy

California Institute of Technology
Pasadena, California

1988
(Submitted July 31, 1987)

*O LORD, our Lord,*

*How majestic is Thy name*

*in all the earth......*

*Psalms 8:1*

# Acknowledgements

It is indeed a real pleasure tó think back on the numerous people who have made my five years of apprenticeship at Caltech a truly memorable experience. Among these, I owed my greatest debt of gratitude to my thesis advisor, Professor Marc-Aurele Nicolet, for providing a superb research environment and letting me discover my strengths and weaknesses at Caltech. His kind words, unfailing support, and keen scientific intuition have guided me through many dark hours of frustrations. I will always remember his graciousness, and treasure the countless lessons he has taught me.

I am glad to acknowledge Dr. Uri Shreter of Yokneam, Israel for his immense patience in getting me started in the thin-film laboratories. Dr. Chuen-Der Lien, now with Digital Equipment Corporations, has been my lifetime collaborator and has inspired in me many useful ideas for this thesis. I am also indebted to Dr. Jawahar Tandon at McDonnell Douglas for his invaluable contributions to our GaAs ohmic contact studies. I have profited a great deal from associating with my 'all-purpose' buddy, Dr. Bruce Ho, who initiated not only the study of nitrogen impurities in metals, but also some far-reaching Southern California social connections. Dr. Elzbieta Kolawa deserves a word of thanks for many fruitful discussions and collaborations. The solar cell studies reported in Chapter 5 would not have been realized without the incessant interest and efforts of Drs. Charlie Chu, Frank Ho, and Peter Iles of Applied Solar Energy Corporation. My sincere thanks go to Professor David Rutledge who has generously granted me access to his photolithographic facilities and various hardware. I also like to thank Dr. Zuyin Zhou in Professor T. A. Tombrello's laboratories for the time she invested in obtaining nitrogen depth profiles by nuclear resonance analysis.

I want to express my special appreciation for Drs. Xin-An Zhao, Sung Joon Kim, Kenneth Kung (M.I.T.), Eric Pan, Tom Banwell, Marc Van Rossum, Hannu Kattelus, and Simon Nieh for their friendship and their unselfish help in times of need. A salute to all those who kindle the dynamic research spirit on the third floor of Steele throughout these years: Drs. Bruce Paine, Meir Bartur, Yang-Tze Cheng, Mei Fang Zhu, David Jamieson, Ilkka Suni, Manuela Finetti, Gang Bai, Tom Workman, and En Ma. Many thanks to David Jamieson for allowing me to produce the illustrations in this manuscript with his marvellous software graphics package. Dr. Adam Kolawa has also offered me the use of his computer workstation. I am extremely grateful to Michell Parks and Arlene Collinwood for their friendship and efficient secretarial accomplishments.

It would be remiss of me not to mention 'Robbie' Gorris for his competent technical support and the many entertaining evening conversations that we have about everything under the sun: from L.A. Lakers to the Hollywood Bowl Jazz Festivals.

Organizations which provide support for this research includes the Army Research Office and Sandia National Laboratories.

I extend my heartfelt appreciation for my ex-roomates, Joseph 'Chi-chi' Hu and John Kao for all the good and bad times we shared together; and to Rosa, Iris, Ken, Dave, Eric, and Spencer of the magnificent *Laser Beam* for introducing me to the glamorous career of a L.A. performing musician.

Last but not least, my deepest gratitude goes to Dad and Mom, and to Joann, for their love and blessings. It is to them that I dedicate this thesis.

# Preface

Most of my work done at Caltech to fulfill the requirements of my thesis is published, or accepted for publication, or in preparation for publication. This thesis will review most of my work but the details are found in the published work. To make this thesis a comprehensive presentation of my work, I have my publications listed separately in the thesis as **References II**, and have them numbered by Roman numerals. These publications constitute an integral part of the thesis. The unpublished part is included in the **Appendix** of this thesis.

# Abstract

This thesis is concerned with diffusion barriers in contact structures to semiconductors. Diffusion barriers are indispensable in present contact technologies to preserve device characteristics from the influence of metal-semiconductor interaction during post-metallization processing.

The absence of grain boundaries makes amorphous W-Zr and Ni-W alloy barriers very attractive for high temperature applications. Nevetheless, in the presence of an adjoining metal layer such as Al, these amorphous barriers are chemically dissociated to form compounds with the metal. The usefulness of these barrier in VLSI metallization schemes is severely limited by their high reactivity with Al within normal processing temperature cycles. Such thermal instability can be removed, however, by adding nitrogen to the barrier layers during sputter deposition.

Becoming aware of the beneficial effects of nitrogen incorporation, we investigate the performance of nitrogen-doped W barrier films in various contact configurations. Reactively sputtered amorphous and polycrystalline W-N layers are demonstrated to be excellent diffusion barriers against interdiffusion between Si-Al, Si-Ag, GaAs-Ag, and GaAs-Au. A novel idea of utilizing W-N as an interconnect in CMOS fabrication is also discussed.

Conducting transition metal oxides emerge as a new class of diffusion barriers. Metallic $Mo_{1-x}O_x$ films are deposited by reactive sputtering a Mo target in controlled $O_2$/Ar ambients. These $Mo_{1-x}O_x$ barriers can effectively protect Si $n^+$-p shallow junctions from Al spiking even beyond the eutectic temperature of

Si-Al. $RuO_2$ films are also found to be equally good in suppressing Si-Al interdiffusion. The present study clearly shows that $Mo_{1-x}O_x$ and $RuO_2$ barriers are the most outstanding performers among all the passive barriers that have been explored so far.

# Table of Contents

*ACKNOWLEDGEMENTS* ........ *iii*

*PREFACE* ........ *v*

*ABSTRACT* ........ *vi*

*TABLE OF CONTENTS* ........ *viii*

Chapter 1. Introduction ........ 1

Chapter 2. Amorphous W-Zr Diffusion Barriers ........ 9

2.1 Introduction ........ 9

2.2 Deposition and crystallization of W-Zr alloy films ........ 11

2.3 Reaction with <Si> substrate ........ 11

2.4 Reactions with metal overlayers ........ 12

2.5 The (111) <Si> /W-Zr/Al contact systems ........ 12

2.6 Conclusions ........ 16

Chapter 3. Amorphous Ni-N-W as Diffusion Barriers Between Al and Si ........ 17

3.1 Introduction ........ 17

3.2 <Si> /Ni-W contacts ........ 18

3.3 Ni-N-W films ........ 18

3.4 Reaction between $Ni_{30}N_{21}W_{49}$ and (100) <Si> ........ 19

3.5 Reactions between $Ni_{30}N_{21}W_{49}$ and Al ........ 19

3.6 Schottky barrier heights of $Ni_{30}N_{21}W_{49}$ on <Si> ........ 19

3.7 Discussions ........ 20

3.8 Summarizing remarks ........ 22

Chapter 4. Tungsten Nitride: Deposition and Properties ........ 23

4.1 Introduction .......... 23

4.2 Deposition behavior and properties of W-N films .......... 26

4.3 Comparision with TiN films .......... 26

Chapter 5. Diffusion Barrier Applications of Tungsten Nitride Films .......... 30

5.1 Introduction .......... 30

5.2 <Si> /W-N/Al contacts .......... 30

5.21 <Si> /$W_{80}N_{20}$ /Al and <Si> /$W_{60}N_{40}$ /Al contacts .......... 32

5.22 <Si> /$W_{90}N_{10}$ /Al and <Si> /W/Al contacts .......... 34

5.23 Summarizing remarks .......... 34

5.3 <Si> /W-N (or W)/Ag contacts to <Si> solar cells .......... 37

5.4 Pt-Mg/W-N (or W)/Ag contacts to p-GaAs .......... 41

5.5 GaAs/W-N (or W)/Au contacts .......... 47

5.6 Conclusions .......... 48

Chapter 6. The Ti/W-N Bilayer .......... 49

6.1 Introduction .......... 49

6.2 The <Si> /Ti/W-N/Al contact system .......... 51

6.3 Application of the Ti/W-N bilayer to the self-aligned $TiSi_2$ process .. 54

Chapter 7. Reactively Sputtered $Mo_{1-x}O_x$ and $RuO_2$ Diffusion Barriers ... 60

7.1 Introduction .......... 60

7.1 Deposition of $Mo_{1-x}O_x$ films .......... 62

7.2 Deposition of $RuO_2$ films .......... 63

7.3 $Mo_{1-x}O_x$ and $RuO_2$ films as diffusion barriers between Al and Si ... 64

7.4 Conclusions .......... 64

Chapter 8. Further Thoughts .......... 66

*Reference I–General* .......... 69

*Reference II–Work published by F. C. T. So* .......... 76

Appendix I–Heat of Reaction of W-based Binary Alloy with Al .......... 79

Appendix II–W-N Alloys as Diffusion Barriers between Al and Si .......... 82

Appendix III–Properties of Reactively Sputtered $Mo_{1-x}O_x$ Films .......... 93

Appendix IV–Reactively Sputtered $RuO_2$ and $Mo_{1-x}O_x$ Diffusion Barriers:

Summary .......... 115

# Chapter 1
# Introduction

Since the early days of microelectronics technology, contacts between metal and semiconductors have been presenting a constant challenge to the electronics industry. There has been a persistent demand for improved contact metallurgy to satisfy device design specifications and still to maintain reasonable processing windows. This requirement is mainly driven by the ever-shrinking device geometries in both Si and GaAs IC's. Device scaling is being extensively employed to improve chip density and device performance. In the case of Si random access memory (RAM), the density and complexity have grown exponentially [1] in the last one and half decade. The minimum feature size of these MOS devices in production dropped from 10 $\mu$m in 1971 to 1.5 $\mu$m in 1985 for a typical 256K DRAM, to 0.7 $\mu$m for the 1987 Fujitsu 4 Mbit DRAM [23]. Not just the lateral dimensions shrink; vertical dimensions such as source/drain junction depth are scaled accordingly [2,3] to overcome deleterious hot-carrier effects. When junctions become shallow, they also become increasingly vulnerable to an interaction between the metal and silicon that causes junction leakage or shorting. Currently, typical junction depths in CMOS devices are in the range of 0.25 $\mu$m – 0.35 $\mu$m. The vertical dimensions of the active device regions in GaAs IC's also fall in the same range [4]. Even in some commercial large-area devices such as <Si> solar cells, the depth of $n^+$-p junctions is ~0.2 $\mu$m [61]. Fabrication of reliable contact schemes to shallow junction and surface barrier devices has thus become a non-trivial task.

Owing to their high conductivities, aluminum, gold and silver are the most

commonly used metals for contacts and interconnects in semiconductor device structures. While Al has always been the sacred metal for Si IC's fabrications [5], Au occupies the most prominent position in metallization schemes to compound semiconductors. Solar cell manufacturers prefer using Ag to the other two for contact grid lines. This thesis is concerned mainly with contacts to Si with Al as the conducting overlayer.

Aluminum has brilliantly solved the wiring problem of the I.C. industry because of its ability to make low resistance contacts to both heavily doped $p^+$ and $n^+$ regions. After aluminum has been deposited and delineated on device wafers, it is customary to carry out a 400 - 500°C sintering to lower the contact resistivity by dissolving the native silicon dioxide [6] and to minimize interface states or radiation damage in the case of MOSFET devices [7]. With the advent of electron beam lithography for submicron VLSI fabrication, post-metallization anneal above 500°C is essential [7]. The Al-Si equilibrium phase diagram shows an appreciable solid solubility of Si in Al at the processing temperatures used (about 0.4 atomic percent at 450°C). During this thermal anneal, Si from the single-crystal substrate diffuses into the top Al layer at a very fast rate to satisfy the silicon solid solubility in aluminum [8,9]. Concomitantly, Al diffuses to the substrate to backfill the vacancies left behind by Si. However, it was observed that this erosion of <Si> occurs at specific sites possibly as a result of of the uneven nature of the native oxide, leading to the creation of deep pits or voids in the substrate silicon. Since the aluminum keeps backfilling the Si voids, an electrical short develops when the Al spikes penetrate the device junction. The depth and size of the dissolution pits depend strongly on the contact size (increase as contact size decreases for fixed amount of Al coverage). This phenomenon imposes a lower limit to practically achievable junction depths when Al is in direct

contact with the Si in a contact window [10]. Diodes of 0.3 $\mu$m junction depth were found to be shorted after a 450°C, 15 min sintering when Al is in direct contact with <Si> [11].

Silicides of transition metals have been extensively investigated as primary contact layers to <Si> . Some silicides are formed from an overlaid metal film via an exceptionally uniform reaction with <Si> [40]. The spiking problem does not occur. For instance, platinum silicide (PtSi) is widely used in bipolar I.C. fabrication to produce Schottky and ohmic contacts [12]. Since Al still remains to be the final interconnect choice, reliable silicide contacts to <Si> can be achieved only if Al overlayers are thermally stable with silicides films in the processing environment. Unfortunately, when Al is heated in contact with metal silicides at temperatures around 400°C, it either decomposes the silicide (e.g. $Pd_2Si$) and triggers a chain of events which quickly leads to contact failure [13], or simply diffuses through the grain boundaries of the silicide layer (e.g. $TiSi_2$ ) to destroy the shallow junction beneath [14]. Therefore, an intermediate layer of silicide alone cannot adequately protect the device junctions from the destructive consequences of Al penetration. To redeem the advantages of a laterally uniform silicide contact, the presence of an extra barrier layer is indispensable.

The concept and application of thin film diffusion barriers have been discussed in great detail by Nicolet [15,16]. The features of an ideal contact barrier layer can be summarized as follows, with particular emphasis on the application to silicon devices with aluminum metallization:

i) The barrier layer should be thermodynamically stable with Al and Si or silicide. In other words, the barrier layer should not react with the Al overlayer and Si or the silicide layer underneath within the processing temperature limits.

ii ) The barrier layer should constitute a kinetic barrier to prevent the trans-

port of Al or silicon across the barrier.

iii) The barrier film should be a good electrically conducting layer and should provide low contact resistivities to Al and Si (or silicide) neighboring layers. The bulk resistivity of the barrier layer is usually not as important as the contact resistivities at the metal-metal or metal-Si interfaces. For a $1\,\mu m^2$ contact area, a $0.1\,\mu m$ thick barrier layer of resistivity as high as $1000\,\mu\Omega$-cm would only contribute $1\ \Omega$ to the total contact resistance. On the other hand, for the same contact dimensions, it takes a contact resistivity of $10^{-8}\,\mu\Omega cm^2$ to achieve the same low series resistance (which is one to three orders of magnitude lower than typical metal-Si contact resistivities). The contact resistivities are the main contributors to to the total series contact resistance.

iv) The barrier layer should adhere well to both <Si> (or silicide) and the Al top layer. It should also have low stress to avoid peeling or delamination after thermal cycles.

An ideal barrier does not exist [16]. Compromises have to be made in reality. A diffusion barrier layer in a particular metallization scheme fails in one way or the other when one or more of the above criteria is not satisfied. A general classification for diffusion barriers has been proposed [16] that distinguishes three types of successful barriers in practical implementation. i) Sacrificial barriers exploit the fact that the thin barrier layer reacts with the metal overlayer to form compounds with predictable rates and in a laterally uniform manner. As long as the barrier layer is not fully consumed in the reaction, a separation between the metal overlayer and the semiconductor can be effectively maintained. Refractory metals such as Ti [17,18], V and Cr [19,42] belong to this category when Si-Al contacts are considered. ii) Stuffed barriers are those whose low atomic diffusivities are attributable to the inhibiting effect of impurities (e.g. O, N)

along grain boundaries which act as fast diffusion paths for metal-semiconductor interdiffusion. Examples of such are Mo and Ti-W alloy films containing a few atomic percent of oxygen or nitrogen [20,21]. iii) Passive barriers are chemically inert with respect to both the overlayer metal and the underlying layers, and have negligible solid solubility and diffusivities for both the top metal and the underlying layers. A good example of such a passive barrier is TiN, but nearly all nitrides, borides and carbides of early transition metals are attractive candidates for stable compound barriers [15,24]. Both passive and stuffed barriers may be deposited in controlled ambients purposely loaded with nitrogen, methane, etc. A clear distinction between these barrier types cannot always be made. Sputtered W and TiN are believed to function in either the stuffed or passive barrier mode [42,61] when they are positioned between Al and Si. However, owing to the strong driving force for reaction between transition metals and Al, Si-Al contact systems with a plain refractory metal barrier (e.g. Ti, Cr, W) deposited in relatively pure state degrades severely at processing temperatures above 450°C [25,26]. The stuffed and passive barriers are definitely favored for contacts exposed to temperature cycles in excess of 500°C [26], and are, in fact, the main subject of this thesis.

From a survey of previous work on stuffed and passive barriers, two valuable lessons on barrier layer design are learned:

1) Grain boundaries in polycrystalline barrier layers can always act as fast diffusion paths for atomic transport and should either be stuffed or preferably be eliminated.

2) Incorporating a light reactive element such as nitrogen, carbon or oxygen into a barrier metal will almost invariably improve the effectiveness of the barrier in any contact scheme.

Based on the above guidelines, this thesis starts with a study of amorphous binary metallic alloys as diffusion barriers (Chapter 2 and 3). By definition, amorphous materials do not contain grain boundaries and should in principle be as effective as stuffed barriers in preventing grain boundary diffusions. The factors that set the limitations of such barrier layers are examined. In addition, the beneficial effect of impurity (nitrogen) incorporation on the diffusion barrier properties of these amorphous layers is established. Chapter 4 and 5 embody a passive-stuffed barrier case study: nitrogen-doped W barrier layers. The deposition process of W-N is first characterized to understand the mode of nitrogen incorporation into W-N films. This is followed by an exploration of the diffusion barrier capability of W-N films in contact schemes to both Si and GaAs. An investigation of the compatibility between W-N and Ti in Chapter 6 leads to a novel idea in utilizing W-N films to implement a self-aligned process in CMOS fabrication. Finally, Chapter 7 presents a new class of material for diffusion barriers between Al and Si: transition metal oxides ($Mo_{1-x}O_x$ and $RuO_2$). These oxide barriers are shown to be superior to any other kind of stuffed or passive compound barriers that have been investigated so far.

Evaluation of the thermal stability of the contact systems covered in this thesis was performed mainly with backscattering spectrometry (BS) [27]. BS provides a depth profile of the elements constituting a thin film system. It allows a direct analysis of chemical interdiffusion and interaction processes. Owing to the rather large area of about 1 - 2 $mm^2$ irradiated on the sample, the lateral resolution of BS is very limited. Metallurgical interactions occurring on a microscopic scale amounting to only a few percent of the total irradiated area cannot be detected by BS. Also, BS is of limited value in analyzing Al-Si systems because the atomic masses of Al (27 a.m.u.) and Si (28 a.m.u.) are very close. Signal

overlaps in a BS spectrum affect the detection sensitivity for Al-Si interdiffusion adversely. In view of these limitations, almost all BS measurements are complemented by electrical measurements performed on actual devices throughout this work. The major test vehicle consists of patterning a contact structure on a Si substrate with a shallow n-p junction (see Chapter 5). Shallow junction diodes are probably the most sensitive devices to use for determining the performance of diffusion barriers. A tiny metal spike or nonuniform reaction can generate a high reverse leakage current or total junction short. Results obtained by BS and electrical measurements are combined to evaluate barrier integrity.

Since more than 80% of my thesis research is devoted to experiments with W-based materials, this written account would appear to be quite incomplete without an update of the role played by W or W-based materials in the state-of-the-art microelectronics technology of today.

1) Owing to its excellent room-temperature bulk resistivity (5.3 $\mu\Omega$-cm), small thermal expansion mismatch with <Si> (4.5 ppm/°C versus 3.0 ppm/°C for Si), high reaction temperature with <Si> (650°C), and high electromigration resistance [28], W is a potential candidate to replace Al as an interconnect material for VLSI applications. Hewlett-Packard Co. has already been using W for the first and second level interconnects in the fabrication of a 32 bit microprocessor for the company's new HP-3000 series computers [29].

The value of W in semiconductor process technologies is enhanced further by breakthroughs in W chemical vapor deposition (CVD) and low pressure chemical vapor deposition (LPCVD). These techniques enable polycrystalline W films with resistivities approaching that of bulk to be produced [30]. Furthermore, the low pressure processes allow selective deposition of W on Si, silicides, and certain metals instead of on dielectric surfaces. Excellent step coverage is another

important feature for these CVD W films. LPCVD W is therefore well-suited for self-aligned diffusion barrier layer formation in submicron contact holes and multilevel interconnect planarization [11,30].

2) Recently, workers at Hitachi Central Research Laboratory have developed a highly reliable W gate process that circumvents the long standing problem of oxidation when a W film is exposed to an oxidizing ambient at elevated temperatures [31]. Such process is currently used to manufacture high-speed 1 Mbit DRAMs.

3) Tungsten nitrides and tungsten silicides are currently employed as high temperature gate electrodes in GaAs MESFETS I.C.'s manufactured by Toshiba and Fujitsu [32].

4) Sputtered Ti-W and Ti-W-N diffusion barriers are widely used as stuffed diffusion barriers between Al and PtSi in bipolar I.C. technologies. Apart from being good diffusion barriers, these alloys also possess excellent corrosion resistance.

The prominence of W and W-based materials in VLSI technology is expected to grow because many advantages offered by the material properties and advanced deposition processes are unsurpassed by those of other metallic elements. Apart from W, refractory metals such as Mo and Ta and their compounds are also gaining ground in VLSI processing. It is hoped that the studies undertaken in this thesis may provide some useful directions in diffusion barrier material research involving the early transition refractory metals.

# Chapter 2

# Amorphous W-Zr Diffusion Barriers

## 2.1 Introduction

Polycrystalline diffusion barrier films have been widely used to improve thermal stability of contacts to devices. It is well known that grain boundaries in polycrystalline films can act as fast diffusion paths [33]. The phenomenon of grain boundary diffusion (GBD) has been found to be largely responsible for the degradation of many metallization schemes [16,22]. For instance, failure in contact systems such as Si/Ti/Al [18] and Si/NiSi/Cr/Al [19] is induced by the consumption of the polycrystalline barrier metals in a chemical reaction. Intermetallic compound formation in these metal-Al couples proceeds through GBD [26,33]. In many other metallization systems, the large driving force for dissolution between the metallic overlayer and the semiconductor causes interdiffusion through the interposed polycrystalline barrier film, even though no chemical reaction between the barrier and the metal overlayer or the semiconductor results (e.g. Si/Mo/Au [20], Si/ $TiSi_2$ /Al [14]). Grain boundaries simply render the polycrystalline barrier 'transparent' to atomic transport. Such failure modes were also observed in some cases when a barrier layer is used to suppress the interaction between a silicide layer and Al. Aluminum penetrates the barrier layers via grain boundaries to react with the underlying silicides at temperatures much lower than the reaction temperatures between Al and the barrier metals [18,34].

To circumvent the problems arising from GBD, amorphous metallic alloy films

offer an obvious advantage over the conventional polycrystalline barriers. Amorphous layers do not have grain boundaries that act as fast diffusion short-cuts. Atomic diffusivities in an amorphous phase are typically orders of magnitude less than in a corresponding polycrystalline phase in the temperature regime where GBD dominantes [35]. At the time when the present work was executed, the structural stability of several amorphous metallic alloys in contact with various semiconductor substrates and metallic overlayers has already been investigated [39,41]. The most basic requirement for the choice of an amorphous barrier in a certain contact scheme is that the barrier film has to remain amorphous throughout thermal cycling. In other words, the crystallization temperature of the amorphous layer should be higher than the processing temperatures used following the deposition of the metallization structures. However, it was not at all clear then what factors actually dominate the failure of these amorphous barriers. One report shows that failure in the Si/$\alpha$-Fe-W/Al system occurs at temperatures below the crystallization temperature of amorphous Fe-W with the consumption of W from Fe-W by Al, to form $WAl_{12}$ [39]. In some other systems, significant interdiffusion is only observed above the crystallization temperatures of the amorphous barriers [41]. The investigation of amorphous W-Zr as described here attempts to elucidate the interplay between crystallization temperature, reactivity with metallic overlayers, and failure temperatures. The thermal stability of W-Zr alloy films in the presence of Al, Au, Ag, Ni, and Si is examined. In particular, special attention is paid to the failure mode in a <Si> /W-Zr/Al system to establish the degree of usefulness of the barrier for VLSI applications. The performance of W-Zr barrier is also compared to its polycrystalline counterpart, Ti-W.

## 2.2 Deposition and crystallization of W-Zr alloy films

The W-Zr pair satisfies the structural difference rule for amorphous phase formation [38], has atomic radii difference of ~14% and possesses a large difference in electronegativities (1.33 for Zr and 2.36 for W on the Pauling scale). The mutual solubilities of W and Zr are very limited up to 1000°C, and the lowest eutectic temperature of W-Zr is ~1700°C. All the above factors favor the formation of amorphous W-Zr phases [36,37].

Thin films of $W_{70}Zr_{30}$, $W_{60}Zr_{40}$ and $W_{40}Zr_{60}$ were deposited by r.f. sputtering of a W target partially covered with narrow Zr stripes [I,II]. The amorphous nature of these films was confirmed by X-ray and Transmission Electron Microscopy (TEM) analysis. Regardless of the composition, x-ray diffraction analysis indicates that these films crystallize on sapphire substrates after 30 min. annealing at 850–900°C. Crystallization results in the formation of W and possibly $W_2Zr$. The crystallization temperatures of W-Zr films are thus much higher than the maximum post-metallization processing temperature (~600°C). The resistivities of these amorphous layers are in the range of 180–280 $\mu\Omega$-cm, which are very acceptable for thin film barrier applications. A raised base pressures prior to deposition and lowered deposition rates result in an increased resistivity of the W-Zr films.

## 2.3 Reaction with <Si> substrate

Interaction between W-Zr films and Si substrates can be detected by backscattering spectrometry after annealing at ~700°C with the formation of the disilicides of W and Zr and also metal-rich silicides such as ZrSi, $Zr_2Si$ and $W_5Si_3$. The reaction between W-Zr alloys and Si are most noteworthy in the following aspects:

i)The reaction sets in at a temperature that coincides more or less with the reaction temperatures of the elemental films of Zr and W with single crystal Si [40], and is about 200°C lower than the crystallization temperature of a W-Zr film.

ii)The reaction, once initiated, proceeds in a laterally uniform fashion.

iii) Unlike the case of amorphous Ni-W [44], there is no detectable low-temperature penetration (by BS) of W or Zr into Si below the temperature at which the reaction begins. We associate this difference with the fact that Ni silicides form by the diffusion of Ni, but $ZrSi_2$ and $WSi_2$ form by diffusion of Si [40]. The low temperature instability of Ni-W or Fe-W on <Si> can therefore be eliminated by substituting Ni with Zr.

## 2.4 Reactions with metal overlayers

Samples of the configuration $SiO_2$/W-Zr/M, where M is a metal layer, were investigated for their thermal stability [I,II]. Metallurgical interactions between W-Zr and Al, Ag and Ni overlayers can be detected by BS in the temperature range of 500-550°C. With a Au overlayer, W-Zr is dissociated at ~400°C. The reaction temperatures of these metal layers with W-Zr are at least 350°C below the crystallization temperature of the barrier layer. Various compound phases could be easily identified by x-ray diffraction analysis in the reacted samples. Thermal instability in such W-Zr/metal couples is therefore dictated by the chemical driving force for compound formation and *not* by the crystallization of the W-Zr layers.

## 2.5 The (111) <Si> /W-Zr/Al contact systems

Interaction between amorphous W-Zr films on <Si> with an Al overlayer occurs after annealing at 500°C for 30 min. Interdiffusion takes place in a laterally

nonuniform manner as determined by BS analysis. In these reacted samples, x-ray analysis confirms the formation of $WAl_{12}$ and $ZrAl_3$, which are also obtained when elemental W and Zr react with Al. W and Zr films have been reported to react with Al in the vicinity of 500°C and 400°C respectively [26,42]. Interestingly enough, the reaction between W or Zr with Al is described to be nonuniform in nature, as in the present case.

Figure 1 shows a SEM micrograph of the surface of a <Si> /W-Zr/Al sample after 30 min annealing at 525°C. Circular pits, typically of a few microns in size, can be observed to form as a result of annealing. These pits are present for all samples in which reaction between Al and W-Zr can be detected by BS. Energy Dispersive X-ray Spectrometry (EDX) showed that W or Zr signals can be detected only at the flat or pit-free regions of the surface. In other words, W and Zr are absent where the pits are. These observations suggest that the W-Zr barrier film fractures during the course of thermal treatment. Naturally, these deeply penetrating pits would constitute the major cause for the failure of W-Zr films to block Al-Si interdiffusion. Identical results were obtained for both W-rich and Zr-rich alloy barriers. The formation mechanisms of the pits are, however, not very certain. A model proposed by Canali et al. [34] to explain the failure mechanism in a <Si> /PtSi/Ti-W/Al contact structure appears to be quite applicable to our <Si> /W-Zr/Al case. We believe that the dominant failure mechanisms in these contact systems is a mechanical instability induced by thermal stress and subsequent chemical reaction. It is relevant to note in this context that although W-Zr is amorphous in contrast to Ti-W, the failure modes in both cases look quite similar.

The thermal stability of a <Si> / $W_{70}Zr_{30}$ /Al contact structure was tested by electrical measurements performed on $n^+$-p shallow junctions of 0.35 $\mu$m junc-

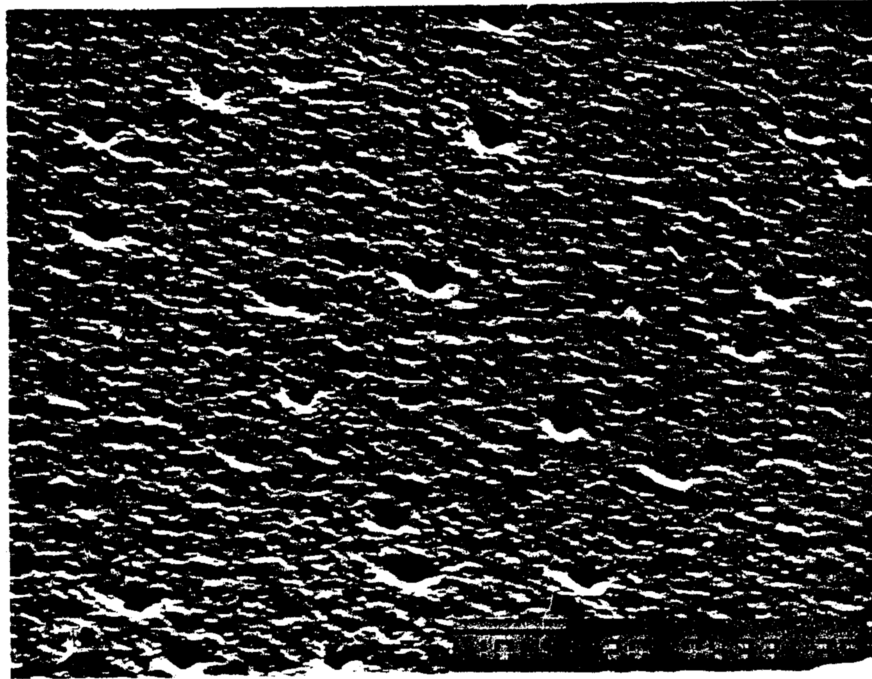


**Figure 1.** SEM micrograph of the surface of a (111) <Si> / $W_{70}Zr_{30}$ / Al sample after a 525°C, 30 min anneal in vacuum.

tion depth. The d.c. characteristics of all the diodes were found to be well behaved up to 450°C annealing for 30 min, but were all shorted after a 500°C, 30 min heat treatment (Fig 2). These results are consistent with the studies conducted with BS, SEM and EDX as described above.

## 2.6 Conclusions

The performance of amorphous W-Zr alloy diffusion barriers is limited by their tendency to interact with adjoining metal layers and <Si> at temperatures well below their crystallization temperatures. In fact, simple reaction enthalpy calculations reveal that W-Zr alloys are probably the most reactive (with Al) among a dozen of W-based binary metallic alloys (see appendix I). W-Zr films were chosen for this study to demonstrate that high crystallization temperatures and low atomic diffusivities alone cannot guarantee successful implementation of an amorphous barrier layer. Work done at Cornell University also supports such findings [46,47]. Moreover, the localized and nonuniform nature of the interaction between Al and W-Zr disqualifies W-Zr films as candidates for sacrificial barrier applications in VLSI processing, and limits their use as passive barriers between Al and Si to temperatures below 500°C. Based on the above observations, the performance of amorphous W-Zr barriers is expected to be just comparable to that of the commonly used polycrystalline Ti-W alloys [34].

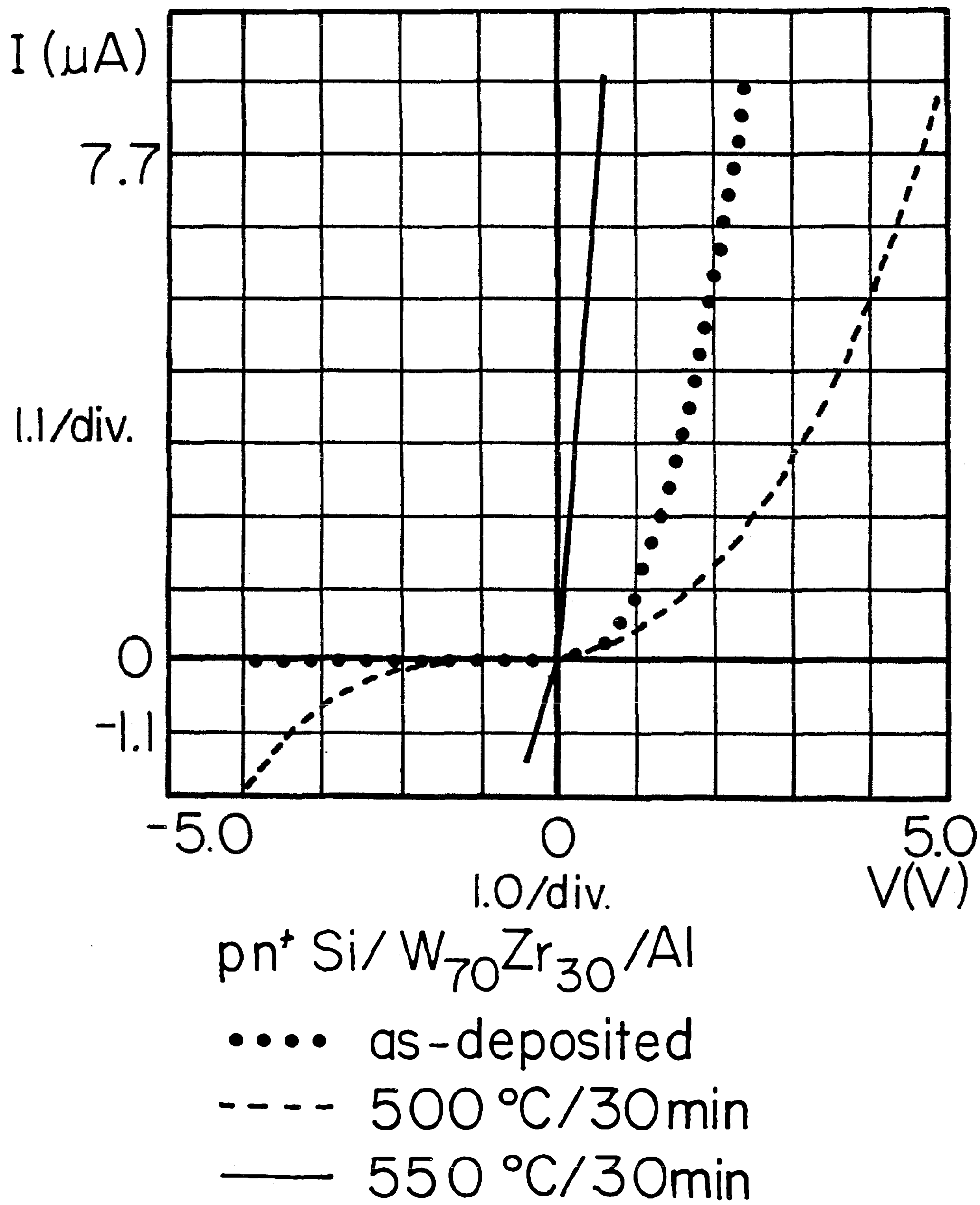


**Figure 2.** I-V characteristics of Si $n^+$-p diodes with the <Si> / $W_{70}Zr_{30}$ /Al contact structures before and after annealing at 500°C and 550°C for 30 min.

# Chapter 3

# Amorphous Ni-N-W as Diffusion Barriers Between Al and Si

## 3.1 Introduction

It was shown in the last chapter that one major problem amorphous W-Zr barriers have in common with ordinary metallic thin films is that they tend to react with adjoining polycrystalline layers. Unless this difficulty with reactivity is overcome, amorphous diffusion barriers will remain as elegant schemes without redeeming importance. To stabilize an amorphous binary alloy against reaction with metal overlayers, one can in principle choose a combination with large formation enthalpy. However, thermal stability data of amorphous binary alloys show a rather small number of systems, such as Ir-Ta, which possess both high crystallization temperatures and large negative heat of mixing. Even in such cases, it has been noted [47] that reactions with Al to form aluminides yield negative enthalpies of reaction. It appears that amorphous binary metallic alloys can hardly serve as reliable diffusion barriers between Al and Si. Some other way is therefore needed to alleviate the problem of reactivity.

It has long been known that the incorporaton of reactive elements, such as oxygen and nitrogen, can have beneficial effects on the thermal stability of metallic diffusion barriers [16,22,49]. As stated in Chapter 1, such improvements of diffusion barrier capability have been attributed to stuffing of grain boundaries or the formation of interstitial compounds such as metallic nitrides that exhibit reduced reactivity with the metal overlayers. This notion of adding an

'impurity' constituent to make a barrier more chemically inert to its reactive environment is now extended to the amorphous Ni-W case. In this chapter, the influence of nitrogen on the reactivity of Ni-W with both <Si> and Al is examined. The sample configurations used in our study are <Si>/barrier(500Å) and <Si>/barrier(500Å)/Al(2500Å). Reactions of nitrogen-doped Ni-W with <Si> and Al overlayers were monitored by Schottky barrier height (SBH) measurements and BS.

### 3.2 <Si>/Ni-W contacts

An important feature in the reaction between (100) <Si> and an amorphous $Ni_{36}W_{64}$ film is that Ni penetrates locally into the Si substrate at around 500°C in the form of NiSi precipitates and epitaxial $NiSi_2$ pyramids [44]. $Ni_{36}W_{64}$ crystallizes at ~650°C on $SiO_2$. The occurrence of such nonuniform reaction results in the degradation of the Schottky behavior of <Si> / $Ni_{36}W_{64}$ diodes at temperatures as low as 450°C, probably due to the presence of strong electric fields generated around the sharp protrusions of Ni silicides (see later). This low temperature instability naturally makes $Ni_{36}W_{64}$ unsuitable for direct contact to shallow junctions.

### 3.3 Ni-N-W Films

Nitrogen is incorporated into Ni-W films by sputter-deposition in a 90% Ar and 10% $N_2$ ambient [III]. The resulting film composition was determined by BS to be $Ni_{30}N_{21}W_{49}$. With nitrogen in the films, the crystallization temperature is lowered from 650°C (30 min) for $Ni_{36}W_{64}$ to 600°C for $Ni_{30}N_{21}W_{49}$. The resistivity of a $Ni_{30}N_{21}W_{49}$ film is ~260 $\mu\Omega$-cm, which is slightly higher than that of $Ni_{36}W_{64}$ (170 $\mu\Omega$-cm).

### 3.4 Reactions between $Ni_{30}N_{21}W_{49}$ and (100) <Si>

Using BS analysis, no low-temperature localized penetration of Ni could be observed in the <Si> / $Ni_{30}N_{21}W_{49}$ system below 725°C. Above that temperature, the tungsten and nickel mixture reacts rapidly with the Si substrate and forms silicide phases [III] in a manner very similar to that of $Ni_{36}W_{64}$ on <Si> [44]. It is interesting to note that a penetration of Ni from $Ni_{30}N_{21}W_{49}$ into Si sets in only after crystallization.

### 3.5 Reactions between $Ni_{30}N_{21}W_{49}$ and Al

The metallurgical interactions between $Ni_{36}W_{64}$ or $Ni_{30}N_{21}W_{49}$ with Al were investigated by BS [III]. In the case of <Si> / $Ni_{36}W_{64}$ /Al, interdiffusion occurs at 500°C (30 min), resulting in the formation of $WAl_{12}$ and $NiAl_3$ intermetallic compounds in these annealed samples. On the other hand, no detectable interdiffusion can be observed for <Si> / $Ni_{30}N_{21}W_{49}$ /Al after it has received an identical heat treatment. The onset of significant intermixing between Al, $Ni_{30}N_{21}W_{49}$ and <Si> takes place only above the eutectic temperature of Al-Si (577°C). Thus, the presence of nitrogen in a Ni-W film greatly enhances its barrier integrity.

### 3.6 Schottky barrier heights of $Ni_{30}N_{21}W_{49}$ on <Si>

The SBH of $Ni_{36}W_{64}$ and $Ni_{30}N_{21}W_{49}$ films on (100) <Si> as a function of thermal treatment are summarized in Table I. For $Ni_{36}W_{64}$ / <Si> diodes, the SBH derived from forward I-V measurements remains more or less constant throughout the whole annealing procedure, but the ideality factor starts to increase dramatically at 450°C. Such a gradual deviation from ideal Schottky behavior is accompanied by an anomalously high reverse current, and can be

explained by a nonuniform interfacial penetration of nickel into the Si substrate during the course of thermal treatment as mentioned above.

In marked contrast to <Si> / $Ni_{36}W_{64}$ , <Si> / $Ni_{30}N_{21}W_{49}$ diodes exhibit stable Schottky characteristics for annealing up to 550°C for 60 min. Heat treatment leaves both the SBH and the ideality factor unchanged. The preservation of diode integrity lends further support to the presence of an unaltered <Si> / $Ni_{30}N_{21}W_{49}$ interface after heat treatment at 550°C.

### 3.7 Discussions

The improvement in the thermal stability of a polycrystalline diffusion barrier such as TiW [21] in contact with metal layers has been attributed to the incorporation of impurities that reduce the atomic diffusivity along the fast diffusion paths in the barrier layer. In the present work, improved thermal stability cannot be explained by stuffing of grain boundaries, since grain boundaries are absent in amorphous materials.

Although amorphous $Ni_{36}W_{64}$ films have a slightly higher crystallization temperature than amorphous $Ni_{30}N_{21}W_{49}$ films, Ni from $Ni_{36}W_{64}$ penetrates into the Si substrate at a temperature much lower than the crystallization temperature, whereas a similar penetration of Ni from $Ni_{30}N_{21}W_{49}$ into silicon sets in only after crystallization. Below that temperature, the incorporation of nitrogen in the amorphous film apparently suppresses the Ni penetration into the Si substrate. Similarly, the reaction of W or Ni with Al is retarded. These results unambiguously show that nitrogen reduces the reactivity of the barrier layer. One explanation of this improvement assumes that nitrogen introduces a kinetic barrier against these reactions by inhibiting the transport and depletion of both Ni and W in the amorphous film. Another explanation is that the heat of forma-

| *Annealing temperature* | *n-Si⟨100⟩/Ni$_{36}$W$_{64}$* | | *n-Si⟨100⟩/Ni$_{30}$N$_{21}$W$_{49}$* | |
|---|---|---|---|---|
| | $\phi_B$ (V) | *n* | $\phi_B$ (V) | *n* |
| As deposited | 0.65±0.01 | 1.04 | 0.59±0.01 | — |
| 400 °C (30 min) | 0.65±0.01 | 1.08 | — | — |
| 450 °C (30 min) | 0.64±0.01 | 1.15 | 0.65±0.01 | 1.03 |
| 500 °C (30 min) | 0.65±0.01 | 1.35 | — | — |
| 450 °C (30 min)+ 500 °C (150 min) | — | — | 0.66±0.01 | 1.04 |
| 450 °C (30 min)+ 500 °C (150 min)+ 550 °C (60 min) | — | — | 0.65±0.01 | 1.05 |

**Table I.** Schottky barrier height and ideality factors for diodes made of amorphous $Ni_{36}W_{64}$ and $Ni_{30}N_{21}W_{49}$ films on n-Si annealed at various temperatures.

tion of the amorphous film is more negative with nitrogen than without, which reduces the driving force for reactions. In general, both kinetic and thermodynamic effects play a role. More elaborations on the stabilization of barriers by impurities will be presented in the next few chapters.

### 3.8 Summarizing remarks

The conventional wisdom of adding nitrogen to enhance the effectiveness of a polycrystalline metallic diffusion barrier also applies to the case of amorphous Ni-W film in contact with Al or Si. The present investigations essentially couple the concept and advantages of an amorphous barrier with those of a stuffed or passive barrier. Whether nitrogen doping will solve the reactivity problem that virtually all amorphous binary metallic alloy barriers confront in chemically reactive environments remains to be investigated. As an extension of the present studies, nitrogen-doped W-Zr alloys were examined for their chemical stability with Al overlayers. No interdiffusion can be detected in a <Si>/W-Zr-N/Al sample up to 550°C (compared to 450°C for nitrogen-free W-Zr). Ironically, incorporation of nitrogen turns the W-Zr films crystalline as revealed by x-ray analysis. Nevetheless, nitrogen remains an indispensable ingredient in diminishing the reactivity of these barriers with Al overlayers.

# Chapter 4
# Tungsten Nitride: Deposition and Properties

## 4.1 Introduction

The investigations reported in the last two chapters reveal the importance of the role played by nitrogen in Ni-W and W-Zr diffusion barriers. When one compares the performance of Ni-W or W-Zr as a barrier between Al and Si to that of plain sputtered or evaporated W, it is amusing to see that the addition of Ni or Zr to W brought little excitement to the diffusion barrier enthusiasts. Tungsten alone is stable on Si up to 650°C, and can block Al-Si diffusion up to 30 min annealing at 450 – 500°C [11,42,45]. Combining W and Ni in fact causes contact spiking problems at 400°C and above. Nitrogen incorporation into the these W-based barrier layers has definitely provided the key advantage, and more important, the inspiration for the next step.

Previous work showed that thin-film reaction rates between Al and various refractory metals depend strongly on the impurity content (e.g. N, O, C) present in the metals [19, 42]. It has been suggested that the fairly equal reaction rates reported by independent investigators may actually result from the presence of impurities in the barrier films above a certain atomic percentage [42]. A good understanding of the mechanisms and consequences of impurity incorporation into a barrier film is therefore very relevant to a successful design of a metallization system with a barrier layer. Apart from the Ni-N-W case reported in the last chapter, nitrogen 'impurity' has appeared in a few other tungsten-based diffusion

barriers. These include the popular Ti-W [21], and W [50]. To save myself from the complications and frustrations of working with ternaries, I have chosen to study the simple case of the binary W-N alloy without other intentionally added elements. One motivation for this work originated from the Ti-W diffusion barrier and the improvement of its properties when nitrogen is added [21]. Two binary nitride systems are associated with Ti-W-N: Ti-N and W-N. The Ti-N system has been extensively investigated for diffusion barrier applications in the past, but the W-N system remained unexplored. Further motivations for this work arose from the ease with which W-N films can be deposited by sputtering of W in an Ar-$N_2$ mixture and the encouraging first results reported on the diffusion barrier properties of W-N [51] and Ni-N-W. The present studies emphasize the dependence of film properties on various deposition parameters and assess the potential of W-N layers for various device applications.

Tungsten, as many other refractory metals, is reactive with nitrogen. Various forms of tungsten nitrides have been reported in the literature, including $W_2N$, hexagonal WN, and rhombohedral $WN_2$ [53]. Affolter et al. reported that $W_2N$ is the dominant phase present in a number of W-N alloy films prepared by reactive sputtering in nitrogen-containing ambients [52]. Likewise, other refractory nitrides such as TiN and ZrN can be deposited in similar manners [54,61]. One of the most general observations associated with the production of compound films by reactive sputtering is that the properties of these films are strong functions of the deposition conditions. Different film properties may eventually lead to differing barrier performance. 'Nitriding' the metal films does not always ensure the satisfactory performance as a barrier. For example, the failure temperatures in the <Si>/TiN/Al system have been reported to range from 450°C [48,55] to 600°C [71] from independent studies conducted in different laboratories. The

discrepancies of these findings call for efforts to probe into the basics of the deposition processes. The barrier attributes of TiN change with almost every property of the film (stoichiometry, intrinsic stress, oxygen content, microstructures, etc.), which in turn depend on how the layers were made.

Reactive sputtering is essentially a low pressure ($10^{-3}$ to $10^{-1}$ Torr) plasma process in which various ions or neutral species are created in a chemically active environment. Different deposition parameters result in the generation of different relative amounts of these ions and neutrals [57]. The flux of particles arriving at the substrate determines the film chemistry and atomic order, from which other properties derive.

The goal of this chapter is to examine in a systematic manner how some of the film properties of W-N may be critically influenced by deposition conditions. From an application standpoint, the factors which affect the reproducibility of a barrier film should be unambiguously identified. With a proper understanding of the process-property relationships, the film properties of W-N may then be tailored for optimum barrier characteristics (Chapter 5).

## 4.2 Deposition behavior and properties of W-N films

Tungsten nitride films were prepared by reactively sputtering a pure W target in an rf $N_2$/Ar plasma. The dependence of the resistivity, intrinsic stress and atomic composition, and deposition rates of the films on the sputtering power, initial total gas pressure, relative partial pressure of nitrogen and negative substrate bias were studied. Detailed results are presented in reference IV.

Our major findings are that the deposition rate and film composition are smooth and continuous functions of various sputtering parameters. No sharp transitions have been observed. The resistivity, stress, and crystallographic structure of W-N films depend only on the nitrogen concentration in the films, regardless of the deposition conditions. This observation also suggests that the microstructure of the W-N films is dictated principally by the amount of nitrogen present in the films. An amorphous W-N phase is observed in the range of 15-30 atomic % nitrogen [52]. These amorphous films crystallize at ~620°C. All the W-N films decompose to bcc $\alpha$W when subjected to a 800°C, 30 min heat treatment, accompanied by a loss of nitrogen to the ambient.

## 4.3 Comparision with TiN films

While it may be difficult to deduce the formation mechanisms of W-N by reactive sputtering from the rather limited amount of information obtained from these experiments, one can compare the deposition behavior of W-N to that of TiN to gain insights into the physics of the deposition process. There have been many studies on reactive sputter deposition of TiN, and a fairly consistent picture can be drawn from the early results obtained at Caltech [61] to the most recent investigations [56,62]. Models have been put forward to account for the sputtering characteristics [60,63,64,65]. Although no conclusive explanations have been

arrived at, the model generally accepted for the reactive sputter deposition of TiN is used as a reference for comparision with our W-N results.

The sputtering behavior of W-N described in the last section differs quite radically from that of TiN in many respects [IV]:

i) When the rf power is increased, all other parameters being fixed, the nitrogen content in the W-N films decreases monotonically and can approach zero (i.e. pure W is deposited) without discontinuity in the deposition rate. That is not so for TiN: there always exists threshold in power level below which TiN can be deposited. Passing through that threshold always results in abrupt change of deposition rate. Also, the ratio of N to Ti in TiN departs negligibly from 1:1 over a wide range of sputtering conditions.

ii) The deposition rate of W-N depends primarily on the dissipated power, and little on total gas pressure and composition. For TiN, large changes in deposition rate are noted with changes in the total pressure and gas composition at fixed power for the same range of total gas pressure and composition used.

iii) To the first order, the resistivity of W-N is a function of the film composition only. Similar observations hold for the stress behavior in the films. In marked contrast to W-N, near-stoichiometric TiN obtained under different sputtering conditions has film resistivities that can vary by an order of magnitude owing to different film densities, oxygen contamination level, stress and grain structures.

iv) A negative dc substrate bias changes the the resistivity and compressive stress of W-N little; for TiN, this bias is critical. Abrupt transitions in the internal stress, the resistivity and the film color of TiN can be observed in a narrow range of negative bias values.

v) The oxygen concentration of all the W-N films is found to be below the

detection limits of BS (about 5 atomic percent) regardless of the sputtering conditions. The extent of oxygen contamination is often much more severe in TiN films than in W-N. The incorporation of oxygen into TiN depends strongly on sputtering parameters.

The contrast observed in the relationship between sputtering parameters and film deposition in the two nitrides implies that their formation mechanisms must be dissimilar. According to reference 58, 59, 63, 64, 65, the deposition behavior of a nitride within a certain range of deposition conditions is solely determined by whether nitrogen is chemically bonded to the metal target surface during the reactive sputtering process. Following this line of thought, TiN sputter-deposition is usually modelled by the formation of a thin layer of TiN on the target surface under the appropriate conditions of nitrogen partial pressures and sputtering power, followed by the ejection of the TiN molecules from the target surface in the form of ions or neutrals and eventual arrival of TiN on the substrate. Abrupt transitions in the sputtering characteristics are thought to be caused by a sudden conversion of a Ti target surface to a TiN target surface, when the partial pressure of nitrogen in the sputtering ambient exceeds a certain threshold [59,60]. On the other hand, a very recent investigation of the reactive sputtering of W in $Ar/N_2$ ambients by Aita [66] using optical and mass spectroscopy technique [57] reveals that W-N formation is most probable to happen on the substrate where the W-N film grows, and not on the target surface. The observed dependence of film composition of W-N on the partial pressure of $N_2$ and sputtering power reported above fits well into the deposition characteristics of an "nitride-free W target" regime as described by Hollands [58]. Titanium and tungsten nitrides form at different locations of the glow discharge, and different deposition behavior results.

From another viewpoint, different formation mechanisms are probably the consequences of the distinct chemistry of TiN and W-N. Tungsten nitrides are not as stable as the nitrides of the titanium or vanadium group; the enthalpy of formation (at 298°K) of $W_2N$ is about -17 kcal/mole while that of TiN is about -80 kcal/mole [51,53]. Unlike W-N, TiN does not decompose upon annealing in vacuum up to at least 1000°C [61]. The affinity of Ti for oxygen is also much greater than that of W [96]. (This may provide the reason why high concentrations of oxygen are sometimes found in TiN films.) The two nitrides dissolve in different mineral acids or alkali [51,67]. All these factors influence the extent to which different particle species are formed in the sputtering glow discharge and hence, the film deposition and growth.

# Chapter 5

# Diffusion Barrier Applications of Tungsten Nitride Films

## 5.1 Introduction

In this chapter, the performance of W-N diffusion barriers are evaluated in three contact schemes. The first investigation deals with W-N barriers between Al and Si, and is pertinent to VLSI process technology, since Al remains a preferred metal for connection to devices. Both amorphous and polycrystalline W-N will be tested and compared for their effectiveness to block Al-Si interaction. The other studies focus on contacts to Si and GaAs solar cells with Ag as the low resistivity overlayers. The advantages of incorporating W or W-N barrier layers between Ag and the contacting underlayers to Si or GaAs are assessed. Some results of W-N as diffusion barriers between Au and GaAs are also described.

### 5.2 <Si> /W-N/Al contacts

The deposition studies described in the last chapter show that the thin-film properties of W-N depend mainly on the nitrogen concentration present in the film. For the benefit of device fabrication, it is of great importance to determine if W-N films with different microstructures and stress also differ in their effectiveness in inhibiting Si-Al interaction, as in the case of TiN [69,70]. Also, by comparing the thermal stability of contact structures with various W-N barrier films of the same stoichiometry but deposited under different sputtering conditions, the validity of the one-to-one relationship between film properties and compositions of W-N can be checked.

Four different barrier layers, W, $W_{90}N_{10}$, $W_{80}N_{20}$ and $W_{60}N_{40}$, were tested for their diffusion barrier capability against Al-Si interaction. The $W_{80}N_{20}$ film is the only one among the four that is amorphous, and has the lowest compressive stress [V]. $W_{60}N_{40}$ consists predominantly of the $W_2N$ phase; $W_{90}N_{10}$ is made up of a mixture of $\alpha$W and $\beta$W. Except for W and $W_{90}N_{10}$, the microstructures of the films are expected to be quite different from each other. The thicknesses of the barrier layers used in the test structures are ~800Å. W-N and Al are deposited sequentially in the same sputtering system without breaking vacuum to avoid effects due to interfacial oxides.

The test vehicles for barrier evaluation consist of Si $n^+$-p diodes of 0.35 $\mu$m junction depth formed by $As^+$ ion implantation (150 keV, $7\times10^{15}$ $As/cm^2$) into 10-20 $\Omega$-cm p-type <Si> and anneal. Details of the fabrication procedure are reported in reference II. The size of the junction areas and contact windows are 500 $\times$ 500 $\mu m^2$ and 300 $\times$ 300 $\mu m^2$ respectively. The W-N/Al contact metallization was delineated by the lift-off technique.

### 5.2.1 <Si> / $W_{80}N_{20}$ /Al and <Si> / $W_{60}N_{40}$ /Al CONTACTS

The effectiveness of $W_{80}N_{20}$ and $W_{60}N_{40}$ as barriers between Al and Si are comparable. Backscattering analysis detects very little interaction between the adjoining layers in both contact structures up to annealing at 575°C for 30 min (the Al-Si eutectic temperature is 577°C). At 600°C, extensive intermixing between Al and the underlying W-N and Si occurs in a highly laterally nonuniform manner [appendix II]. However, no W-Al intermetallic compound can be detected in the annealed sample by x-ray analysis, indicating that contact failure cannot be attributed to the consumption of W-N by Al to form $WAl_{12}$ (as in a W/Al couple). Also, no metallurgical interactions can be detected at 600°C if <Si> is replaced by $SiO_2$. This shows that the presence of Si promotes Al penetration at 600°C.

Measurements of the change in junction leakage of the $n^+$-p diodes with the <Si> /W-N/Al contact structures further our understanding of the failure mechanisms. The dc electrical characteristics of the diodes are preserved up to annealing at 575°C, in agreement with BS analysis. Even after a 600°C, 30 min anneal, a large percentage of the measured diodes still survive [appendix II] without increase in leakage currents (72% for amorphous and 48% for polycrystalline W-N) despite BS already showed barrier breakdown which is laterally nonuniform, however. This suggests that diode failure is caused by highly localized or nonuniform penetration of Al into the Si substrate. Inspection of the diode contact areas by Scanning Electron Microscopy (SEM) and Optical Microscopy revealed three distinct types of surface features after annealing. The first type comprises micron-size bubbles scattered over all the contact areas after annealing at 550°C and above. These irregular-shaped bubbles probably arise as a result of a partial loss of adhesion between Al and the W-N layers. When the Al overlayer

is selectively etched off from the contact areas of the good diodes after this annealing, the exposed surfaces of W-N are smooth and bubble-free. These bubbles are evidently not fatal to the leakage currents of the $n^+$-p diodes underneath. The second type consists of square pits that show up only in the contact areas of the shorted diodes, and are unremovable by Al selective etch. The presence of these square pits is indicative of Al spiking into (100) <Si> [10]. They also reflect the localized nature of Al-Si intermixing through the W-N layers. Each contact area to a leaky diode contains no more than two such pits whose sizes range from a few microns square to about $50 \times 50\,\mu m^2$. The third type consists of droplets which surround the square pits and give rise to extremely rough surface morphologies before an Al selective etch. These droplets appear to be resolidified material formed as a result of Si-Al intermixing and melting above 577°C, the eutectic temperature of Si-Al [87]. In fact, the whole surface of the sample (~1cm × 1cm in size) used for BS analysis is also found to be covered by such droplets after the 600°C sintering. It can therefore be inferred that the lateral expansion of Si-Al melting can take place quite rapidly if the contact metallization areas are not isolated from one another. Surface of contact regions to the good diodes with unchanged I-V characteristics are generally much smoother than those of the shorted diodes.

The Si/W-N/Al samples were also taken through a heat treatment at 500°C for 13 hours of thermal treatment to simulate the worst-case processing exposure [29]. The percentage of diode failure is a factor of two lower for contacts with an amorphous $W_{80}N_{20}$ barrier (23% ) than those with a polycrystalline $W_{60}N_{40}$ barrier (46% ). The failure mechanisms at 500°C may be very different from those at 600°C, and are not pursued here.

Experiments with other $W_{80}N_{20}$ and $W_{60}N_{40}$ barrier layers deposited under

different sets of sputtering parameters (total gas pressure, power, and substrate bias) show that these barriers also perform satisfactorily up to 575°C for 30 min annealing. In the light of these results, I conclude that both amorphous $W_{80}N_{20}$ and polycrystalline $W_{60}N_{40}$ barriers are about equally effective as diffusion barriers between Al and Si up to the Al-Si eutectic temperature, and that their diffusion barrier properties do not vary strongly with deposition conditions.

5.2.2 <Si> / $W_{90}N_{10}$ / Al and <Si> / W / Al CONTACTS

A polycrystalline $W_{90}N_{10}$ film is inferior as a barrier between Al and Si to $W_{80}N_{20}$ or $W_{60}N_{40}$. A reaction between Al and $W_{90}N_{10}$ leading to the formation of $WAl_{12}$ can be detected at 550°C by BS. Accordingly, the leakage currents of all the measured diodes are preserved up to 500°C annealing for 30 min but increase tremendously after a 550°C, 30 min heat treatment. Similarly, plain W fails by BS as a metallurgical barrier between Al and Si after a 500°C, 30 min as a result of the consumption of W by Al, in agreement with previous work [42, 45]. However, all the diodes with the <Si> / W / Al contact structure were shorted after annealing at 450°C for 30 min. This astonishing failure at 450°C is likely to be caused by diffusion of Al or Si through the grain boundaries of the W barrier undetected by BS analysis. As noted in Chapter 1, electrical measurements are more sensitive in detecting Al penetration than BS depth profiling. By comparing the performance of W and $W_{90}N_{10}$ barriers, one recognizes that the introduction of 10 atomic % of nitrogen into a W film creates a useful stuffed barrier effect and raises the diode failure temperature from 450°C to 550°C. Our observations with the four barrier layers also implied that W-N films must contain enough nitrogen so that Al-W reaction can be suppressed.

The percentage of diode failure as a function of annealing temperature (30 min) for the four barriers are summarized in Figure 3.

### 5.2.3 SUMMARIZING REMARKS

Both amorphous $W_{80}N_{20}$ and polycrystalline $W_{60}N_{40}$ films compare favorably with the best TiN layers [56,71] as diffusion barriers between Al and <Si>. The real strength of W-N diffusion barriers lies in their smooth dependence of film properties on the deposition conditions which derives from the one-to-one relationship between the various film properties and the composition. This monoparametric dependence is consistent with the comparable effectiveness of the barriers (against Al and Si intermixing) made of various W-N films with the same stoichiometry but deposited with different sputtering parameters. The diffusion barrier capability of W-N in a <Si>/W-N/Al contact scheme does not depend critically on how the films are deposited, provided enough nitrogen is present in the film. TiN films , on the other hand, exhibit strong dependence of barrier properties on deposition conditions even if they all have the same Ti to N ratio of 1:1. Optimization of sputter deposition for diffusion barrier applications is therefore much more demanding for TiN than that for W-N. Two additional advantages are present in using W-N barrier layers instead of TiN in Si-Al contact systems. A W-N layer is a good etch-stop for the chlorine-based dry etching processes currently used for Al interconnect patterning, whereas TiN is not [73]. Also, the best W-N barrier ($W_{80}N_{20}$) has the lowest compressive stress, while the opposite is true for TiN [69]. Based on the above findings and considerations, W-N qualifies as an attractive candidate for VLSI diffusion barrier applications.

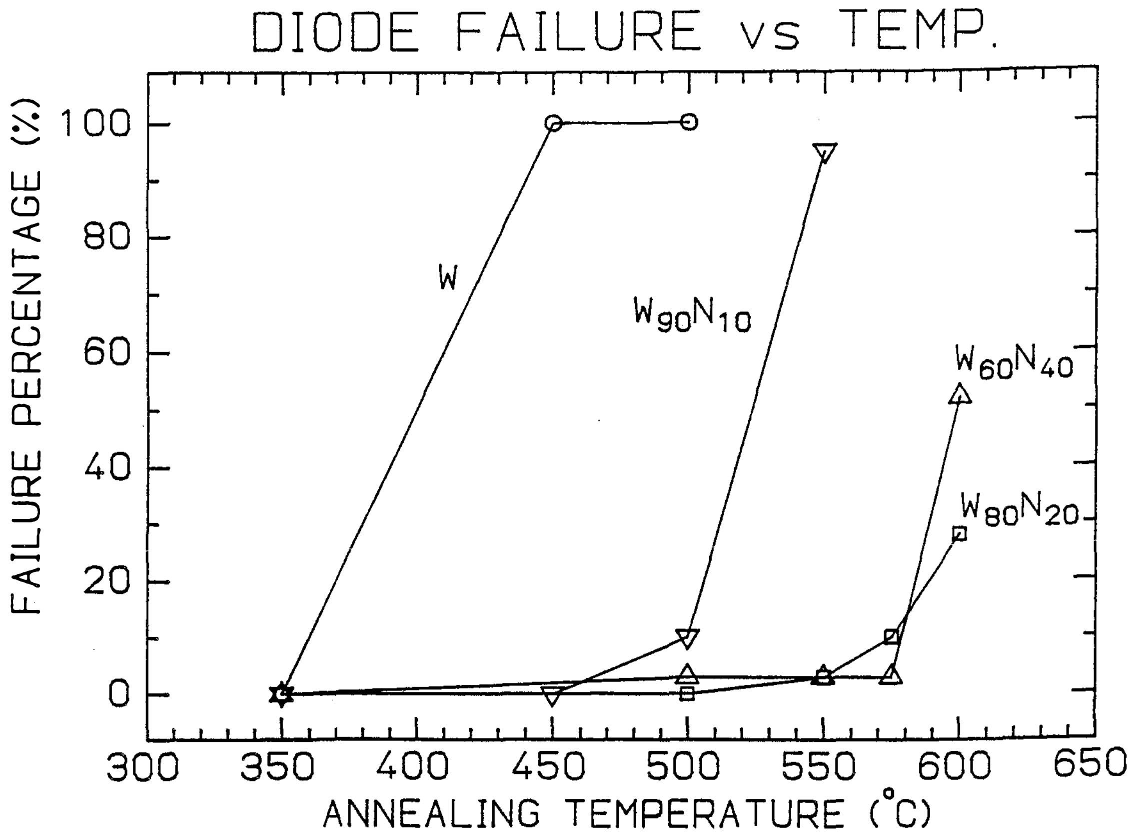


**Figure 3.** Percentage of diode failure as a function of annealing temperature (30 min) for diodes with the <Si> /W-N/Al contacts.

### 5.3 <Si> /W-N (or W)/Ag contacts to <Si> solar cells

Silicon shallow junction solar cells with the conventional Ti/Pd/Ag contact system degrade in Si shallow junction solar cells during a 600°C, 10 min electrostatic bonding step in the packaging process [61]. Significant intermixing takes place between Ag and Si at such temperature. It was shown by Kattelus et al. that a W layer can act as a metallurgical barrier between Ag and Si up to 600°C for 30 min, while W-N can suppress Si/Ag interaction up to even higher temperatures [51]. (From the phase diagram of Ag-W, Ag does not form compounds or solid solutions with W.) The electrical tests performed here serve to determine if W or W-N barriers can be used to enhance the the stability of the electrical contacts to a solar cell; simultaneously the performance of W and W-N barriers at 600°C may be compared with previous results.

Our test structures consist of 45 $\mu$m wide Si/Ti/$W_{80}N_{20}$ (or W)/Ti/Ag grid line contact structures fabricated by the lift-off technique onto 2 cm $\times$ 2 cm <Si> solar cells with shallow $n^+$-p junctions of ~2000Å depth supplied by Applied Solar Energy Corporation. The Ag layers (4 $\mu$m thick) were e-beam evaporated from a separate system after 800Å of amorphous W-N (or W) has been deposited by reactive sputtering. The thin Ti layers (100Å ) were introduced to ensure satisfactory adhesion and contact resistivities between the adjoining layers. We found that the thick Ag layers delaminate very easily from the W or W-N films if the Ti glue layers are absent. Control cells with the conventional Ti/Pd/Ag contacts were also prepared. After a standard 400°C, 15 min sintering in forming gas for the reduction of contact resistivities, the cells were evaluated electrically and then subjected to an additional 600°C, 10 min anneal that simulates the electrostatic bonding process.

The I-V characteristics of a typical control cell under AM0 illumination degrade radically after the 600°C treatment: the open circuit voltage $V_{oc}$ drops from 0.623±0.002 volt to 0.176±0.011 volt as a result of the heat the treatment (Figure 6a). The short circuit current $I_{sc}$ decreases slightly. This implies that the failure of the cells is caused predominantly by short-circuits across the diode junction, presumably as a result of Ag-Si interaction. Similar results were reported by Cheung [61].

In comparision to the control cells, the electrical characteristics of the cells with W or W-N incoporated into the grid line contacts change much less appreciably after annealing. Only a slight decrease of $V_{oc}$ from 0.620±0.002 volt to 0.608±0.001 volt is measured (Figure 6b). $I_{sc}$ also changes slightly as in the control cells. These results apply to both type of cells with either W or amorphous W-N, indicating that W and W-N are equally effective in inhibiting Si-Ag intermixing for the thermal cycle considered here. However, the small drop in $V_{oc}$ suggests that the diffusion of metal atoms into the vicinity of the device junction is not completely eliminated by the presence of the diffusion barriers. Inspection by SEM shows evidence of Ag flow down the edge of some of the grid lines. The reduction of $V_{oc}$ may be connected with this movement of the thick Ag overlayer along the contact edges into the $n^+$-p junction. The possibility of Ag diffusing through the bulk of the W or W-N layers cannot, however, be totally eliminated. To clarify if geometrical effects play the dominant role in governing the thermal stability of the cells, another set of cells were fabricated with narrow Ag lines (23 $\mu$m) on top of wide W or W-N layers (45 $\mu$m). These cells show, on average, only about 0.003 volt reduction in $V_{oc}$ after the 600°C anneal, as compared to 0.012 volt in the cells described above. Vertical flow of Ag probably lessens when the Ag lines are recessed from the edges of the barrier layer. The degradation in

$I_{sc}$ is also removed by such a geometrical modification.

From the above results, I conclude that both W and $W_{80}N_{20}$ perform excellently as diffusion barriers between Ag and Si for the electrostatic bonding thermal cycle.

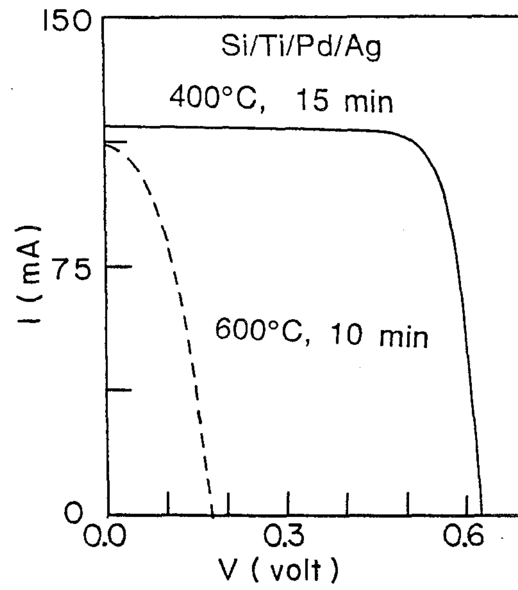


(a)

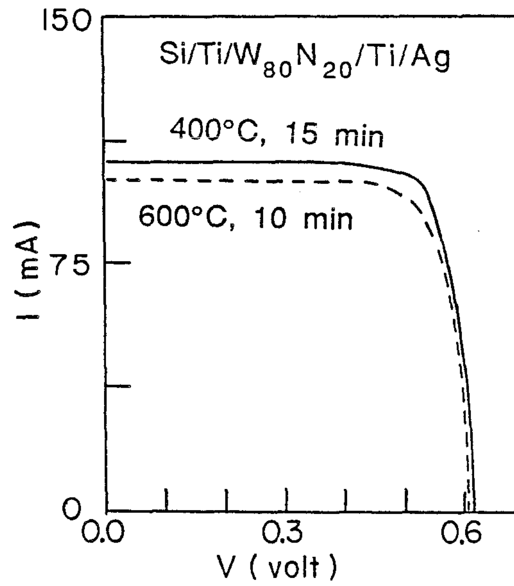


(b)

**Figure 6.** I-V characteristics of solar sells with (a) the conventional Ti/Pd/Ag contacts (b) the Ti/$W_{80}N_{20}$/Ti/Ag contacts before and after a 600°C, 10 min sintering.

### 5.4 Pt-Mg/W-N (or W)/Ag contacts to p-GaAs

The concept and importance of diffusion barriers has not yet been implemented in GaAs contact technologies. Although ohmic contacts to GaAs have been studied extensively, the present contact schemes used in devices are still far from satisfactory. A conventional ohmic contact structure involves a metal (e.g. Au, Ag) combined with a dopant element (e.g. Ge for n-type and Zn, Be for p-type) [74]. The ohmic behavior in these systems is realized by alloying the metal-dopant layers with GaAs in a quenched liquid-phase reaction. Melting and quenched resolidification usually result in lateral and compositional inhomogeneties which have detrimental effects in subsequent contact bondings of shallow junction devices and their operations. The contact resistivities are critical functions of the alloying parameters [74] and are therefore hard to reproduce.

To obtain reproducible and stable ohmic contacts on GaAs, a process based on steady-state solid phase reactions that is analogous to the silicide contacts formed on Si offers obvious advantages [VIII]. To implement this concept, we follow a strategy that exploits the advantages of a diffusion barrier layer and separates the metallic film that reacts with GaAs below the barrier layer from the low resistivity metal overlayer above the barrier layer. Figure 7 depicts the solid-phase contact scheme we advocate alongside, with a conventional contact scheme. The reacting metal film below the diffusion barrier should be chosen such that it reacts with GaAs in the solid phase to form a stable contacting layer of intermetallic compounds. Simultaneously, that contacting layer has to provide adequately low and thermally stable contact resistivities to GaAs. A low resistivity metal overlayer (Au, Ag, Al) is invariably needed for interconnection and bonding purposes. The barrier layer confines the reaction between the metallic

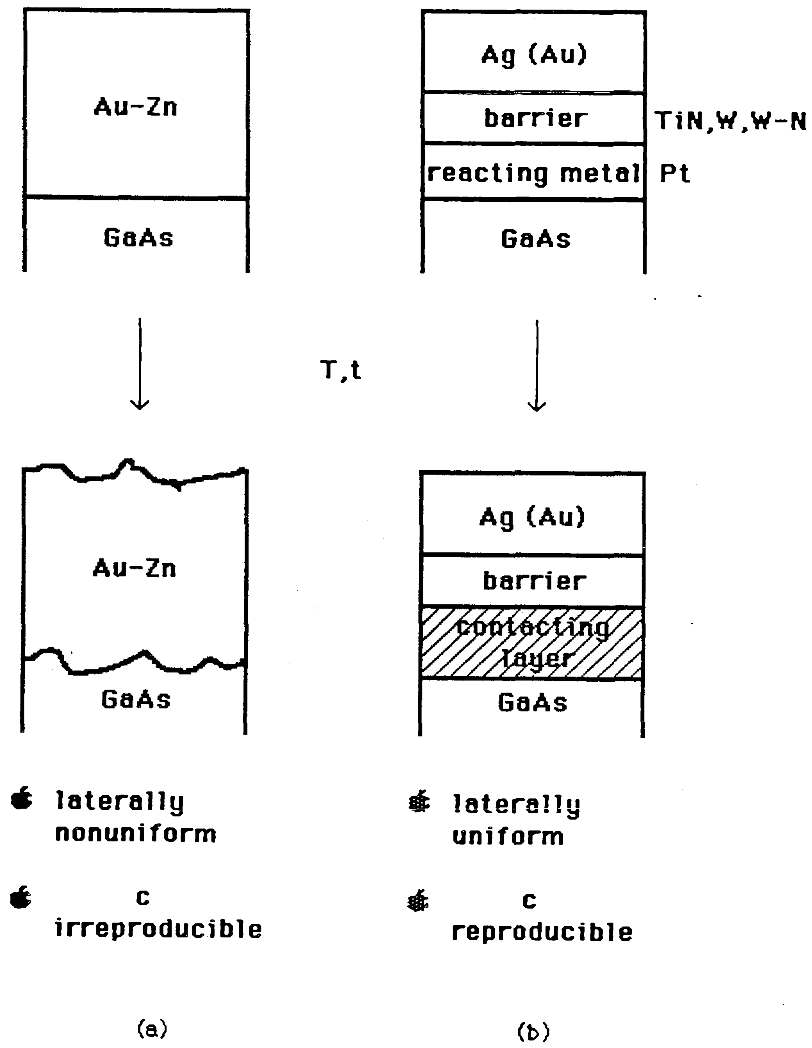


Figure 7. a) The conventional contact scheme to GaAs with Au-Zn (or Au-Ge); b) The solid-phase contact scheme.

layer and GaAs and prevents the top overlayer from interfering with this reaction. The contacting layer is generally necessary even when the diffusion barrier layer happens to have an acceptable contact resistivity to GaAs. The problems of electrical reproducibility of that interface are always more difficult to handle in practice than for an interface that is formed *in situ* by a solid-phase reaction, as is the case for a contacting layer. The major conceptual difference between such a contact scheme and a conventional one is that the metal overlayer is no longer involved in the ohmic contact formation. (The use of Au and Ag as a constituent in the primary contacting layer usually accounts for the nonuniformity problems.) Proper choices of the barrier layer and the reacting metallic film are therefore crucial in the implementation of a solid-phase contact. We are concerned here mainly with the diffusion barrier aspect in one such contact scheme.

The thermal stability of the GaAs/ Pt-Mg/ $W_{70}N_{30}$ (or W)/ Ag metallization scheme to p-GaAs are examined [VI, VIII]. Platinum is chosen as the reacting metal layer because it reacts with GaAs in a laterally uniform fashsion and forms stable intermetallic phases (PtGa and $PtAs_2$) at 350°C and above [76,VI]. A reacted Pt contact to p-GaAs provides acceptable contact resistivities that are thermally stable at least up to 550°C [75]. About 3 atomic percent of Mg is incoporated into the Pt layer by sputter deposition performed at Applied Solar Energy Corporation from a nominally Pt-2% Mg composite target. The motivation for the Mg incorporation springs from reference 75 where it is shown that a thin Mg layer at the interface between Pt and GaAs can lower the contact resistivity much. As in the Si solar cell studies described in the last section, both W and W-N (in this case amorphous $W_{70}N_{30}$ ) are evaluated as barrier layers in the contact structures. The W or W-N (~800Å ) barrier layers and the Ag

overlayers (~2500Å) were deposited sequentially without breaking vacuum in the same deposition chamber. To evaluate the thermal stability of the contacts, all the samples were annealed at 550°C up to 5 hours in forming gas.

Backscattering analysis shows that both W and W-N act as excellent diffusion barriers and confine the reaction of Pt with GaAs up to 5 hours annealing at 550°C [VI, VIII]. Interdiffusion between Ag and the underlying films in the contact structures cannot be detected. The presence of Mg does not have any noticeable effect on the Pt-GaAs reaction. SEM and EDX reveal rather smooth surface morphologies and no compositional inhomogeneities for the annealed samples. Some micron size bubbles are spotted on the sample surface, presumably as a result of a localized loss of adhesion between Ag and W-N(W). In contrast, heat treatment at 550°C for only 15 min causes significant intermixing between Ag and Pt or GaAs when the barrier layers are absent. Very rough surface morphologies and compositional inhomogeneities typical of nonuniform alloying can be observed. (Ag-As eutectic temperature is 540°C; Ag-Ga eutectic temperature is $\leq$ 100°C.)

The GaAs/Pt-Mg/Ag contacts yield contact resistivities to p-GaAs ($p = 1 \times 10^{18}$ $cm^{-3}$) of $\sim 10^{-2}$ $\Omega\,cm^2$ after 15 min of annealing at 550°C. On the other hand, the contact resistivities of contacts with W and W-N diffusion barriers are measured to be $5 \times 10^{-4}$ $\Omega\,cm^2$ after 30 min annealing at 550°C (Table II). The contact resistivities in the latter case increase only by a factor of two even after 5 hours of prolonged heat treatment. This slight increase in contact resistivities is probably connected with the loss of dopants or minute amount of Ag penetration into GaAs not detected by BS [VI]. These measurements clearly demonstrate the advantage of the presence of W or W-N barrier layers in isolating the Pt-GaAs reaction from the influence of the top Ag layer.

| | $\rho_c$ ($\Omega$-cm$^2$) | |
|---|---|---|
| | 550°C 30′ | 550°C 5h |
| GaAs/Pt-Mg/Ag | 1(±0.3) x $10^{-2}$ | |
| GaAs/Pt-Mg/W/Ag | 5(±2) x $10^{-4}$ | 10(±3) x $10^{-4}$ |
| GaAs/Pt-Mg/W-N/Ag | 5(±2) x $10^{-4}$ | 9(±3) x $10^{-4}$ |
| GaAs/Mg/Pt/TiN/Ag | 3 x $10^{-4}$ | |
| GaAs/Pt/TiN/Ag | 3 x $10^{-3}$ | |

**Table II.** Contact resistivities of various metallization schemes to p-GaAs.

The contact resistivities obtained here with the Pt-Mg/W-N(W)/Ag systems are comparable to those obtained on Mg/Pt/TiN/Ag contacts taken through the same thermal cycle [75]. This result is, in fact, expected if ohmic behavior in these systems is the consequence of the reaction products formed at the GaAs/Pt interface, and independent of the overlayers. It is also worth noting that 3 atomic percent of Mg contained in the Pt layer has the same effect as the 100Å of Mg layer interposed between Pt and GaAs in reducing the contact resistivities to p-GaAs [75]. End resistance measurements [77] indicate that the sheet resistance of the p-layer benneath the contacts drops dramatically after heat treatment at 350°C and above in both cases [VI]. This drop in the p-layer sheet resistance presumably results from the doping action of Mg. Without Mg, contact resistivities are about $3\times10^{-3}\,\Omega\,cm^2$ after annealing at 550°C for 30 min. No reduction of the p-layer sheet resistance is observed when Mg is absent.

The successful implementation of a solid-phase contact to GaAs cannot be realized unless appropriate barriers layers are used. As in the case of Si, both W and W-N are excellent diffusion barriers between Ag and the underlying Pt or GaAs at the processing temperatures considered here. The contact resistivities provided by the Pt-Mg alloy layer is adequately low for wafer-size solar cell device requirements, but are still too high for LSI GaAs IC applications. So far, very few efforts have been devoted to exploring suitable materials that make good solid-phase ohmic contacts to p or n-type GaAs. A lack of appropriate contacting layers would discourage the practice of the ideas discussed here. The systematic study of contacting layers and their suitability for GaAs contacts– both ohmic and rectifying– is clearly needed critical for further progress in this field.

## 5.5 GaAs/W-N (or W)/Au Contacts

Gold is the most widely used contact and interconnection material in GaAs device fabrication. It is particularly challenging to find an effective diffusion barrier between Au and GaAs because of the low eutectic temperature between Au and Ga (340°C). A GaAs/W-N (or W)/Au system is presently used as gate electrode in the manufacturing of GaAs MESFET [32]. Using backscattering analysis and sheet resistance measurements, W and W-N layers were found to be excellent diffusion barriers between Au and GaAs up to 550°C annealing for 30 min in forming gas [VII]. Problems of adhesion between Au and W-N (or W) can be observed, however, as in the case of Ag overlayer.

## 5.6 Conclusions

Both amorphous and polycrystalline W-N films are far superior than W and compete favorably with TiN as diffusion barriers between Al and Si. The diffusion barrier properties of W-N do not depend strongly on the deposition conditions of the layers, provided a certain minimum amount of nitrogen is incorporated into the films.

In the case of Ag overlayers, W is as good as amorphous W-N in inhibiting interactions between Ag and the underlying contact layers to both GaAs and Si up to at least 550°C and 600°C respectively. Tungsten nitrides also hold promise as candidates for diffusion barrier applications in Au-based metallizations to GaAs.

# Chapter 6

# The Ti/W-N Bilayer

## 6.1 Introduction

We have seen in the last chapter that the adhesion between W-N barriers and Al, Au, or Ag overlayers is generally unsatisfactory. This adhesion problem can be a major hindrance to the application of W-N in real-life contact structures, especially when contact areas are small. In the study of grid-line contacts to <Si> solar cells with Ag overlayers, the use of thin layers of Ti in the contact structure was found to be extremely effective in enhancing the adhesion between W-N or W with Ag. As a matter of fact, Ti is a very common glue layer used in many MOS and bipolar IC metallizations. It is also widely exploited as a primary contact layer to <Si> to provide low contact resistivities [18] and as an underlayer to Al interconnects for relieving problems due to hillocks formation [78]. Although the <Si> /W-N/Al contact structures are shown to have good thermal stability, an extra contact layer between W-N and <Si> is probably necessary in the design of a realistic contact structure. The contact resistivities of W-N to $n^+$-Si are evaluated to be in the $10^{-5}\,\Omega\,\text{cm}^2$ range, which are unacceptably high for VLSI applications. (With the present VLSI feature size of $\sim 1\,\mu$m, contact resistivities in the $10^{-7}\,\Omega\,\text{cm}^2$ range are desired.) Under these circumstances, the compatibility between Ti and W-N becomes a relevant subject for careful investigation, since the two elements are expected to abide side by side in a contact structure. In the first part of this chapter, the effect of an adjacent Ti layer on the diffusion barrier performance of W-N against Ai-Si interdiffusion is presented. In the second part, we demonstrate how the inherent

thermal instability in a Ti/W-N bilayer may actually be converted usefully into a novel self-aligned process for CMOS fabrication.

### 6.2 The <Si> /Ti/W-N/Al contact system

A 900Å layer of amorphous $W_{70}N_{30}$ can effectively inhibit interaction between Al and Si up to 575°C. However, with an extra Ti layer of 1500Å in thickness in contact with <Si>, significant interactions between Al and the underlying layers can be observed in a <Si> /Ti/W-N/Al contact structure by BS after annealing at 550°C for 30 min [IX]. As depicted by the BS spectra, W-N reacts with Al in a similar fashion as pure W does. The whole W-N film is fully consumed in the reaction with Al after the heat treatment. $WAl_{12}$ formation is evident from x-ray analysis of such a reacted sample. Apparently, the presence of a sublayer of Ti reduces the effectiveness of $W_{70}N_{30}$ alloy as a passive barrier barrier between Al and Si. Similar results are obtained with polycrystalline $W_{54}N_{46}$.

Auger Electron Spectroscopy (AES) has been used to determine the depth distribution of nitrogen in a bilayer of Ti/W-N on <Si> before and after annealing in order to understand the cause of failure in the <Si> /Ti/W-N/Al system. The evolution of nitrogen in a Si/Ti/W-N sample at 500 and 550°C is portrayed in the AES depth profiles shown in Figure 8. Clearly, redistribution of nitrogen from W-N into Ti occurs as a result of the thermal treatment. (Due the overlapping between of Ti and N signals, quantitative information of nitrogen in Ti cannot be provided by AES. Nevetheless, the relative change in nitrogen levels gives a convincing picture of the nitrogen movement.) With this knowledge, failure in the <Si> /Ti/W-N/Al metallization system can then be rationalized by a partial depletion of nitrogen from W-N followed by Al reacting with the nitrogen-deficient W-N layer.

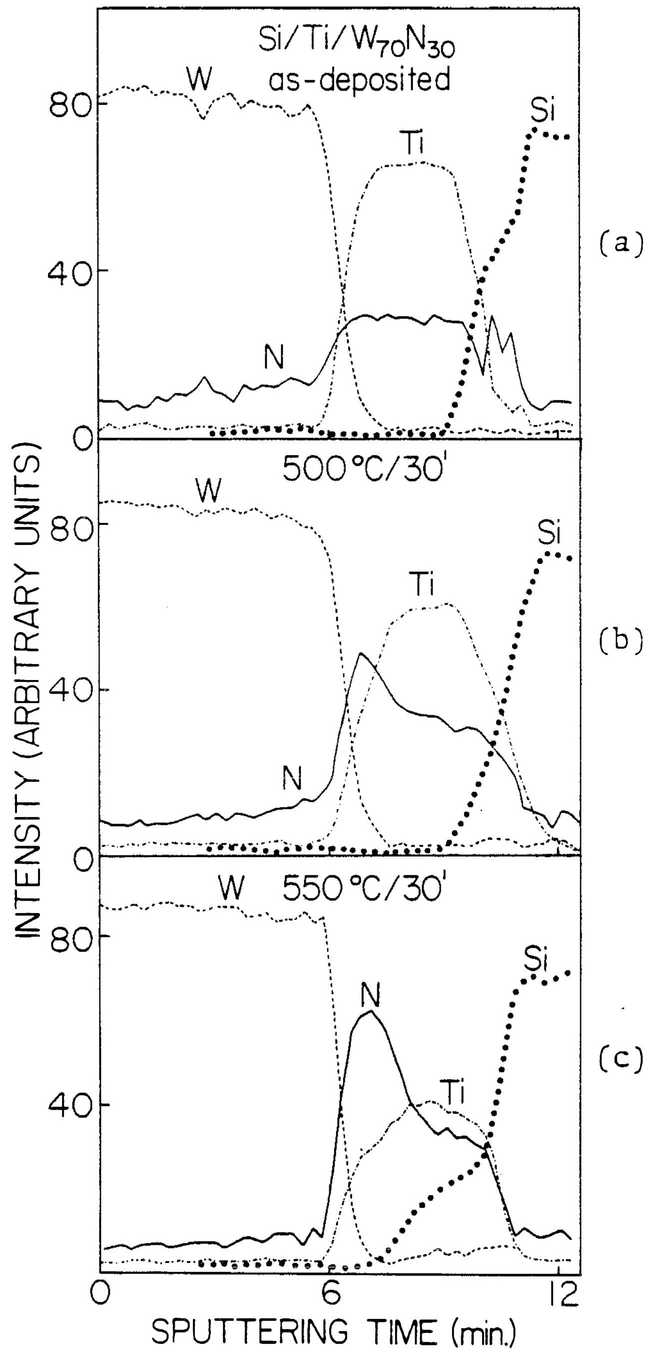


**Figure 8.** AES depth profiles of a <Si> $/Ti/W_{70}N_{30}$ sample before and after annealing at 500°C and 550°C for 30 min.

One obvious question to ask is what force drives such movement of nitrogen. As mentioned in Chapter 4, the heat of formation of TiN (-80 kcal/mole) is much more negative than that of $W_2N$ (-17 kcal/mole). It follows that nitrogen is more strongly bound to Ti than to W by a large amount. The redistribution of nitrogen from W-N into Ti is thus thermodynamically favorable. On the other hand, estimations of diffusion length of nitrogen in W and Ti [IX] show that nitrogen is quite mobile in the Ti/W-N couple at temperatures above 500°C. It thus appears that the displacement of nitrogen into the Ti layer is driven by a chemical potential and facilitated by a high diffusivity.

Nitrogen redistribution, however, does not occur at 550°C if the Ti sub-layer is replaced by a sputtered $TiSi_{2.3}$ from AES depth profiles. Significant interaction between nitrogen and $TiSi_2$ usually takes place at temperatures in excess of 850°C [79]. The integrity of the W-N barrier is indeed preserved in the <Si>/$TiSi_{2.3}$/W-N/Al contact system after 30 min annealing at 550°C. The above findings also suggest that a preformed $TiSi_2$ layer is preferred to Ti as the contacting layer to Si if W-N is used as a diffusion barrier.

### 6.3 Application of the Ti/W-N bilayer to the self-aligned $TiSi_2$ process

The thin-film reactions and nitrogen redistribution in a polycrystalline $Ti/W_{60}N_{40}$ bilayer on both <Si> and $SiO_2$ have investigated in the temperature range of 600 - 850°C [X]. The major results are summarized as follows:

I) On <Si>

i) Between 600°C and 750°C annealing, the Ti/W-N bilayer on <Si> is transformed into a <Si> / $TiSi_2$ /TiN/W-N structure. Nitrogen is released preferentially from the W-N layer near the Ti interface. This results in a W-N outer layer whose nitrogen concentration vary with depth. The atomic fraction of N in the TiN layer varies from 0.4 at 600°C to 0.55 at 700°C and above. Formation of the cubic TiN phase in all the annealed samples is confirmed by X-ray analysis. The thicknesses of TiN and $TiSi_2$ remain more or less constant for the whole temperature range.

ii) Between 800°C and 850°C, the W-N layer loses most of its nitrogen to both TiN and the ambient. Consequently, the TiN layer grows slightly at the expense of the $TiSi_2$ layer. Only 5 - 10 atomic percent of nitrogen still resides in the the W-N layer. The W-N layers consists of $\alpha$W only, meaning that the tungsten nitride phases present in the as-deposited $W_{60}N_{40}$ are chemically reduced. Above 850°C, W(W-N) reacts with <Si> to form $WSi_2$.

II) On $SiO_2$

In the $SiO_2$/Ti/W-N system, nitrogen moves in much the same way as in the former case. As nitrogen diffuses into Ti, Ti also interacts slightly with $SiO_2$ at 600°C and above. Oxygen from a decomposed interfacial layer of $SiO_2$ layer probably dissolves in the Ti film [80]. Consequently, a $SiO_2$ /Ti-N-O /W-N

structure forms in the temperature range of 600 – 750°C. No titanium oxide or silicide phases can be detected by x-ray diffraction. Reaction between Ti and $SiO_2$ remains very limited up to 850°C due to the competing reaction between Ti and nitrogen. Without the W-N layer, Ti reacts rapidly with $SiO_2$ at 700°C or above leading to the formation of Ti-rich silicides and $TiO_x$ [80]. The resistivities of the W(W-N) and Ti-O-N layers are determined to be about 40 $\mu\Omega$-cm and 77 $\mu\Omega$-cm respectively after a 30 min, 800°C anneal. (For details, see reference X.)

The nitridation of Ti resembles the outcome in the self-aligned $TiSi_2$ process where a Ti film on <Si> or $SiO_2$ is annealed in a nitrogen ambient above 600°C, as reported by numerous authors [97]. In the present case, it is simply the W-N film that acts as a source of nitrogen for the conversion of Ti to TiN.

The advantages of self-aligned silicide (SALICIDE) processes for submicron CMOS manufacturing have been elaborated in many papers (see references 11, 12, 16, 17, 18, 19 of X). In a recent report on the self-aligned $TiSi_2$ process [98], a local interconnection (LI) level has been realized by utilizing the TiN layer formed during silicidation. Figure 9 shows the process flow that leads to the formation of TiN local interconnection lines between gates and source/drain junctions. The key step in such a process is that silicidation of Ti proceeds in an ambient containing nitrogen. Nitrogen diffuses readily into and reacts with the blanket Ti to form a top layer of TiN. The formation of TiN over the oxide spacers, in addition, effectively prevents silicon from diffusing laterally from the gate and junction regions into the Ti located over the oxides regions. Following the reaction, TiN and any unreacted Ti may be selectively etched with a standard sulfuric acid /hydrogen peroxide cleanup so that gates and junctions would not be electrically shorted together. The $TiSi_2$ layers are left intact over the Si

regions. To form the TiN LI, an additional mask is used to define the LI pattern before the etching step (Figure 9) Such a LI scheme has a number of advantages over the conventional buried interconnection schemes [98]. However, a major disadvantage is that W does not nucleate and grow on a TiN LI surface in a LPCVD process which is advocated for via filling and the formation of second level interconnects (see Chapter I).

As an alternative to the TiN LI technology just described, a Ti/W-N bilayer may be used to implement the self-aligned $TiSi_2$ process with the simultaneous formation of a *W LI* (see Figure 10). A blanket Ti/W-N bilayer is deposited in lieu of a single Ti layer. Upon annealing at 600-700°C, nitrogen will redistribute everywhere from the W-N layer into the Ti films as in a typical self-aligned process. Following this heat treatment, the LI photoresist is again laid down, and the W-N and TiN are then selectively etched off one after another, leaving a TiN/W-N LI running between source drain contacts and gates. Subsequent annealing at 800°C reduces the $TiSi_2$ and TiN resistivities further and also releases nitrogen from W-N to form a LI composed predominantly of bcc $\alpha$W.

The implementation of the $TiSi_2$ self-aligned process with a W LI from the Ti/W-N bilayer offers the following advantages over the conventional process:

1) A W LI provides a lower sheet resistance than its TiN counterpart because of the lower resistivity of the annealed W(W-N) layer. (TiN formed by nitriding Ti in a nitrogen ambient has a typical resistivity of $\sim 100\,\mu\Omega$-cm.)

2) No additional photolithographic step is required to pattern the W LI. However, an additional deposition step and selective etch step for W-N is necessary.

3) A W LI that forms from the Ti/W-N bilayer can act as a platform for nucleating LPCVD W growth for possible second level interconnects or filling of vias. However, since not all the nitrogen is removed from the W layer even after

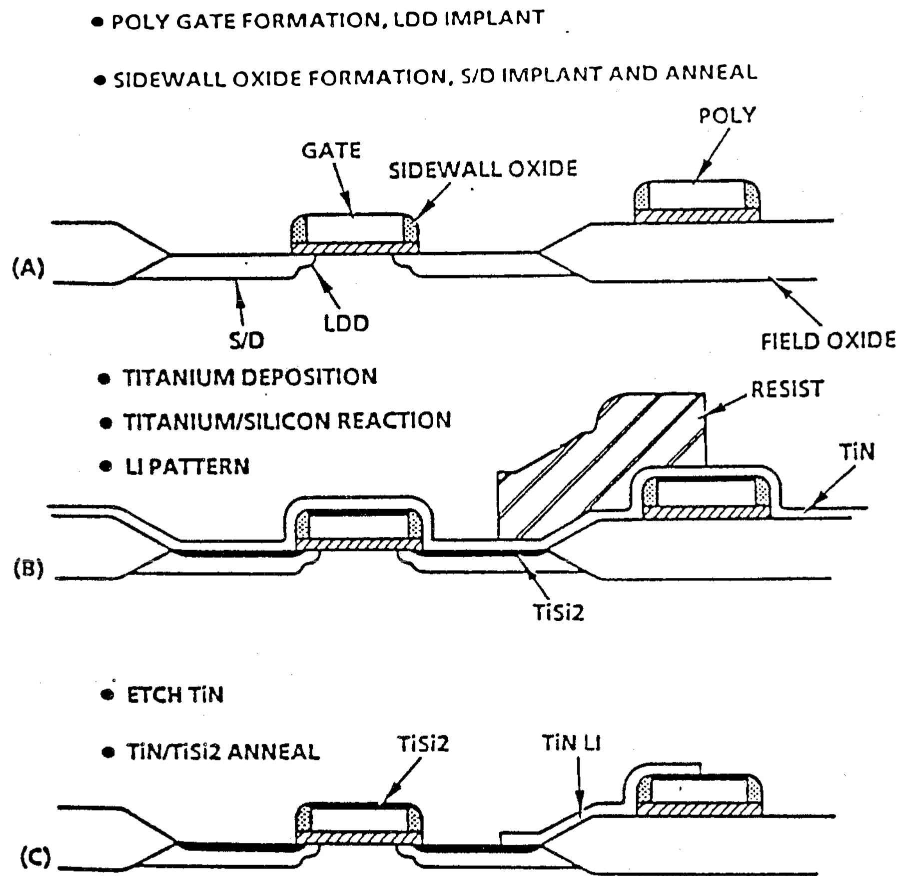


Self-aligned TiSi2 process showing the TiN LI patterning step.

**Figure 9** Conventional self-aligned $TiSi_2$ process showing the TiN LI patterning step, (from reference 98).

- poly gate formation
- spacer , s/d implant ,anneal

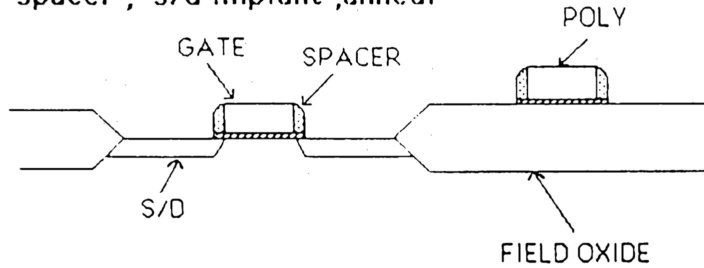


- Ti deposition + W-N deposition
- Ti / Si reaction , TiN formation
- L I pattern

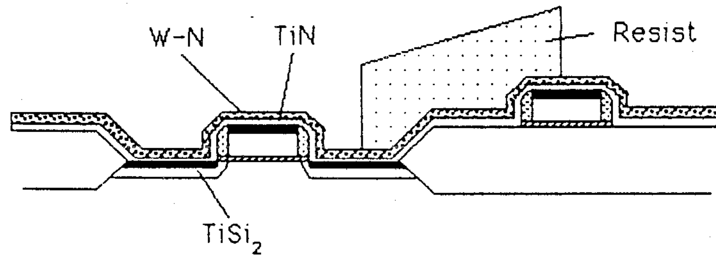


- etch W-N , TiN
- $TiSi_2$/ TiN /W-N anneal ( 800° C )
- W-N reduction to W

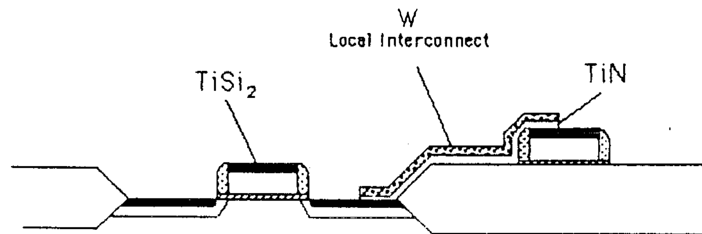


**Figure 10** Self-aligned $TiSi_2$ process with a W (W-N) LI.

annealing at 800°C, the particularities of growing LPCVD W in the temperature range of 150-600°C on such a W LI remains to be investigated.

4) The W-N layer can possibly act as a cap to protect the underlying Ti from undesirable oxidation. Recent work by Wei [81] has already shown that an overlayer of W on <Si>/Ti provides excellent protection against Ti oxidation. Also, since the nitrogen for Ti nitridation in a Ti/W-N bilayer is supplied from W-N and not from the ambient, a dielectric cap like Phosphosilicate glass (PSG) or Borophosphosilicate glass (BPSG) can always be deposited on top of W-N for extra protection against Ti oxidation during the silicidation step.

One limitation of this novel process remains. As mentioned earlier, the <Si>/ $TiSi_2$ /TiN /(W)W-N structure is thermally stable only up to 850°C. Above that temperature, W reacts with Si and forms silicide. This implies that the final heat treatment for resistivity reduction cannot exceed 850°C by furnace annealing. However, such a temperature limit is not expected to be a major hindrance to implementing the process because the maximum annealing temperature that can be tolerated in the conventional self-aligned $TiSi_2$ process does not exceed 900°C. A $TiSi_2$ layer on <Si> is morphologically unstable beyond 900°C [82]. Rapid thermal annealing may offer an attractive alternative.

# Chapter 7

# Reactively Sputtered $Mo_{1-x}O_x$ * and $RuO_2$ Diffusion Barriers

## 7.1 Introduction

Apart from refractory metal nitrides, a number of other interstitial alloys such as borides [83] and carbides [84] have also been investigated for diffusion barrier applications. However, no attention was paid to the suitability of thin films of conducting transition metal oxides as barrier layers. This attitute probably springs from the fact that most transition metals are electrically insulating (e.g. $TiO_2$); some are volatile (e.g. $WO_3$). There are, however, transition metal oxides that exhibit metallic conductivities at room temperatures. One type of conducting oxides has an oxygen to metal ratio of 2. Two groups can be distinguished. The first one consists of the dioxides of the Pt group which crystallizes in the rutile structure: $RuO_2$, $OsO_2$, $IrO_2$ and $RhO_2$. Among the four, $RuO_2$ is reported to possess the lowest bulk resistivity (about 46 $\mu\Omega$-cm) [85]. The other group is made up of the dioxides that adopt distorted variants of the rutile structures: $CrO_2$, $MoO_2$ and $WO_2$. Single crystals of $MoO_2$ are monoclinic and have

---

* We adopt $Mo_{1-x}O_x$ to designate molybdenum-oxygen alloys of variable compositions. This nomenclature has not been extended to tungsten-nitrogen, nickel-nitrogen-tungsten, or tungsten-zirconium alloys described in the previous chapters because of the traditional representations. Strictly speaking, W-N, Ni-N-W, and W-Zr should have been rewritten as $W_{1-x}N_x$, $Ni_{1-x-y}N_xW_y$, and $W_{1-x}Zr_x$ respectively for clarity and consistency.

a room temperature resistivity of ~90 $\mu\Omega$-cm [85]. $RuO_2$ and $MoO_2$ are dissimilar in their stability. $RuO_2$ is the only thermodynamically stable oxide of Ru (86,87). On the other hand, there exist higher oxides of Mo that are electrically insulating and volatile ($MoO_3$). The different oxide chemistry correlates with a different behavior of oxygen incorporation into Mo and Ru films during reactive sputtering. In this chapter, the important aspects of the deposition behavior of $Mo_{1-x}O_x$ films formed by rf reactive sputtering are presented. The preparation of $RuO_2$ will only be briefly mentioned and compared to that of $Mo_{1-x}O_x$. The two oxide films are also tested as diffusion barriers against interdiffusion in Al-Si couples.

## 7.2 Deposition of $Mo_{1-x}O_x$ films

The film composition, microstructure, resistivity and stress of $Mo_{1-x}O_x$ have been investigated as functions of various sputtering parameters in much the same way as in the case of W-N (reference IV). Detailed results can be found in appendix III. The major observations are summarized as follows:

i) $Mo_{1-x}O_x$ films of a wide range of compositions can be deposited in $O_2$ /Ar gas ambients.

ii) For a fixed initial total gas pressure and relative initial partial pressure of oxygen (defined as $p(O_2)/p(O_2+Ar)$ ), the oxygen concentration (x) in the $Mo_{1-x}O_x$ films decreases continuously as sputtering power increases, and can assume any value between 0 to 75 atomic percent.

iii) The amount of oxygen in the films increases smoothly with initial oxygen partial pressure at a fixed initial total gas pressure and sputtering power.

iv) When the initial total gas pressure is kept constant, the deposition rate follows a more or less linear dependence on sputtering power, and is affected insignificantly by variations in initial partial pressure of oxygen.

v) All as-deposited $Mo_{1-x}O_x$ films are electrically conducting and consist predominantly of polycrystalline Mo with oxygen probably stuffing the grain boundaries, except for $Mo_{25}O_{75}$ which contains a single phase of $MoO_3$. Annealing at 600°C or above leads to the formation of $MoO_2$ in the conducting $Mo_{1-x}O_x$ films.

vi) The resistivity of the $Mo_{1-x}O_x$ films increases monotonically with x, regardless of the sputtering conditions used. This indicates that conduction mechanisms in the $Mo_{1-x}O_x$ films are governed by the amount of oxygen contained in the films.

vii) The stress of all conducting $Mo_{1-x}O_x$ is compressive. At a fixed sputtering power, lower film compression is obtained with a higher total gas pressure. However, no simple relationship between film stress and composition can be seen.

A straightforward side-by-side comparision of the the behavior of $Mo_{1-x}O_x$ and W-N deposition shows that they are very much alike. Similar formation mechanisms are therefore expected. Our observation that the oxygen content in the $Mo_{1-x}O_x$ films may be continuously varied for the entire range of sputtering parameters is consistent with the picture of an oxide-free Mo target surface during sputter deposition as proposed by Hollands [58]. The absence of discontinuous change in deposition rate as the oxygen partial pressure and sputtering power are varied is also indicative of deposition from an unoxidized target surface. Under these circumstances, incorporation of oxygen into a $Mo_{1-x}O_x$ film probably takes place by a surface reaction between Mo and chemisorbed oxygen on the substrate as the film grows [58].

### 7.3 Deposition of $RuO_2$ films

The deposition behavior of $RuO_2$ contrasts that of $Mo_{1-x}O_x$ in two major respects. The amount of oxygen incorporated into the ruthenium-oxygen alloy films is discontinuous: either Ru or $RuO_2$ is deposited at one time [88]. In addition, $RuO_2$ films are formed from a Ru target only within a very narrow range of depositions when sputtering in an $O_2$/Ar ambient. However, with a $O_2$/Ne glow discharge, $RuO_2$ film deposition can be realized over a wide range of partial pressure, substrate bias and sputtering powers. This difference can be attributed to the fact that metastable excited Ne atoms can ionize oxygen molecules from their ground state by the Penning process [89], whereas metastable argon atoms cannot. The generation of $O_2^+$ promotes $RuO_2$ formation much. All the as-deposited $RuO_2$ films have resistivities around 170 $\mu\Omega$-cm.

The formation of $RuO_2$ can be correlated with that of Pt-O, since Pt and Ru have very similar oxide chemistry [85]. After a careful study of Pt-O bond formation under different sputtering conditions, Aita [89] concluded that oxide formation in the films is controlled by a reaction which occurs at the target surface and is enhanced when neon carrier gas is used. It is believed that $RuO_2$ forms via very similar mechanisms, since its deposition behavior bears a close resemblance to that of Pt-O.

## 7.4 $Mo_{1-x}O_x$ and $RuO_2$ films as diffusion barriers between Al and Si

The diffusion capability of $Mo_{1-x}O_x$ and $RuO_2$ films have been evaluated by BS analysis and electrical measurements performed on shallow junctions as in the case of W-N. Although a small outdiffusion tail of Mo can be seen in the BS spectrum of a <Si> / $Mo_{80}O_{20}$ / Al sample after a 550°C, 30 min anneal, the interaction of Al with the barrier layer or the Si substrate remains very limited even after annealing at 600°C for 20 min [appendix III]. Indeed, a $Mo_{80}O_{20}$ barrier layer is proved to be very effective in protecting a shallow $n^+$-p junction from Al penetration after the same thermal treatment [appendix IV]. No junction shorting can be observed. The diffusion barrier performance of $Mo_{60}O_{40}$ films is found to be equally good. $RuO_2$ films perform comparably as $Mo_{1-x}O_x$ as diffusion barriers between Al in Si [XI]. Failure in a <Si> / $TiSi_2$ / $RuO_2$ / Al contact system is dominated by localized defects in the $RuO_2$ barrier layer [XI].

## 7.5 Conclusions

In spite of the different deposition mode and film characteristics of $Mo_{1-x}O_x$ and $RuO_2$, the diffusion barrier barrier performance of these oxides are equally outstanding and are superior to any nitride, carbide barrier layers investigated to date. The implication is plain to see: it is the presence of oxygen that accounts

for the extreme effectiveness of such oxide barriers between Al and Si. The potential for applications in VLSI circuits and discrete devices is obvious.

# Chapter 8
# Further Thoughts

Tungsten nitride, molybdenum oxide and ruthenium oxide are undoubtedly excellent passive barriers against Al-Si interdiffusion. It is, however, not very clear why these layers are inert with respect to an adjoining Al overlayer. Table III on the next page reveals that the heat of formation ($\Delta H_{298^\circ}$) of aluminum oxide is in fact much more negative than those of $RuO_2$ and $Mo_{1-x}O_x$. AlN is also more stable than W-N by the same comparision. Decomposition of these oxide or nitride barriers by Al to form aluminum oxide or nitride [26,90] is therefore thermodynamically favorable. In the present investigations, none of the barrier films are chemically dissociated by Al to an appreciable extent according to BS and x-ray diffraction analysis. (Localized failure in W-N and $RuO_2$ barriers precedes *any* observable chemical reaction.) It is therefore likely that a kinetic barrier controls the accessibility of such reactions. Very recent findings of Zhao et al. show that a 45Å layer of interfacial $Al_2O_3$ can effectively inhibit the reactions of Cr [91], Ni [92], or Mo [93] with a single crystal Al substrate. It is suspected that $Mo_{1-x}O_x$, $RuO_2$, and W-N are decomposed interfacially by Al in the contact structures, but that the formation of a thin $Al_2O_3$ or AlN layer prevents atomic transport from taking place any further. The use of Cross-sectional Transmission Electron Spectroscopy can furnish evidence of the existence of such interfacial layers.

In this thesis, the stability of diffusion barriers is evaluated by measurements made on relatively large and planar surfaces when compared to VLSI dimensions. As contact holes sizes in VLSI approach the submicron regime, the ratio between

TABLE I

| Oxide | $\Delta H_{298^\circ}$ (kcal/g-oxygen atom) |
|---|---|
| $Al_2O_3$ | -133.0 |
| $RuO_2$ | -26.25 |
| $MoO_2$ | -65.0 |

| Nitride | $\Delta H_{298^\circ}$ (kcal/g-nitrogen atom) |
|---|---|
| AlN | -76.5 |
| $W_2N$ | -17.0 |

**Table III** Heat of formation ($\Delta H_{298^\circ}$) of various oxides and nitrides.

the linear dimension of the contact at the interface to the Si substrate and the height of the sidewalls of the dielectric is about 1:1. (This ratio is usually defined as the *aspect ratio.*) Severe surface topography and a nonplanar configuration pose stringent requirements on the delineation of a barrier film in the contact hole. It was shown that a sputter-deposited TiN barrier fails to operate in a micron size contact due to poor step coverage at sharp corners of the contact hole edge [55] and compositional inhomogeneities [48]. In these cases, the relationship between barrier layer deposition and contact configuration has to to be reanalyzed.

While non-uniform step coverage is inherent in a sputter-deposited film, chemical vapor deposition (CVD) offers the advantage of providing metal or dielectric layers of superior conformal coverage even in submicron size contact holes [11,30]. Operating in a low pressure mode, a W barrier layer can even be deposited selectively in contact regions without photolithographic masking, as mentioned in Chapter 1 [30]. These self-aligned approaches are definitely attractive for barrier layer formation in the next generation VLSI metallization schemes. Deposition of $RuO_2$ [94] and TiN [95] by CVD has been demonstrated; the feasibility of forming W-N or $Mo_{1-x}O_x$ by chemical vapor deposition remains to be explored.

## References I–General


1. K. C. Saraswat and F. Mohammadi, IEEE Trans. on Elect. Dev. ED-**29**, 645 (1982).
2. W. Fichtner, in *VLSI Science and Technology/1984*, edited by K.E. Bean and G.A. Rozgonyi (The Electrochemical Society, Pennington, 1984), Proceedings Volume 84-7, p.133.
3. R. S. Muller and T. I. Kamins, *Device Electronics for Integrated Circuits* (Wiley, New York, 1986), p.490.
4. S. I. Long, B. M. Welch, R. Zucca, P. Asbeck, C.-P. Lee, C. G. Kickpatrick, F. S. Lee, G. R. Kaelin, and R. C. Eden, IEEE Proceedings **70**-1, 35 (1982).
5. P. A. Totta and R. P, Sopher, IBM J. Res. Dev. **13**, 226 (1969).
6. R. Rosenburg, M. J. Sullivan, and J. K. Howard, *Effects of Thin Film Interactions on Silicon Device Technology*, in *Thin Films- Interdiffusion and Reactions*, edited by J. M. Poate, K. N. Tu, J. W. Mayer (Wiley, New York, 1978), p.13.
7. J. M. Aitken and C. Y. Ting, *Int. Electron Devices Meet., Tech. Dig., Washington, DC, December 1981*, (IEEE, New York, 1981), p.50.
8. J. O. McCaldin and H. Sankur, Appl. Phys. Lett. **19**, 524 (1971).
9. H. Sankur, J. O. McCaldin, and J. Devaney, Appl. Phys. Lett. **22**, 64 (1973).
10. S. Vaidya, J. Electron. Mat. **10**, 337 (1981).
11. T. Moriya and H. Itoh, in *Tungsten and Other Refractory Metals for VLSI Applications*, edited by R. S. Blewer, (MRS, Pittsburg, 1986), p.21.
12. P. B. Ghate, Thin Solid Films **53**, 117 (1978).
13. P. S. Ho, J. E. Lewis ,and U. Koster J. Appl. Phys. **53**, 7445 (1982).
14. C. Y. Ting and M. Wittmer, J. Appl. Phys. **54**, 937 (1983).

15. M-A. Nicolet, Thin Solid Films, **54**, 415 (1978).

16. M-A. Nicolet, and M. Bartur, J. Vac. Sci. Technol. **19**, 786 (1981).

17. R. W. Bower, Appl. Phys. Lett. **23**, 99 (1973).

18. C. Y. Ting and B. L. Crowder, J. Electrochem. Soc. **129**, 2590 (1982).

19. M. Bartur and M-A. Nicolet, J. Electrochem. Soc. **131**, 1118 (1984).

20. R.S. Nowicki and I. Wang, J. Vac. Sci. Technol. **15**, 232 (1978).

21. R.S. Nowicki, J.M. Harris, M-A. Nicolet and I.V. Mitchell, Thin Solid Films **53**, 195 (1978).

22. R. S. Nowicki and M-A. Nicolet, Thin Solid Films **96**, 317 (1982).

23. P.H. Singer, ed., "4M DRAM Technology – IBM Leads U.S.," Semiconductor International, May 1987, p.50.

24. C. W. Nelson, *Proceedings of the International Symposium on Hybrid Microelectronics, Sept. 29-Oct. 1, 1970, Dallas, Texas* (Int. Soc. of Hybrid Microelectronics, Montgomery, 1969), p.413.

25. M. Wittmer, J. Vac. Sci. Technol. A **2**(2), 273 (1984).

26. J. K. Howard, R. F. Lever, P. J. Smith, and P. S. Ho, J. Vac. Sci. Technol. **13**, 68 (1976).

27. W. K. Chu, J. W. Mayer, and M-A. Nicolet, *Backscattering Spectrometry*, (Academic Press, New York, 1978).

28. S. Mehta, in *Tungsten and Other Refractory Metals for VLSI Applications II*, edited by E. K. Broadbent, (MRS, Pittsburg, 1987), p.411.

29. J. P. Roland, in *Tungsten and Other Refractory Metals for VLSI Applications II*, edited by E. K. Broadbent, (MRS, Pittsburg, 1987), p.419.

30. K. C. Saraswat, S. Swirhun, and J. C. McVittie, in *VLSI Science and Technology/1984*, edited by K.E. Bean and G.A. Rozgonyi (The Electrochemical Society, Pennington, 1984), Proceedings Volume 84-7, p.409.

31. N. Kobayashi, S. Iwata, N. Yamamoto, and N. Hara, in *Tungsten and Other*

*Refractory Metals for VLSI Applications II*, edited by E. K. Broadbent, (MRS, Pittsburg, 1987), p.159.

32. N. Toyoda, N. Uchitomi, Y. Kitaura, M. Mochizuki, K. Kanazawa, T. Terada, Y. Ikawa, and A. Hojo, IEEE Journal of Solid-State Circuits SC-**20**(5), 1043 (1985).
33. D. Gupta, D. R. Campell, P. S. Ho, *Grain Boundary Diffusion*, in *Thin Films-Interdiffusion and Reactions*, edited by J. M. Poate, K. N. Tu, J. W. Mayer (Wiley, New York, 1978), p.161.
34. C. Canali, G. Celotti, F. Fantini, and E. Zanoni, Thin Solid Films **88**, 9 (1982).
35. H. S. Chen, L. C. Kimerling, J. M. Poate, and W. L. Brown, Appl. Phys. Lett. **32**, 461 (1978).
36. S. Mader, A. S. Norwick, and H. Wildmer, Acta Meta **15**, 203 (1967).
37. S. Takayama, J. Mat. Sci. **11**, 164 (1976).
38. B. X. Liu, W. L. Johnson, M-A. Nicolet, and S. S. Lau, Appl. Phys. Lett. **42**, 45 (1983).
39. I. Suni, M-A. Nicolet, C. S. Pai, and S. S. Lau, Thin Solid Films **107**, 73 (1983).
40. M-A. Nicolet and S.S. Lau, in *VLSI Electronics : Microstructure Science*, N.G. Einspruch, Series Ed., Vol.6, G.B. Larrabee and N.G. Einspruch, eds. (Academic Press, New York, 1983), Chap. 6.
41. P. L. Doyle, P. S. Peercy, J. D. Wiley, and J. H. Perepezko, J. Appl. Phys. **53**, 6186 (1982).
42. M. Bartur, *Ph.D. thesis*, (California Institute of Technology, Pasadena, 1984).
43. E.G. Colgan, *Ph.D. thesis* (Cornell University, Ithaca, 1987).
44. M. F. Zhu, I. Suni, M-A. Nicolet, and T. Sands, J. Appl. Phys. **56**, 2740 (1984).

45. G. J. van Gurp, J. L. C. Daams, A. van Oostrom, L. J. M. Augustus, and Y. Tamminga, J. Appl. Phys **50**, 6915 (1979).

46. F. M. Saris, L. S. Hung, M. Nastasi, J. W. Mayer, and B. Whitehead, Appl. Phys. Lett. **46**, 646 (1985).

47. L. S. Hung, E. G. Colgan and J. W. Mayer, J. Appl. Phys. **60**, 4177 (1986).

48. K. Park, S. Mihara, Y. Sato, H. Tsuchikawa, and M. Yoshida in *Tungsten and Other Refractory Metals for VLSI Applications II*, edited by E. K. Broadbent (MRS, Pittsburg, 1987), p.275.

49. W. K. Chu, J. K. Howard, and J. F. White, U.S.Patent 4 206 472 (June 3, 1980).

50. R. S. Nowicki, Gold Bull **15**, 21 (1982).

51. H. P. Kattelus, E. Kolawa, K. Affolter, and M-A. Nicolet, J. Vac. Sci. Technol. A**3**(6), 2246 (1985).

52. K. Affolter, H. P. Kattelus, and M-A. Nicolet, Mat. Res. Soc. Symp. Proc. Vol. 47, edited by C. R. Aita and K. S. SreeHarsa (MRS, Pittsburgh, 1985), p.167.

53. H. J. Goldschmidt, *Interstitial Alloys* (Plenum, New York, 1967).

54. L. Krusin-Elbaum, M. Wittmer. C. Y. Ting, and J. J. Cuomo, Thin Solid Films **104**, 81 (1983).

55. H. Norstrom, S. Nygren, P. Wiklund, M. Ostling, R. Buchta, and C. S. Petersson, Vacuum **35**, 547 (1985).

56. N. Kumar, K. Pourrezaei, T. Begley, B. Lee, and E. C. Douglas, Solid State Technol. **4**, 100 (1987).

57. C. R. Aita, J. Vac. Sci. Technol. A**3**(3), 625 (1985).

58. E. Hollands, and D. S. Campell, J. Mater. Sci. **3**, 544 (1968).

59. J. Heller, Thin Solid Films **17**, 163 (1973).

60. T, Abe and T. Yamashina, Thin Solid Films **19**, 19 (1975).

61. N. W. Cheung, *Ph.D. Thesis* (California Institute of Technology, Pasadena, 1980).

62. D. S. Williams and S. P. Muraka, in *Proceedings of Workshop on Silicides and Metals for VLSI Applications V*, San Juan Bautista, May 1987; to be published in J. Vac. Sci. Technol.

63. J. E. Sundgren, B. O. Johansson, and S. E. Karlsson, Thin Solid Films **105**, 353 (1983).

64. J. E. Sundgren, B. O. Johansson, S. E. Karlsson, and H. T. G. Hentzell, Thin Solid Films **105**, 367 (1983).

65. J. E. Sundgren, B. O. Johansson, H. T. G. Hentzell, and S. E. Karlsson, Thin Solid Films **105**, 385 (1983).

66. C. R. Aita, private communications.

67. J. L. Vossen and W. Kern, *Thin Film Processes* (Academic Press, New York, 1978), p.474-475.

68. G. V. Samsonov and I. M. Vinitski, *Handbook of Refractory Compounds* (IFI/Plenum, New York, 1980).

69. H. P. Kattelus, J. L. Tandon, C. Sala, and M - A. Nicolet, J. Vac. Sci. Technol. A**4**(4), 1850 (1986).

70. S. Kanamori, Thin Solid Films **136**, 195 (1986).

71. A. Armigliato, M. Finetti, J. Garrido, S. Guerri, P. Ostoja, and A. Scorzoni, J. Vac. Sci. Technol. A**3**(3), 2237 (1985).

72. M. Wittmer, J. Appl. Phys. **53**, 1007 (1982).

73. J. Stimmell, J. Vac. Sci. Technol. B**4**(6), 1377 (1986).

74. A. Piotrowska, A. Guivarc'h, and G. Pelous, Solid-State Electron. **26**, 179 (1983).

75. H. P. Kattelus, J. L. Tandon, and M-A. Nicolet, Solid-State Electron. **29**, 903 (1986).

76. C. Fontaine, T. Okumura, and K. N. Tu, J. Appl. Phys. **54**, 1404 (1983).

77. G. K. Reeves, Solid-State Electron. **23**, 487 (1980).

78. D. S. Gardner, T. L. Michalka, K. C. Saraswat, T. W. Barbee, Jr., J. P. McVittie, and J. D. Meindl, IEEE Trans. Electron Dev. **32**, 174 (1985).

79. H. Kaneko, M. Koyanagi, S. Shimizu, Y. Kubota, and S. Kishino, IEEE Trans. Electron Dev. **33**, 1702 (1986).

80. C. Y. Ting, M. Wittmer, S. S. Iyer, and S. B. Brodsky, *VLSI Science and Technology/1984*, edited by K.E. Bean and G.A. Rozgonyi (The Electrochemical Society, Pennington, 1984), Proceedings Volume 84-7, p.397.

81. C. S. Wei, J. Van der Spiegel, M. Setton, J. Santiago, M. Tanielian and S. Blackstone, in Mat. Res. Soc. Symp. Proc. Vol. 52, edited by T. O. Sedgwick, T. E. Seidel, and B. Y. Tsaur (MRS, Pittsburg, 1986), p.297.

82. C. Y. Wong, L. K. Wang, P. A. McFarland, and C. Y. Ting, J. Appl. Phys. **60**, 243 (1986).

83. J. R. Shappiro, J. J. Finnegan, and R. A. Lux, J. Vac. Sci. Technol. B**4**(6), 1409 (1986).

84. M. Eizenberg, R. Brener, and S. P. Muraka, J. Appl. Phys. **55**, 3799 (1984).

85. D. B. Rogers, R. D. Shannon, A. W. Sleight, and J. L. Gillson, Inorg. Chem. **8**, 841 (1969).

86. F. A. Shunk, *Constitution of Binary Alloys, Second Supplement* (McGraw-Hill, New York, 1969).

87. R. P. Elliott, *Constitution of Binary Alloys, First Supplement* (McGraw-Hill, New York, 1965).

88. E. Kolawa, F. C. T. So, E. T-S. Pan, and M-A. Nicolet, to be published.

89. C. R. Aita and N. C. Tran, J. Appl. Phys. **56**, 958 (1984).

90. X.-A. Zhao, E. Kolawa, and M-A. Nicolet, J. Vac. Sci. Technol. A**4**(6), 3139 (1986).

91. X.-A. Zhao, T. C. Banwell, and M-A. Nicolet, in *Advanced Processing and Characterization of Semiconductors III*, SPIE Vol. 623 (SPIE, Bellingham, 1986), p.255.

92. X.-A. Zhao, H. Y. Yang, E. Ma, and M-A. Nicolet, to be published in J. Appl. Phys. **62**, August 1987.

93. X.-A. Zhao, private communications.

94. M. L. Green, M. E. Gross, L. E. Papa, K. J. Schones, and D. Brasen, J. Electrochem. Soc. **132**, 2077 (1985).

95. *See for example*, K.-H. Habig J. Vac. Sci. Technol. **A4**(6), 2832 (1986).

96. *Handbook of Chemistry and Physics, 61st edition*, edited by R. C. Weast and M. J. Astle (CRC, Boca Raton, 1980).

97. *See for example*, M. E. Alperin, T. C. Hollway, R. A. Haken, C. D. Gosmeyer, R. V. Karnaugh, and W. D. Parmantie, IEEE Trans. on Electron Dev. ED**32**-2, 141 (1985).

98. T. E. Tang, C. C. Wei, R. A. Haken, T. C. Holloway, L. R. Hite, and T. G. Blake, IEEE Trans. Electron Dev. ED**34**-3, 682 (1987).

99. A. R. Miedema, P. E. de Chatel, and F. R. de Buer, Physica **100B**, 1 (1980).

100. A. R. Miedema, Philips Tech. Rev. **36**, 217 (1976).

## References II–Work published by F. C. T. So

I. M. F. Zhu, F. C. T. So, E. T-S. Pan, and M-A. Nicolet, *Investigation of Amorphous W-Zr Film as a Diffusion Barrier in Metallization Schemes*, Phys. Stat. Sol. (A) **86**, 471 (1984).

II. F. C. T. So, X.-A. Zhao, E. Kolawa, J. L. Tandon, M. F. Zhu, and M-A. Nicolet, *Amorphous W-Zr Films as Diffusion Barriers between Al and Si*, Mat. Res. Soc. Symp. Proc. Vol. 54, edited by R. J. Nemanich, P. S. Ho, and S. S. Lau (MRS, Pittsburg, 1986), p.139.

III. M. F. Zhu, F. C. T. So, and M-A. Nicolet, *Amorphous Ni-N-W Film as a Diffusion Barrier between Al and Si*, Thin Solid Films **130**, 245 (1985).

IV. E. Kolawa, F. C. T. So, X.-A. Zhao, and M-A. Nicolet, *Properties of Reactively Sputtered* $WN_x$ in *Tungsten and Other Refractory Metals for VLSI Applications II*, edited by E. K. Broadbent (MRS, Pittsburg, 1987), p.311.

V. F. C. T. So, E. Kolawa, X.-A. Zhao, E. T-S. Pan, and M-A. Nicolet, *W-N Alloys as Diffusion Barriers between Al and Si*, to be submitted to J. Appl. Phys. (see appendix II).

VI. F. C. T. So, E. Kolawa, J. L. Tandon, and M-A. Nicolet, *Solid-Phase Ohmic Contacts to p-GaAs with W and W-N Diffusion Barriers*, J. Electrochem. Soc. **134**, 1755 (1987).

VII. E. Kolawa, F. C. T. So, J. L. Tandon, and M-A. Nicolet, *Reactively Sputtered W-N Films as Diffusion Barriers in GaAs Metallizations*, J. Electrochem. Soc. **134**, 1759 (1987).

VIII. J. L. Tandon, K. D. Douglas, G. Vendura, E. Kolawa, F. C. T. So, and M-A. Nicolet, *Metallization Systems for Stable Ohmic Contacts to GaAs*, in *Tungsten and Other Refractory Metals for VLSI Applications*, edited by

R. S. Blewer, (MRS, Pittsburg, 1986), p.331.

IX. F. C. T. So, E. Kolawa, H. P. Kattelus, X.-A. Zhao, C. - D. Lien, and M-A. Nicolet, *Thermal Stability and Nitrogen Redistribution in the <Si> /Ti/W-N/Al Metallization Scheme*, J. Vac. Sci. Technol. A**4**(6), 3078 (1986).

X. F. C. T. So, C. - D. Lien, E. Kolawa, X.-A. Zhao, and M-A. Nicolet, *Thermal Stability and Nitrogen Redistribution in the Ti/W-N Bilayer*, in *Tungsten and Other Refractory Metals for VLSI Applications II*, edited by E. K. Broadbent (MRS, Pittsburg, 1987), p.300.

XI. E. Kolawa, F. C. T. So, E. T-S. Pan, and M-A. Nicolet, *Reactively Sputtered $RuO_2$ Diffusion Barriers*, Appl. Phys. Lett. **50**, 854 (1987).

XII. F. C. T. So, E. Kolawa, X.-A. Zhao, and M-A. Nicolet, *$WN_x$: Properties and Applications*, Thin Solid Films (in press).

XIII. F. C. T. So, E. Kolawa, X.-A. Zhao, E. T-S. Pan, and M-A. Nicolet, *Reactively Sputtered $RuO_2$ and $Mo_{1-x}O_x$ Diffusion Barriers :Summary*, in *Proceedings of Workshop on Silicides and Metals for VLSI Applications V*, San Juan Bautista, May 1987; to be published in J. Vac. Sci. Technol. (see appendix IV).

XIV. F. C. T. So, E. Kolawa, S. C. W. Nieh, X.-A. Zhao, and M-A. Nicolet, *Properties of Reactively Sputtered $Mo_{1-x}O_x$ Films*, to be submitted to J. Appl. Phys. (see appendix III).

XV. F. C. T. So, C. - D. Lien, and M-A. Nicolet, *Formation and Electrical Properties of $HfSi_2$ Grown Thermally from Evaporated Hf and Si Films*, J. Vac. Sci. Technol. A**3**(6), 2284 (1985).

XVI. F. C. T. So, U. Shreter and M-A. Nicolet, *Investigation of the Formation Kinetics of $CrSi_2$, $TaSi_2$, and $Pt_2Si$ by Ion Beam Mixing*, SPIE Vol. 530, 145 (1985).

XVII. C. - D. Lien, F. C. T. So, and M-A. Nicolet, *An Improved Forward I-V for Non-Ideal Schottky Diodes with High Series Resistance*, IEEE Trans. Electron Dev. ED-**31**(10), 1502 (1984).

XVIII. E. Kolawa, M-A. Nicolet, and F. C. T. So, *W-N and $RuO_2$ Thin Films for Diffusion Barriers in Al Contacts to Si*, in *Proceedings of the European Workshop on Refractory Metals and Silicides*, (1987).

XIX. U. Shreter, F. C. T. So, and M-A. Nicolet, *Chromium Silicide Formation by Ion Mixing*, J. Appl. Phys. **55**, 3500 (1984).

XX. U. Shreter, F. C. T. So, B. M. Paine, and M-A. Nicolet, *Investigation of a Thermal Spike Model for Ion Mixing of Metals with Si*, Mat. Res. Soc. Symp. Proc. Vol. 27, edited by G. K. Hubbler, O. W. Holland, C. R. Clayton, and C. W. White (MRS, Pittsburg, 1984), p.109.

# APPENDIX I

# HEAT OF REACTION

# OF W-BASED BINARY METALLIC ALLOY WITH Al

It was demonstrated in Chapter 2 that the effectiveness of an amorphous W-Zr barrier is essentially limited by the strong driving force for reaction between the alloy and the metal overlayers. We have also mentioned that W-Zr is in fact most reactive with Al among a number of polycrystalline or amorphous W-based binary alloys. This is evident from Figure 11, in which the heat of reaction ($\Delta H_{298^\circ}$) between Al and M-W (where M= Ti, Zr, Hf, V, Nb, Ta, Cr, Mo, Ni, Pd) is plotted as a function of the atomic number of M. The following reaction is assumed to occur:

$$\text{M-W} + (\text{x}+12)\text{Al} \longrightarrow \text{MAl}_x + \text{WAl}_{12}$$

For simplicity, the ratio of M to W is taken to be unity. The aluminide phases ($MAl_x$) are taken as those observed to form as the first phase from reactions in binary couples of M/Al, as reported by Colgan [43]. The heat of formation of the aluminides are obtained from Goldschmidt [53], and from calculations (supplied by Dr. X-A. Zhao at Caltech) based on Miedema's model [99,100] when data are not avaliable from Goldschmidt. On the other hand, the heat of mixing of the M-W alloys are all taken from Miedema's tables [100].

In the course of collecting these data, an interesting fact caught my attention: W-Zr has the most negative heat of mixing (-1.67 kcal/g-atom), and yet is most reactive with Al. On the contrary, Cr-W possesses a positive heat of mixing (+0.12 kcal/gatom), but has almost the least tendency to interact with Al. In

general, the magnitude of these heat of reaction is dominated by those between the individual metallic elements and Al. The heat of mixing of the binary alloys M-W contributes insignificantly to the heat of reaction.

One can easily see that none of the M-W alloys are thermodynamically stable with Al. Based on these information and experience with W-Zr and Ni-W barriers, we believe that all the polycrystalline or amorphous W-based alloy barriers under considered here will react with Al.

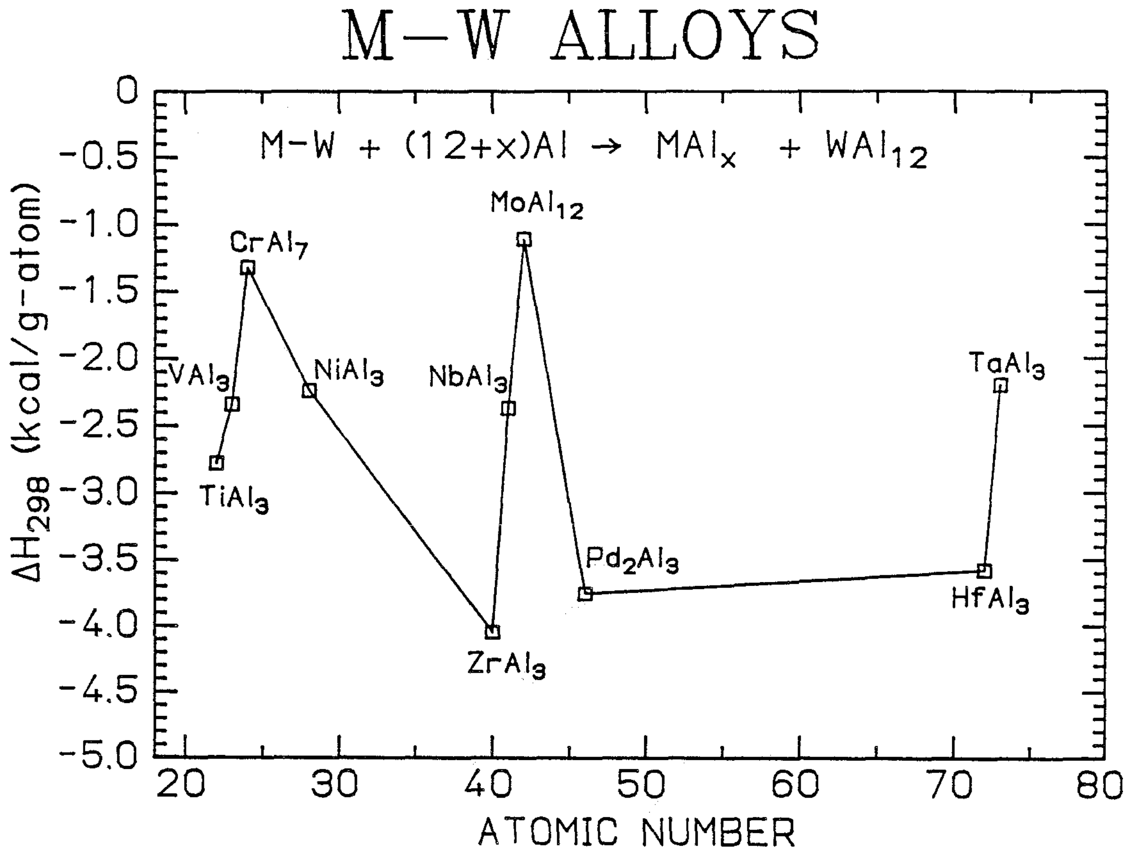


**Figure 11.** Heat of reaction between Al and various M-W alloys as a function of the atomic number of M. The aluminide phases expected to form are shown against the data points.

To be submitted for publication as a communication in J. Appl. Phys., August, 1987

## APPENDIX II

# W-N Alloys as Diffusion Barriers between Al and Si

F. C. T. SO[a], E. KOLAWA, X.-A. ZHAO[b], E. T-S. PAN, and M-A. NICOLET

California Institute of Technology, Pasadena, CA 91125.

a) Present address: Optoelectronics Division, Hewlett-Packard Co., San Jose, CA 95131.

b) Permanent address: Shanghai Institute of Metallurgy, Academy of Sciences of China, Shanghai, China.

*Abstract* — Reactively-sputtered tungsten nitride (W-N) layers are investigated for the first time as diffusion barriers between Al overlayers and Si shallow $n^+$-p junctions. Both amorphous and polycrystalline W-N films were found to be extremely effective in preserving the integrity of the $n^+$-p diodes for annealing up to 575°C. Diode failure at higher temperatures is caused by localized penetration of Al into <Si> through the W-N barriers.

As device dimensions in integrated circuits are continuously scaled down, incorporation of diffusion barriers into contact structures to semiconductors becomes essential for device reliability. The high reactivity of refractory metals, such as Ti and W, with Al limits their use as diffusion barriers between Si and Al to post metallization sintering below 450°C [1,2]. For processing temperatures above 450°C and long-term stability, nitrides of refractory metals are highly favored as barrier materials [3]. Titanium nitride has been studied very extensively for barrier implementation in many process environments [4,5]. With the advent of LPCVD processes [6], tungsten-based barrier materials are expected to play increasingly important roles in contact metallurgy. Since the presence of impurities (O, N, C) in refractory metal diffusion barriers has always been found to be beneficial in enhancing the stability of contact structures [7], we consider here the simple case of nitrogen-doped W deposited by sputtering of tungsten in Ar-$N_2$ mixture.

Kattelus et al. have shown previously by MeV $He^+$ Backscattering Spectrometry (BS) and sheet resistance measurements [8] that W-N are far superior than W as diffusion barriers between Si and Al. In this work, the effectiveness of W-N barriers is evaluated by electrical measurements performed on shallow implanted $n^+$-p diodes with <Si>/W-N/Al contact structures, in addition to BS depth profiling analysis. Shallow junction diodes are probably the most sensitive devices to detect Al-Si interaction that occurs on a microscopic scale. Both polycrystalline and amorphous W-N were deposited [8,9] and their performance as diffusion barriers is compared.

Our test vehicles consist of Si $n^+$-p diodes of $0.35\,\mu$m junction depth formed by $As^+$ ion implantation (150 keV, $7\times10^{15}$As/cm$^{-2}$) and anneal. Details of the

fabrication procedure have been reported elsewhere [10]. The size of the junction areas and contact windows are 500 × 500 $\mu m^2$ and 300 × 300 $\mu m^2$ respectively. The W-N/Al contact metallization was delineated by the lift-off technique.

Depositions of W-N and Al were carried out in an r.f. sputtering system equipped with a diffusion pump and a cryogenic baffle. The sputtering chamber was evacuated to a base pressure of $\sim 1 \times 10^{-6}$ Torr before deposition. Tungsten nitride films were obtained by sputtering a 99.9% W target in premixed Ar and $N_2$ gas ambients. Three W-N films were chosen for diffusion barrier tests: $W_{90}N_{10}$, $W_{80}N_{20}$ and $W_{60}N_{40}$. The sputtering parameters for obtaining these W-N films have been described elsewhere and are not repeated here [11]. Plain tungsten barriers sputter deposited in Ar were also examined for comparision purpose. Following the W-N deposition, Al overlayers of ~5000Å in thicknesses were deposited sequentially without breaking vacuum to complete the formation of the <Si> /W-N/Al contact structures. Such a layer configuration were also instituted on unpatterned Si substrates and $SiO_2$ for depth profiling analysis by BS. In these samples, the thicknesses of Al are in the range of 2800-3500Å.

$W_{90}N_{10}$ and $W_{60}N_{40}$ are polycrystalline and have resistivities of about 100 $\mu\Omega$-cm and 350 $\mu\Omega$-cm respectively [9,11]. $W_{60}N_{40}$ consists predominantly of the $W_2N$ phase while $W_{90}N_{10}$ is made up of a mixture of $\alpha$W and $\beta$W with the nitrogen residing probably in the grain boundaries. On the other hand, as-deposited $W_{80}N_{20}$ films were determined by x-ray read camera diffraction analysis to be amorphous and crystallize at ~620°C. The resisitivity of $W_{80}N_{20}$ film is ~200 $\mu\Omega$-cm. The amorphous barrier has the lowest compressive stress among the four; the stress levels of the other three are comparable.

Annealing of the samples were carried out in a vacuum of better than $1 \times 10^{-6}$ Torr in the temperature range of 350-600°C. Unless otherwise stated, the annealing duration for each temperature cycle is 30 min. The reverse leakage currents

of 30-40 diodes were measured for every heat treatment. Elemental depth profiles of the samples were analysed by 2 MeV $^4He^+$ BS analysis with a $He^+$ beam spot of $\sim 1 \times 2 mm^2$ in size.

Figure 1 shows the BS spectra of <Si> /$W_{80}N_{20}$ /Al before and after annealing at 575°C and 600°C for 30 min. Very little interdiffusion between the adjoining layers can be detected up to annealing at 575°C (Fig 1b). Heat treatment at 600°C leads to a significant interaction between Al and the underlying W-N layer and <Si>. This is evident from a partial disappearance of the Al plateau and the movement of the whole W signal towards the surface position in the BS spectrum. X-ray analysis, however, did not indicate the presence of any W-Al intermetallics in any of the annealed samples. This shows that failure of the <Si> /$W_{80}N_{20}$ /Al system can not be attributed to the consumption of the W-N layer by Al to form $WAl_{12}$, as in the case of a W/Al couple [2]. Also, no metallurgical interactions can be detected at 600°C if <Si> is replaced by $SiO_2$. This shows that <Si> acts as a sink for Al penetration at 600°C.

The histograms of the reverse leakage current distributions of the $n^+$-p diodes with the <Si> /$W_{80}N_{20}$ /Al contact structure after annealing at 350°C, 575°C and 600°C are shown in Fig.2. The reverse currents remain narrowly distributed for annealing up to 550°C. At 575°C, about 10% of the diodes develop high leakage currents. ( Diodes with reverse current densities higher than $8 \times 10^{-8}$A-cm$^{-2}$ are regarded as failure.) Even after a 600°C sintering, a substantial percentage of diodes still survive (72% ) despite BS analysis reveals barrier breakdown. This suggests that Al penetration is likely to proceed in a highly localized manner through the $W_{80}N_{20}$ layers into the device junctions. SEM inspection showed that the contact areas of diodes which survive the 600°C treatment retain their smooth surface morphologies. On the contrary, one or two square pits are easily

visible in the contact region of a shorted diode. Surrounding the square pits in such contact areas are droplets of resolidified material that arises probably from Si-Al melting at 600°C. (The eutectic temperature of Al-Si is 577°C.) The presence of square pits reflects failure modes pertaining to Al spiking into (100) <Si> through localized weak spots or defects in the $W_{80}N_{20}$ layers covering the contact holes.

Similar results were obtained with polycrystalline $W_{60}N_{40}$ barrier layers. Extremely low diode failure rates were found up to annealing at 575°C. A 600°C thermal cycle caused ~52% of the measured diodes to fail. This failure percentage is slightly higher than that in the case of amorphous $W_{80}N_{20}$ barriers. BS and SEM analysis suggest that failure mechanisms in both cases should be very much alike. Diodes with $W_{80}N_{20}$ or the $W_{60}N_{40}$ barrier layers in their contact structures were also subjected to extended heat treatments at 500°C for 13 hours to simulate the worst case processing exposure [12]. The failure rates were a factor of 2 lower for amorphous W-N (23% ) than for $W_{60}N_{40}$ (46% ). Failure mechanisms of these contact systems at 500°C may be quite different than those which dominate above the Al-Si eutectic temperature, and are not examined here.

Polycrystalline $W_{90}N_{10}$ film is inferior as a barrier between Al and Si than $W_{80}N_{20}$ or $W_{60}N_{40}$. A reaction between Al and $W_{90}N_{10}$ leading to the fomation of $WAl_{12}$ system can be detected at 550°C by BS and x-ray analysis. Accordingly, all the diodes with <Si> / $W_{90}N_{10}$ /Al contacts were shorted after a 550°C anneal. Our observations also imply that a W-N barrier must contain enough nitrogen in the films in order to function effectively as a barrier between Al and Si at 550°C and above. Similarly, plain W fails as a metallurgical barrier between Al and Si after a 500°C anneal as a result of the consumption of W by Al, in agreement with previous work [2]. However, all the diodes with W

barrier layers were shorted after annealing at 450°C. This unexpected failure at 450°C is probably caused by grain boundary diffusion of Al or Si through the W barrier that is undetected by BS. The percentage of diode failure as a function of annealing temperature (30 min) for the four barriers are summarized in Figure 3.

Both amorphous and polycrystalline W-N are far superior than W in suppressing Si-Al interaction up to 575°C annealing for 30 min, provided enough nitrogen is present in the barrier films. Since the failure of <Si>/W-N/Al contacts at 600°C is dominated by localized defects or pinholes in the W-N barriers, contact hole size may have a significant effect on the performance of the barriers. Also, the contact resistivities between W-N and <Si> deserve some future attention. An additional silicide contact layer between W-N and <Si> may be appropriate for implementing W-N barriers in realistic contact structures to ensure acceptable contact resistivities.

This work is supported by the Army Research Office under Contract No. DAAG29-85-K-0192. Dr. D.B. Rutledge is gratefully acknowledged for granting us access to his HP Semiconductor Parameter Analyser and photolithographic facilities.

## REFERENCES


1. C. Y. Ting and B. L. Crowder, J. Electrochem. Soc. **129**, 2590 (1982).
2. G. J. van Gurp, J. L. C. Daams, A. van Oostrom, L. J. M. Augustus, and Y. Tamminga, *J. Appl. Phys.*, **50**, 6915 (1979).
3. M-A. Nicolet, and M. Bartur, J. Vac. Sci. Technol. **19**, 786 (1981).
4 S. Kanamori, Thin solid Films, **136**, 195 (1986).
5. K. Park, S. Mihara, Y. Sato, H. Tsuchikawa, and M. Yoshida in *Tungsten and Other Refractory Metals for VLSI Applications II*, edited by E. K. Broadbent (MRS, Pittsburg, 1987), p.275.
6. T. Moriya and H. Itoh, in *Tungsten and Other Refractory Metals for VLSI Applications*, edited by R. S. Blewer, (MRS, Pittsburg, 1986), p.21.
7. R. S. Norwicki and M-A. Nicolet, Thin Solid Film **96**, 317 (1982).
8. H. P. Kattelus, E. Kolawa, K. Affolter, and M-A. Nicolet, J. Vac. Sci. Technol. A **3**(6), 2246 (1985).
9. K. Affolter, H. P. Kattelus, and M-A. Nicolet, Mat. Res. Soc. Symp. Proc., Vol. 47, edited by C. R. Aita and K. S. SreeHarsha (MRS, Pittsburgh, 1985), p.167.
10. F. C. T. So, X.-A. Zhao, E. Kolawa, J. L. Tandon, M. F. Zhu, and M-A. Nicolet, in Mat. Res. Soc. Symp. Proc. Vol. 54, edited by R. J. Nemanich, P. S. Ho, and S. S. Lau (MRS, Pittsburg, 1986), p.139.
11. E. Kolawa, F. C. T. So, X.-A. Zhao, and M-A. Nicolet, in *Tungsten and Other Refractory Metals for VLSI Applications II*, edited by E. K. Broadbent (MRS, Pittsburg, 1987), p.311 .
12. J. P. Roland, in *Tungsten and Other Refractory Metals for VLSI Applications II*, edited by E. K. Broadbent, (MRS, Pittsburg, 1987), p.419.

## Figure Captions

Figure 1. 2 MeV $^4He^+$ BS spectra of a <Si> /$W_{80}N_{20}$ (800Å )/Al(3400Å ) sample before and after annealing at 575°C and 600°C for 30 min. The detector angle is kept at 10°; the angle between the incident beam and the sample normal is 7°.

Figure 2. Histograms of reverse current distributions of Si $n^+$-p diodes with <Si> /$W_{80}N_{20}$ /Al contacts annealed at 350°C, 575°C and 600°C for 30 min.

Figure 3. Percentage of diode failure with <Si> /W-N(W)/Al contacts as a function of annealing temperature.

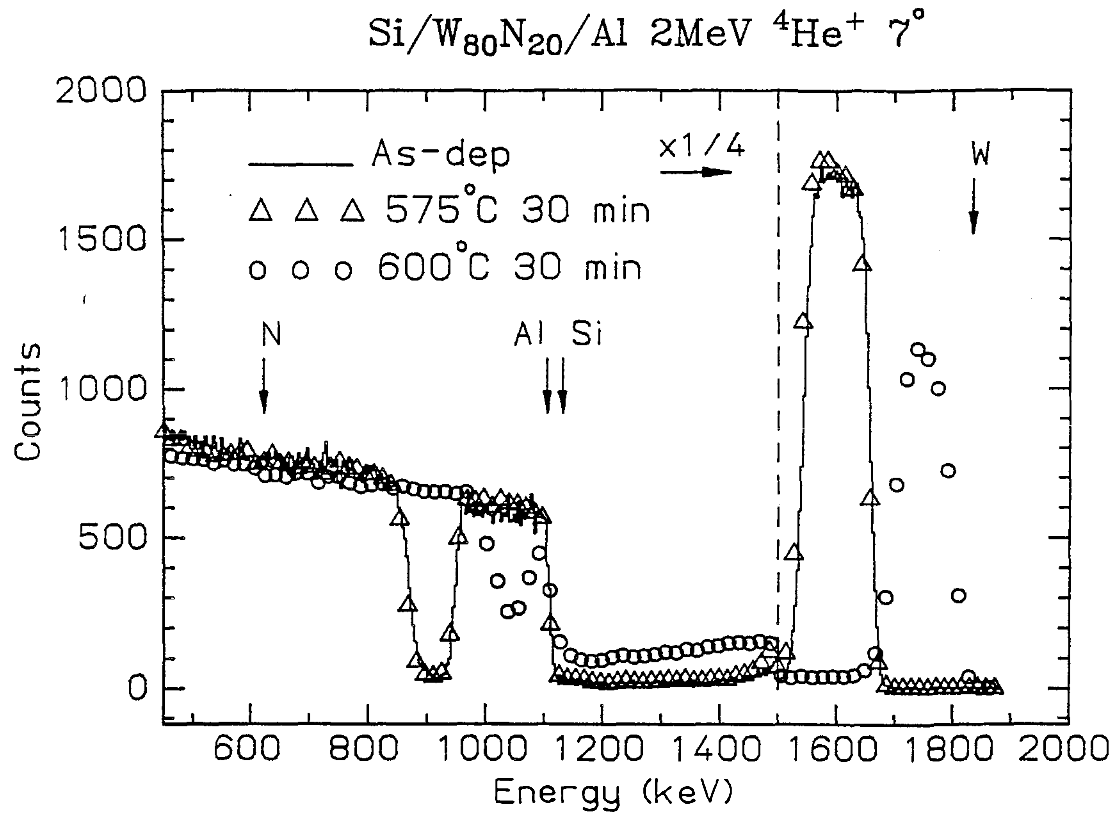


**Figure 1.** 2 MeV $^4He^+$ BS spectra of a <Si> / $W_{80}N_{20}$ (800Å )/Al(3400Å ) sample before and after annealing at 575°C and 600°C for 30 min. The detector angle is kept at 10°; the angle between the incident beam and the sample normal is 7°.

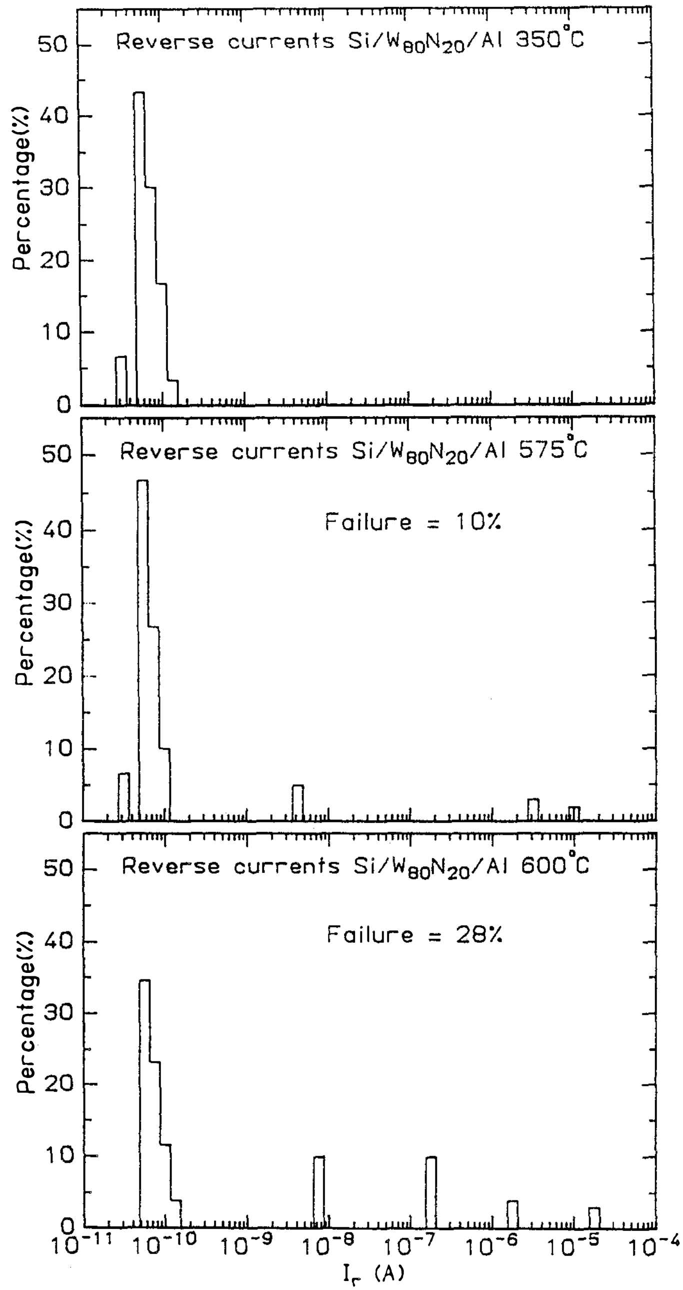


**Figure 2.** Histograms of reverse current distributions of Si $n^+$-p diodes with <Si> / $W_{80}N_{20}$ / Al contacts annealed at 350°C, 575°C and 600°C for 30 min.

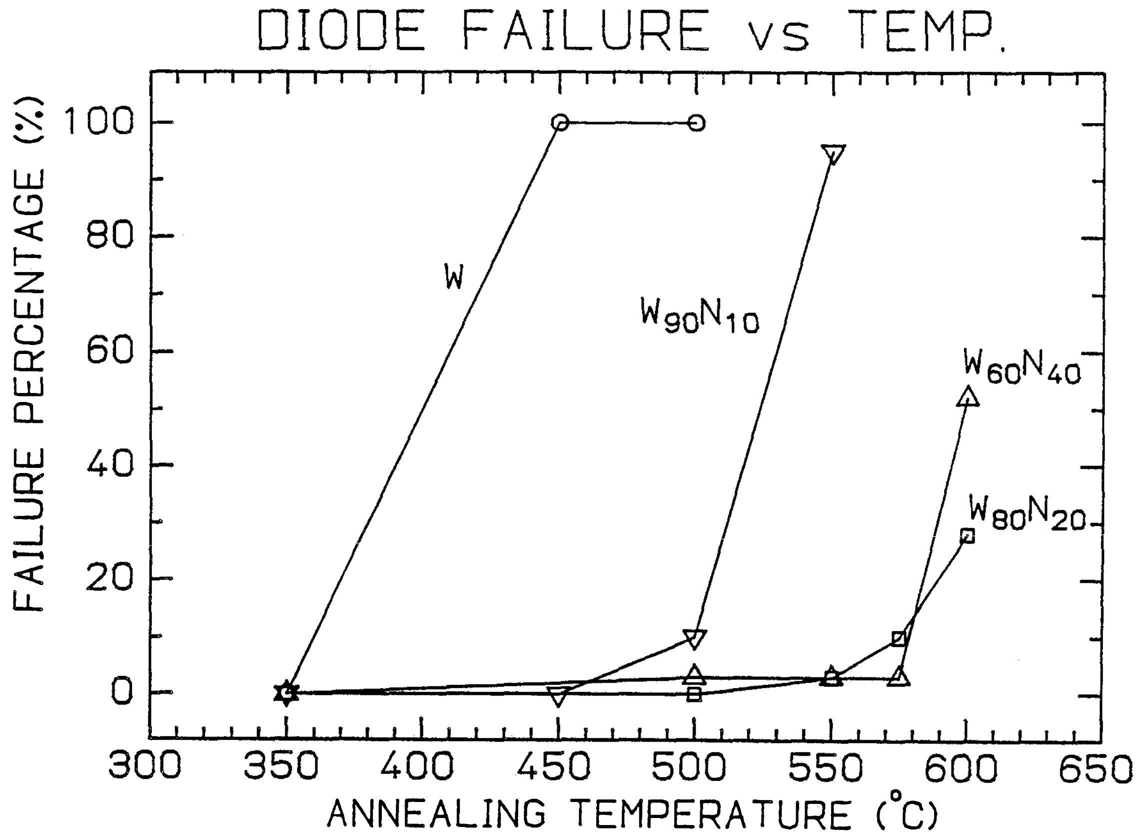


**Figure 3.** Percentage of diode failure with <Si> /W-N(W)/Al contacts as a function of annealing temperature.

## APPENDIX III

# Properties of Reactively Sputtered $Mo_{1-x}O_x$ Films

F.C.T. So[a], E. Kolawa, S.C.W. Nieh, X.-A. Zhao[b], and M-A. Nicolet

California Institute of Technology, Pasadena, CA 91125.

a) Present address: Optoelectronics Division, Hewlett-Packard Co., San Jose, CA 95131.

b) Permanent address: Shanghai Institute of Metallurgy, Academy of Sciences of China, Shanghai, China.

ABSTRACT

Molybdenum oxide ( $Mo_{1-x}O_x$ ) films were prepared by reactive rf sputtering of a Mo target in $O_2$ /Ar plasma. The dependence of film properties on various sputtering parameters is investigated. The atomic percentage of oxygen (x) in the $Mo_{1-x}O_x$ films decreases with sputtering power and increases with the partial pressure of oxygen. $Mo_{1-x}O_x$ films that exhibit metallic conductivities can be obtained over a wide range of sputtering conditions. The intrinsic film stress of conducting $Mo_{1-x}O_x$ is compressive. Such $Mo_{1-x}O_x$ films were shown by backscattering spectrometry to be excellent diffusion barriers between Al and Si up to 600°C annealing for 30 min.

## INTRODUCTION

Electrically conducting $RuO_2$ [1,2] and $Mo_{1-x}O_x$ [3] films have recently emerged as potential candidates for diffusion barrier applications in VLSI contact metallurgy. These barrier layers can typically inhibit interdiffusion between Al and Si substrate up to 600°C annealing for 30 min. It is well known that the diffusion barrier properties of a reactively sputtered compound layer (such as TiN) can depend critically on sputtering conditions [4]. In view of that, the present work aims at providing a concise account and basic understanding of the deposition behavior of $Mo_{1-x}O_x$ films. $Mo_{1-x}O_x$ can be formed easily by reactively sputtering a Mo target in a $O_2$/Ar gas mixture. The influence of various sputtering process parameters, such as power, initial total gas pressure, partial pressure of oxygen on the composition, deposition rate, resistivity and intrinsic stress of $Mo_{1-x}O_x$ films have been examined.

## EXPERIMENTAL PROCEDURE

Silicon wafers, carbon substrates and thin cover glasses were used as substrates for the $Mo_{1-x}O_x$ films. The experimental procedures were very similar to those used in previous work for W-N characterization [5]. All $Mo_{1-x}O_x$ films of this study were deposited by rf reactive sputtering using a planar magnetron Mo (99.95% ) cathode of 7.5 cm diameter. The substrate holder was placed about 7 cm below the target and was neither cooled nor heated externally. A base pressure of $\sim 1\times 10^{-6}$ Torr in the sputtering chamber was attained prior to $Mo_{1-x}O_x$ sputter-deposition in $O_2$/Ar ambients. The $O_2$/Ar gases were premixed, and were admitted into the sputtering system with a variable leak valve. The total gas pressure measured before striking the discharge was monitored

with a capacitive manometer (subsequently refered to as an "initial" gas pressure). $Mo_{1-x}O_x$ films of thicknesses in the range of 1000-2500Å were deposited with initial total gas pressures of 5 and 10mTorr. The relative partial pressure of oxygen, defined as the ratio of the partial pressure of $O_2$ to the total gas pressure, $p(O_2)/p(O_2+Ar)$, was varied from 0% to 40% .

The methods used to determine film compositions, thicknesses, resistivities and stress have been described in detail previously [5]. A combination of x-ray Read camera diffraction and transmission electron microscopy was used to study the phases and microstructures of the $Mo_{1-x}O_x$ films.

<Si> / $Mo_{1-x}O_x$ /Al samples were also prepared for evaluating the diffusion barrier capability of the $Mo_{1-x}O_x$ films against Al-Si interdiffusion. Prior to loading into the sputtering chamber, Si wafers of <100> orientation were oxidized slightly in an oxygen plasma for 10 min followed by etching in a 10% dilute HF solution for 2 min. $Mo_{1-x}O_x$ barrier films (700 -1000Å ) and Al overlayers (3000 -5000Å ) were sputter-deposited sequentially onto the Si substrates without breaking vacuum. Subsequent annealing of all samples were carried out in a vacuum of better than $1\times10^{-6}$ Torr. 2 MeV $^4He^+$ backscattering spectrometry (BS) was used to determine compositional profiles and to monitor interdiffusion or reactions in the samples.

## RESULTS AND DISCUSSIONS

### *A. Film composition and deposition rate*

Figure 1a shows the dependence of the oxygen content of the $Mo_{1-x}O_x$ films on the dissipated sputtering power for three different relative partial pressures of $O_2$. The initial total gas pressure is kept at a constant level of 10mTorr. The oxygen concentration decreases continuously as the sputtering power is raised from 100W to 600W. Also, for fixed sputtering power, increasing the initial relative partial pressure of oxygen leads to an increase in x of the $Mo_{1-x}O_x$ films, in agreement with previous results by Ohfuji et al. [7]. These observations resemble closely those found when W-N films are reactively sputtered in $N_2/Ar$ mixtures [5] but are in sharp contrast with findings for sputter deposition of $RuO_2$ [3,6]. When Ru is sputtered in a $O_2/Ar$ or $O_2/Ne$ glow discharge, the amount of oxygen incorporated into the ruthenium-oxygen alloys varies discontinuously with sputtering power: either Ru or $RuO_2$ is deposited at one time. Sputtering power clearly exerts a strong influence on the stoichiometry of $Mo_{1-x}O_x$. With 30% of oxygen in the gas, the oxygen concentration in the films falls below the detection limit of backscattering analysis when sputtering is carried out at a 400W power level or above, but soars to 75 atomic percent at 100W. However, for each partial pressure of oxygen, there appears to exist a threshold in sputtering power below which rapid incorporation of oxygen into the $Mo_{1-x}O_x$ films occurs (Figure 1a). The threshold value increases with the initial relative partial pressure of oxygen. In other words, it takes an elevated sputtering power level to keep oxygen out of Mo films as the oxygen in the chamber increases. On the other hand, changing the relative partial pressure of $O_2$ influences the deposition rate insignificantly (Figure 1a) except at 100W, when $Mo_{1-x}O_x$ films of high oxygen concentration

(exceeding 60 atomic percent) are formed; the deposition rate drops noticeably from 140Å /min for 10% $O_2$ to 65Å /min for 30% $O_2$ in gas. For all three partial pressures of oxygen, the deposition rate is linearly related to the sputtering power with more or less the same slope, and is close to that when Mo is deposited in 100% argon. (Deposition rates for Mo in an argon ambient at sputtering powers of 100W, 200W and 300W are also shown in Figure 1a.)

Our observation that the oxygen content in the $Mo_{1-x}O_x$ films may be varied continuously is consistent with the picture of an unoxidized Mo target surface when $Mo_{1-x}O_x$ films are deposited as proposed by Hollands [8,9]. The absence of a steplike drop in deposition rate as the partial pressure of oxygen is varied (at a fixed sputtering power) also suggests strongly that the Mo target surface is oxidized very little during sputter deposition for nearly the entire range of sputtering parameters used here. The formation of stoichiometric $MoO_3$ (see below) and the drop in sputtering rate at a sputtering power of 100W as noted above probably signifies the onset of transition from of an unoxidized Mo target surface to an oxidized Mo target surface [8].

Similar interdependence between $p(O_2)/p(O_2+Ar)$ , sputtering power, deposition rate and oxygen concentration in $Mo_{1-x}O_x$ films were obtained when the initial total gas pressure is 5mTorr (Figure 1b). However, for the same sputtering power and relative partial pressure of $O_2$, oxygen incorporation into $Mo_{1-x}O_x$ occurs to a much less extext than for 10mTorr total gas pressure.

*B. Phases and Microstructure*

Phase and microstructural information of the $Mo_{1-x}O_x$ films obtained by x-ray Read camera analysis and TEM is summarized in Table I. Molydenum films whose oxygen content falls below the detection limit of BS contain the bcc Mo phase only. $Mo_{90}O_{10}$ film is observed to contain bcc Mo grains embedded in a

background material that appears amorphous under TEM. The average grain size is about 500Å . A single fcc Mo phase is consistently detected in all the $Mo_{80}O_{20}$ , $Mo_{60}O_{40}$ and $Mo_{40}O_{60}$ films. The three dominant x-ray or electron diffraction lines that we observed for this fcc phase correspond to lattice spacings of 2.37Å , 2.05Å , and 1.45Å , which are in excellent agreement with those given by Chopra et al. in reference 10. There is no evidence of $MoO_2$ or $MoO_3$ formation in these films in spite of the significant amount of oxygen incorporated. Oxygen probably decorates the grain boundaries in such $Mo_{1-x}O_x$ layers. $Mo_{25}O_{75}$ is composed of a single phase of $MoO_3$. As indicated in Table I, we also see a trend of diminishing grain size as the oxygen content in the film increases. Previous work by Ohfuji et al. [7], reveals the formation of the bcc Mo phase only in reactively sputtered $Mo_{1-x}O_x$ films.

According to the Chopra et al. [10,11], the 'normal' bcc Mo phase is sputter deposited only when the substrate temperature exceeds 400°C. An amorphous Mo film is obtained when no substrate heating is applied, while the fcc Mo phase dominates at substrate temperatures between 200°C and 400°C. The fact that all the relatively oxygen-free ($\leq$5 atomic percent) Mo films prepared in our experiment contain invariably the bcc phase suggests that the surface mobility of Mo atoms on the substrate are probably high enough so that the normal bcc phase is accessed. (even if the substrate is not intentionally heated). The preferential formation of the fcc phase in $Mo_{1-x}O_x$ occurs clearly as a result of oxygen incorporation. We surmise that the surface mobility of Mo atoms on the substrate are probably reduced by the the presence of oxygen during film growth. Such a lowering of kinetic energies leads eventually to the nucleation of the fcc phase [10,11] instead of the bcc phase, and is also reflected in the shrinking grain size as oxygen is gradually added to the $Mo_{1-x}O_x$ films. The conversion of bcc

Mo into an amorphous phase as observed by Ohfuji can also be explained in the same way.

A 600°C, 30 anneal in vacuum transforms the fcc Mo phase in all samples into bcc Mo according to the x-ray diffraction analysis. Moreover, lines corresponding to the conducting $MoO_2$ phase are observed in the diffraction patterns of $Mo_{60}O_{40}$ and $Mo_{40}O_{60}$ films after the same heat treatment. A 30 min anneal at 800°C and 900°C leads to $MoO_2$ formation in both $Mo_{90}O_{10}$ and $Mo_{80}O_{20}$ as well. $Mo_{40}O_{60}$ then consists predominantly of the $MoO_2$ phase with faint diffraction lines of Mo. TEM analysis has not been applied to the annealed samples.

*C. Resistivity*

All the as-deposited $Mo_{1-x}O_x$ films are electrically conducting except when x=3. This corresponds to the insulating $MoO_3$ phase as mentioned before. For 10mTorr initial total gas pressure, such insulating films are obtained only at 100W sputtering power and $p(O_2)/p(O_2+Ar) = 30\%$ or 40% . Figure 2 shows the resistivities of the $Mo_{1-x}O_x$ films as a function of film compositions (up to 50 atomic percent oxygen). The resistivity values are taken from all our films deposited under every sputtering condition discussed in this paper. It is clear that the resistivity of $Mo_{1-x}O_x$ increases monotonically with the oxygen content in the films, regardless of the sputtering parameters. As-deposited Mo films sputtered with 100% Ar or that have oxygen content below the BS detection limit (~3-5 at.% ) exhibit resistivities in the range of 15 - 25 $\mu\Omega$-cm, which are 3-5 times higher than the bulk resistivity of Mo (5.3 $\mu\Omega$-cm). The resistivity rises slowly with oxygen concentration up to about 40 atomic percent. Above that, the increase in resistivity steepens. $Mo_{40}O_{60}$ films have resistivities approaching 2000 $\mu\Omega$-cm. It has been stated [10] that the fcc and bcc Mo phases possess

comparable resistivities. The fact that resistivity correlates with the oxygen concentration regardless of the sputtering conditions used suggests that the conduction mechanism of the as-deposited $Mo_{1-x}O_x$ is controlled by the amount of oxygen present in the films. A similar monotonic relationship between resistivity and composition has also been established for W-N films [5].

If the oxygen in $Mo_{1-x}O_x$ really resides in the grain boundaries, a major contribution to the resistivity of $Mo_{1-x}O_x$ films is expected to originate from grain boundary scattering, since the grain size of our $Mo_{1-x}O_x$ films is comparable to the mean free path of electrons in bulk Mo (395Å ) [21]. Oikawa et al. suggested that resistivity in a polycrystalline Mo film is largely due to grain boundary electron scattering [20]. Furthermore, there is enough evidence to show that the reflection coefficient of conduction electrons at grain boundaries increases drastically with the amount of oxygen segregated along the grain boundaries [20]. The increase of film resistivity of $Mo_{1-x}O_x$ with oxygen concentration can then be rationalized by a combination of two factors: a reduction in grain size and a rise in oxygen scatterers in the grain boundaries.

The resistivities of the $Mo_{1-x}O_x$ films are unaffected by vacuum anealing for 30 min at 600°C but drop abruptly for anneals between 600°C and 800°C. Table II presents the range of resistivities obtained for different conducting $Mo_{1-x}O_x$ films before and after heat treatment at 800°C. Annealed $Mo_{1-x}O_x$ films containing up to 20 atomic percent of oxygen are almost as conductive ($\sim 10\,\mu\Omega$-cm) as plain Mo films taken through the same treatment. Backscattering analysis detects no oxygen loss from these $Mo_{1-x}O_x$ films by annealing. Heat-treated $Mo_{40}O_{60}$ films experience the greatest resistivity reduction (20 fold). In a recent report, Ahn observed from TEM images that the $WO_2$ phase precipitates out in a W matrix after an oxygen-doped W layer was subjected to heat treatments [12]. A similar

precipitation phenomenon probably occurs in our annealed $Mo_{1-x}O_x$ samples, resulting in films composed of Mo and $MoO_2$ grains. Their presence was indeed confirmed by x-ray analysis. Since the bulk resistivity of $MoO_2$ (88-200 $\mu\Omega$-cm) [13] much exceeds that of pure Mo (5.3 $\mu\Omega$-cm), the Mo grains must establish the main electrical conduction path in the annealed $Mo_{1-x}O_x$ films, except for $Mo_{40}O_{60}$ in which the major structural component is $MoO_2$.

*D. Stress*

The stress of all conducting $Mo_{1-x}O_x$ films is compressive (perpendicular to the cover glass substrate). Insulating $MoO_3$ films, on the other hand, exhibit tensile or almost zero stress. Figure 3 shows the film stress of $Mo_{1-x}O_x$ as a function of the relative partial pressure of oxygen $p(O_2)/p(O_2+Ar)$ at sputtering powers 200W, 300W and 600W. The initial total gas pressure is 10mTorr. At a fixed sputtering power, the film stress varies little with the oxygen partial pressure in the gas. This also suggests that the stress level of $Mo_{1-x}O_x$ is not altered significantly by the addition of oxygen. However, there appears to be a tendency for the compression in $Mo_{1-x}O_x$ films to increase slightly with sputtering power, as in the case of dc sputtered Mo films [15]. When an initial total gas pressure of 5mTorr is used, film stress is in the range of 4 - 5 GPa, which is higher than for depositions performed at 10mTorr [14,15].

Although the sputtering characteristics of $Mo_{1-x}O_x$ and W-N are similar in many ways, we have not been able to obtain a meaningful relationship between film composition and stress for $Mo_{1-x}O_x$ as in the case of W-N [5]. A more complicated interplay between stress and various sputtering parameters seems to prevail in the present study of $Mo_{1-x}O_x$ layers. More detailed and systematic investigations are needed.

*E.* $Mo_{1-x}O_x$ *films as diffusion barriers between Al and Si*

Interactions between Al and Mo films have been investigated by numerous authors [16,17,18] who showed that $MoAl_{12}$ forms as a result of the diffusion of Al through $MoAl_{12}$ and a reaction at the $MoAl_{12}$/Mo interface at temperatures above 450°C. Figure 4 depicts the BS spectra of a <Si> /Mo/Al sample before and after vacuum annealing at 550°C for 30 min. Evidently, heat treatment induces the disruption of the whole Mo layer by a reaction with Al and possibly Si [19]. In contrast, BS detects relatively little interdiffusion in a <Si> /$Mo_{80}O_{20}$ /Al sample taken through the same heat treatment (Figure 5). Although a little outdiffusion of Mo can still be seen, the extent of the interaction remains very limited even after a 600°C, 40 min sintering. The presence of oxygen in the $Mo_{1-x}O_x$ barrier layer is clearly effective in suppressing the reaction between Mo and Al. Such a $Mo_{80}O_{20}$ barrier has been demonstrated to be capable of protecting a Si $n^+$-p shallow junction from Al spiking during a 600°C, 40 min thermal cycle [3]. $Mo_{80}O_{20}$ barriers deposited under different sputtering conditions appear to be equally effective in suppressing Al-Si interaction at 600°C. $Mo_{60}O_{40}$ films are also found to have comparable performance as diffusion barriers. Preliminary results show that a $Mo_{1-x}O_x$ barrier must contain at least 15 atomic percent of oxygen in order to function effectively as a barrier between Al and Si at 600°C.

## CONCLUSIONS

We have investigated the properties of reactively sputtered $Mo_{1-x}O_x$ films as functions of various sputtering parameters. The reasons behind the formation of the fcc Mo phase are poorly understood and deserve further attention. Electrical conduction in $Mo_{1-x}O_x$ is dictated principally by the oxygen concentration

in the films. Most importantly, these $Mo_{1-x}O_x$ films act as excellent barrier layers between Al and Si beyond the eutectic temperature of Al-Si (577°C). The deposition behavior of $Mo_{1-x}O_x$ and $RuO_2$ differ markedly from each other, meaning that the formation mechanisms of the two oxides by reactive sputtering are probably dissimilar.

## ACKNOWLEDGEMENTS

The financial support from the Army Research Office under contract number DAAG29-85-K-0192 and Intel Corporation is gratefully acknowledged.

# REFERENCE


1. M. L. Green, M. E. Gross, L. E. Papa, K. J. Schones, and D. Brasen, J. Electrochem. Soc. **132**, 2077 (1985).
2. E. Kolawa, F. C. T. So, E. T-S. Pan, and M-A. Nicolet, Appl. Phys. Lett. **50**(13), 854 (1987).
3. F. C. T. So, E. Kolawa, X.-A. Zhao, E. T-S. Pan, and M-A. Nicolet, in *Proceedings of Workshop on Silicides and Metals for VLSI Applications V*, San Juan Bautista, May 1987; to be published in J. Vac. Sci. Technol.
4. S. Kanamori, Thin Solid Film **136**, 195 (1985).
5. E. Kolawa, F. C. T. So, X.-A. Zhao, and M-A. Nicolet, in *Tungsten and Other Refractory Metals for VLSI Applications II*, edited by E. K. Broadbent (MRS, Pittsburg, 1987), p.311.
6. E. Kolawa, F. C. T. So, E. T-S. Pan, and M-A. Nicolet, to be published in J. Appl. Phys.
7. S. Ohfuji, C. Hashimoto, T. Amazawa, and J. Murota, J. Electrochem. Soc. **131**, 446 (1984).
8. E. Hollands, and D. S. Campell, J. Mater. Sci. **3**, 544 (1968).
9. J. Heller, Thin Solid Film **17**, 163 (1973).
10. K. L. Chopra, M. R. Randlett, and R. H. Duff, Phil. Mag. **16**, 261 (1967).
11. K. L. Chopra, *Thin Film Phenomena* (McGraw-Hill, New York, 1969) p.199-214.
12. K. Y. Ahn, S. B. Brodsky, C. Y. Ting, and J. Kim, J. Vac. Sci. Technol. A**4**(6), 3111 (1986).
13. D. B. Rogers, R. D. Shannon, A. W. Sleight, and J. L. Gillson, Inorg. Chem. **8**, 841 (1969).

14. K. Y. Ahn, C. Y. Ting, S. B. Brodsky, P. M. Fryer, and B. Davari, in *Tungsten and Other Refractory Metals for VLSI Applications*, edited by R. S. Blewer (MRS, Pittsburg, 1986), p.239.

15. A. Bensaoula, J. C. Wolfe, A. Ignatieve, F-O. Fong, and T-S. Leung, J. Vac. Sci. Technol. A**2**(2), 389 (1984).

16. M. Kitada and N. Shimizu, J. Mater. Sci. **19**, 1339 (1984).

17. P. Merchant and J. Amano, J. Vac. Sci. Technol. A**1**, 459 (1983).

18. R. N. Singh, D. M. Brown, M. J. Kim, and G. A. Smith, J. Appl. Phys. **58**, 4598 (1985).

19. K. T. Ho , *Ph.D. Thesis*, (California Institute of Technology, Pasadena, 1984).

20. H. Oikawa and T. Tsuchiya, J. Vac. Sci. Technol. **15**(3), 1117 (1978).

21. E. Fawcett and D. Griffiths, J. Phys. Chem. Solids **23**, 1631 (1962).

# FIGURE CAPTIONS

Figure 1a. Oxygen concentration in the $Mo_{1-x}O_x$ films and deposition rates for samples sputtered in 10, 20, and 30% of oxygen in the sputtering gas. The initial total gas pressure is 10mTorr.

Figure 1b. Oxygen concentration in the $Mo_{1-x}O_x$ films and deposition rates for samples sputtered in 20 and 30% of oxygen in the sputtering gas. The initial total gas pressure is 5mTorr.

Figure 2. Resistivity of $Mo_{1-x}O_x$ films as a function of their oxygen concentration. The data are obtained from all our films deposited under all different sputtering conditions.

Figure 3. Compressive stress of $Mo_{1-x}O_x$ films as a function of the relative partial pressure of oxygen at sputtering powers of 200W, 300W, and 600W. The initial total gas pressure is 10mTorr.

Figure 4. 2 MeV $^4He^+$ BS spectra of Si/Mo(800Å)/Al(3200Å) before and after vacuum annealing at 550°C for 30 min.

Figure 5. 2 MeV $^4He^+$ BS spectra of $Si/Mo_{80}O_{20}$ (1000Å)/Al(3700Å) before and after vacuum annealing at 550°C for 30 min and 600°C for 20 min.

| film | phases (as dep.) | average grain size (Å) | phases after 600°C | phases after 800°C |
|---|---|---|---|---|
| Mo | bcc Mo | - | bcc Mo | bcc Mo |
| $Mo_{90}O_{10}$ | bcc Mo + amor. | 500 | bcc Mo | bcc Mo + $MoO_2$ |
| $Mo_{80}O_{20}$ | fcc Mo | 400 | bcc Mo | bcc Mo + $MoO_2$ |
| $Mo_{60}O_{40}$ | fcc Mo | 100 | bcc Mo + $MoO_2$ | bcc Mo + $MoO_2$ |
| $Mo_{40}O_{60}$ | fcc Mo | 100 | bcc Mo + $MoO_2$ | $MoO_2$ (+ Mo) |
| $Mo_{25}O_{75}$ | $MoO_3$ | - | - | - |

**Table I.** Phases in $Mo_{1-x}O_x$ films before and after vacuum annealing at 600°C and 800°C for 30 min. The table also contains gain size information of as-deposited $Mo_{1-x}O_x$ films.

| film | $\rho(\mu\Omega\text{-cm})$ as dep. | $\rho_{800^\circ C-anneal}(\mu\Omega\text{-cm})$ |
|---|---|---|
| Mo | 15–25 | 9–10 |
| $Mo_{90}O_{10}$ | 60–80 | 10–11 |
| $Mo_{80}O_{20}$ | 100-140 | 10–11 |
| $Mo_{60}O_{40}$ | 350–450 | 25–30 |
| $Mo_{40}O_{60}$ | 2000–2600 | 100–150 |
| $Mo_{25}O_{75}$ | insulating | – |

**Table II.** Resistivities of $Mo_{1-x}O_x$ films before and after vacuum annealing at 800°C for 30 min.

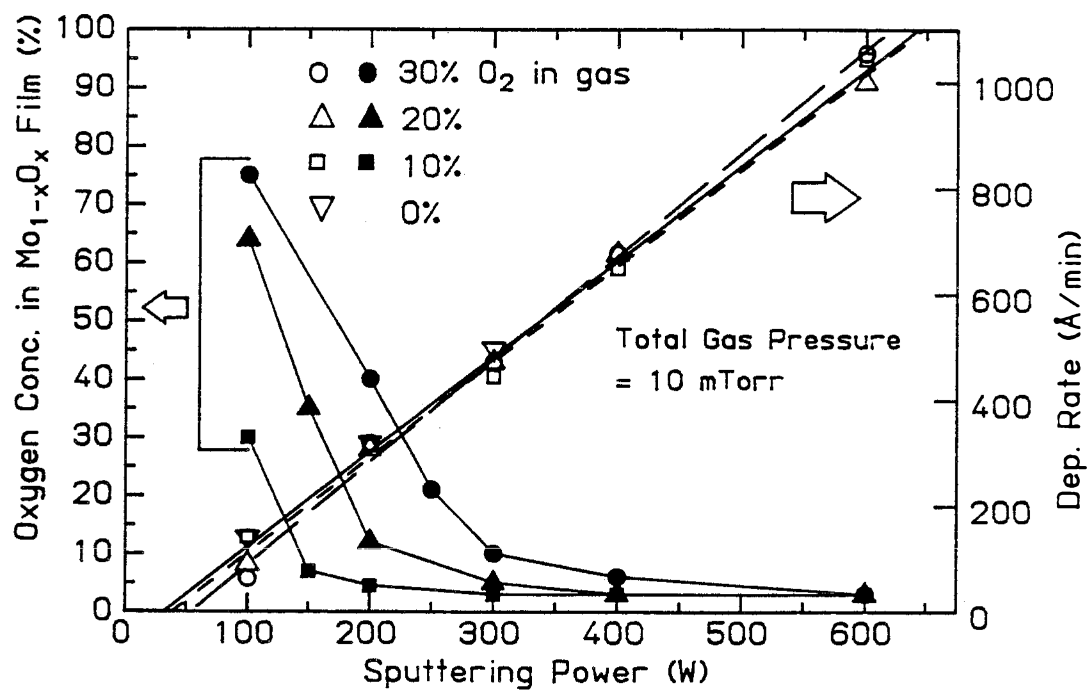


**Figure 1a.** Oxygen concentration in the $Mo_{1-x}O_x$ films and deposition rates for samples sputtered in 10, 20, and 30% of oxygen in the sputtering gas. The initial total gas pressure is 10mTorr.

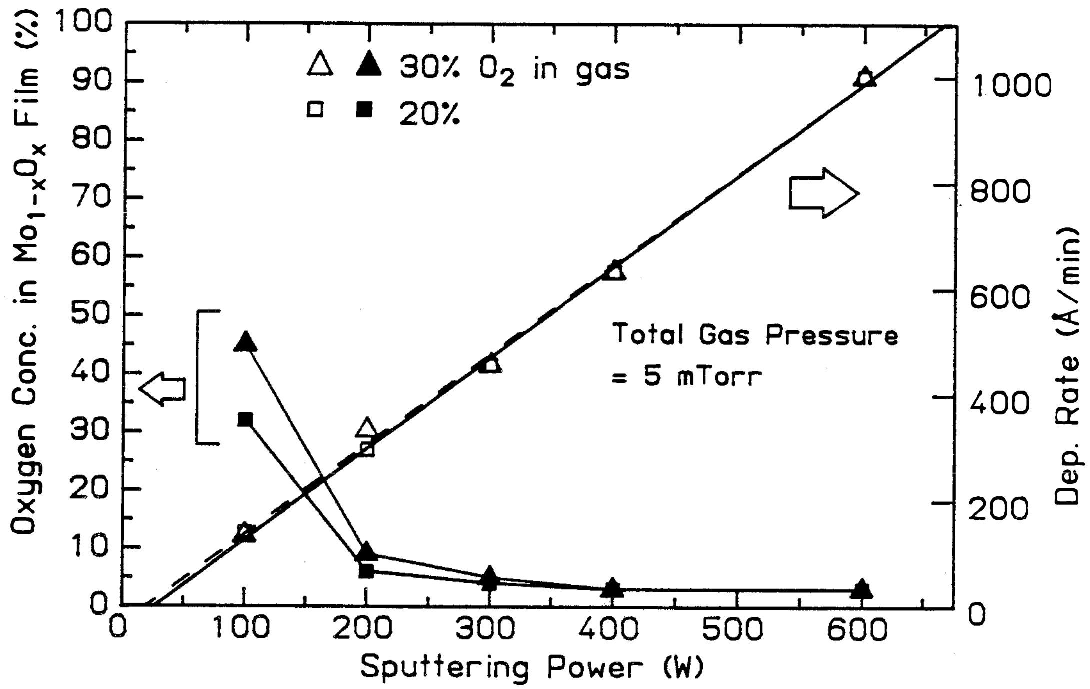


**Figure 1b.** Oxygen concentration in the $Mo_{1-x}O_x$ films and deposition rates for samples sputtered in 20 and 30% of oxygen in the sputtering gas. The initial total gas pressure is 5mTorr.

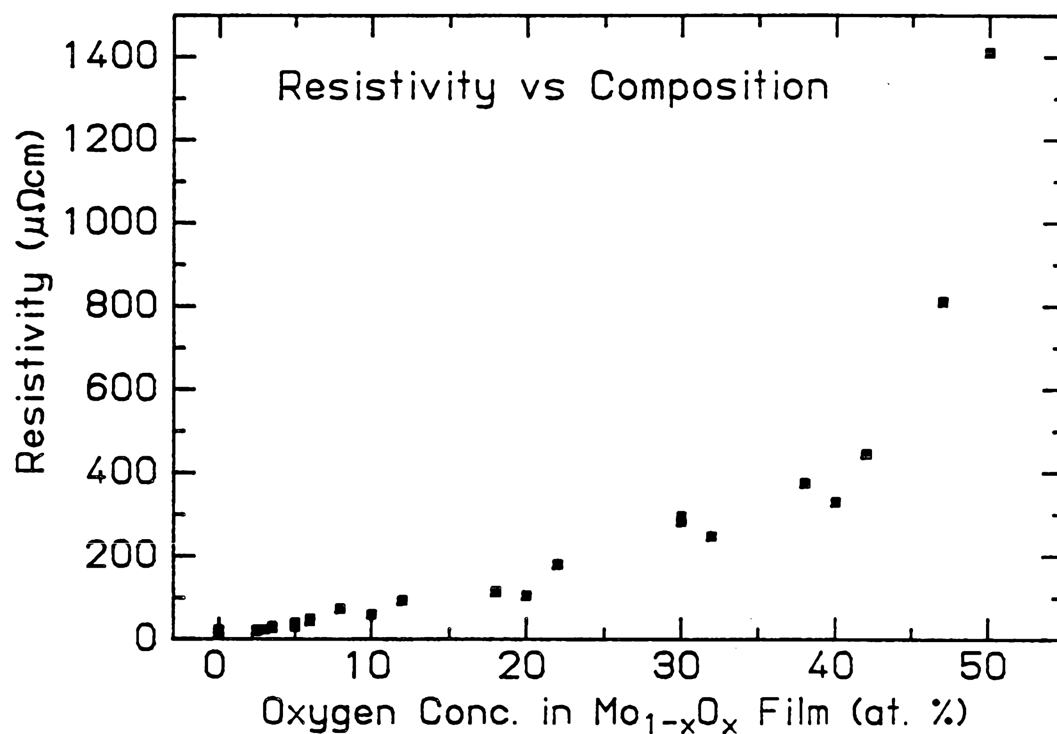


**Figure 2.** Resistivity of $Mo_{1-x}O_x$ films as a function of their oxygen concentration. The data are obtained from all our films deposited under all different sputtering conditions.

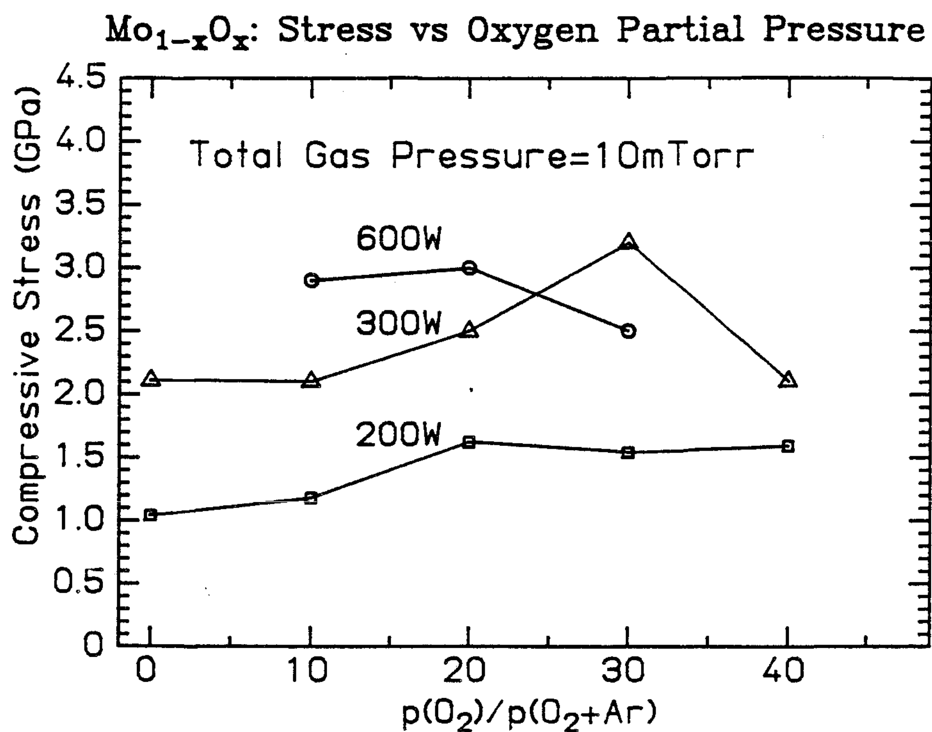


**Figure 3.** Compressive stress of $Mo_{1-x}O_x$ films as a function of the relative partial pressure of oxygen at sputtering powers of 200W, 300W, and 600W. The initial total gas pressure is 10mTorr.

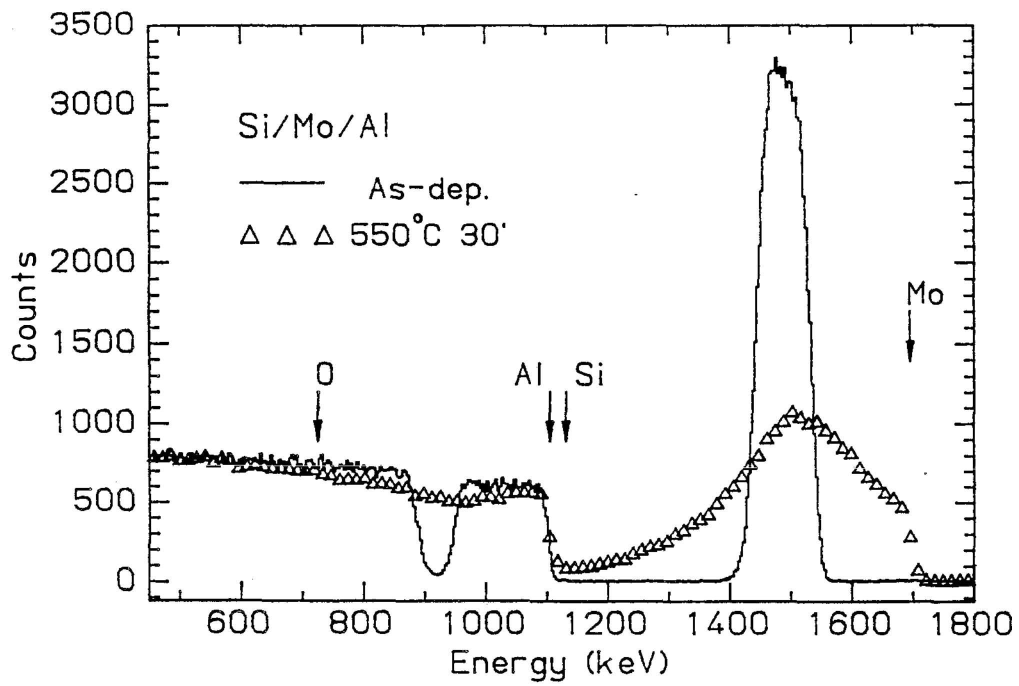


**Figure 4.** 2 MeV $^4He^+$ BS spectra of Si/Mo(800Å )/Al(3200Å ) before and after annealing at 550°C for 30 min.

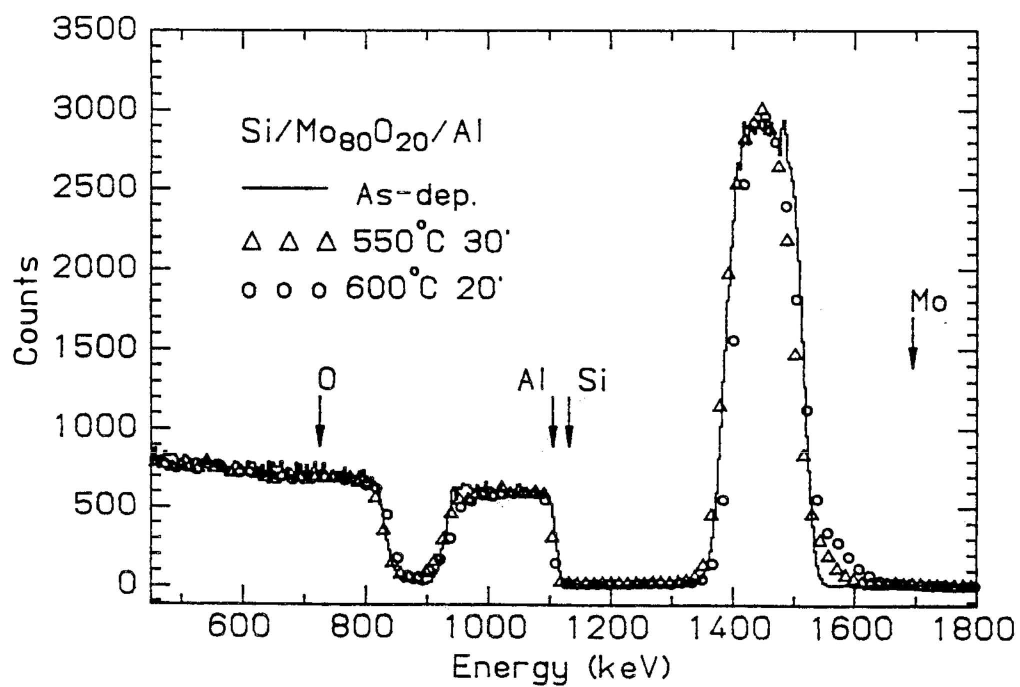


**Figure 5.** 2 MeV $^4He^+$ BS spectra of $Si/Mo_{80}O_{20}$ (1000Å)/Al(3700Å) before and after annealing at 550°C for 30 min and 600°C for 20 min.

To appear in J. Vac. Sci. Technol.

# APPENDIX IV

# Reactively Sputtered $RuO_2$ and Mo-O Diffusion Barriers: Summary

F.C.T. So[1], E. Kolawa, X.-A. Zhao[2], E.T-S. Pan and M-A. Nicolet

California Institute of Technology, Pasadena, CA 91125

## ABSTRACT

Conducting $RuO_2$ and Mo-O emerge as the forerunners of a new class of diffusion barriers. Thin layers of the oxide films are extremely effective in suppressing interdiffusion between Al and Si up to 600°C annealing for 30 min.

Diffusion barriers are indispensable in present VLSI contact technologies to preserve the integrity of shallow junctions and Schottky barriers from Al spiking during post-metallization processing. While a mamouth effort has been devoted to refractory metal nitrides [3], little attention is paid to the suitability of thin films of conducting transition metal oxides for diffusion barrier applications. This attitute probably springs from the fact that most transition metal oxides are electrically insulating (e.g. $TiO_2$); some are volatile (e.g $WO_3$). There are, however, transition metal oxides that exhibit metallic conductivities at room temperatures. One type of conducting oxides has an oxygen to metal ratio of 2. Two groups can be distinguished. The first one consists of the dioxides of the Pt group metals which crystallize in the rutile structure: $RuO_2$, $OsO_2$, $IrO_2$ and $RhO_2$. Among the four, $RuO_2$ is reported to possess the lowest bulk resistivity (about 46 $\mu\Omega$-cm [4]). The other class is made up of the dioxides that adopt distorted variants of the rutile structure: $CrO_2$, $MoO_2$ and $WO_2$. Single crystals of $MoO_2$ are monoclinic and have a room temperature resistivity of ~90 $\mu\Omega$-cm [4]. In this report, we summarize the important aspects of the deposition behavior of $RuO_2$ and Mo-O films formed by rf reactive sputtering and their diffusion barrier properties against interdiffusion in Al-Si couples.

$RuO_2$ and $MoO_2$ are dissimilar in their stability. $RuO_2$ is the only stable oxide of Ru below 800°C [5,9]. On the other hand, there exists higher oxides of Mo which are electrically insulating and volatile ($MoO_3$) [10]. The different oxide chemistry correlates with a different behavior of oxygen incoporation into Ru and Mo films during reactive sputtering. In our sputtering system, $RuO_2$ films are formed from a Ru target only within a very narrow range of deposition conditions when sputtering in an $Ar/O_2$ ambient. However, with a $Ne/O_2$ glow discharge,

$RuO_2$ film deposition can be realized over a wide range of oxygen partial pressures, substrate bias and sputtering powers [6]. The physics behind sputtering in $Ne/O_2$ plasmas is elaborated in reference 4. The amount of oxygen incoporated into the ruthenium-oxygen alloy films is found to be more or less discontinuous: either Ru or stoichiometric $RuO_2$ is deposited at one time. The compositions of and the phases contained in the deposited films are confirmed by backscattering and TEM analysis. All the as-deposited $RuO_2$ films have resistivities near 170 $\mu\Omega$-cm. Contrary to the discontinuous mode of oxygen incoporation into Ru, oxygen can be incoporated into Mo films continuously from 0 to 75 atomic percent by sputter-deposition in $Ar/O_2$ ambients [7]. Generally, for a fixed initial total sputtering gas pressure, the amount of oxygen contained in the Mo-O films increases with the relative partial pressure of oxygen and decreases with the input sputtering power. All the as-deposited Mo-O films are electrically conducting and polycrystalline, consisting predominantly of Mo and perhaps $MoO_2$, except for $Mo_{25}O_{75}$ which is composed of a single phase of insulating $MoO_3$. Such insulating films are formed only under extremely low sputtering power levels or with very high partial pressures of $O_2$ in the sputtering gas. The resistivity of Mo-O film increases monotonically with their oxygen content (from ~60 $\mu\Omega$-cm for $Mo_{90}O_{10}$ to ~2000 $\mu\Omega$-cm for $Mo_{40}O_{60}$ ). Mo-O films which are conducting in their as-deposited state remain conducting after annealing (in vacuum or nitrogen) up to at least 900°C. Sharp drops in the resistivities of all the conducting Mo-O layers are observed for heat treatment above 600°C. Such annealed layers invariably contain a mixture of the Mo and $MoO_2$ phases.

Backscattering analysis of a <Si> / $RuO_2$ /Al sample shows that Al-Si interdiffusion can be effectively suppressed by the $RuO_2$ barrier up to 650°C for 30 min [8]. A <Si> / $TiSi_2$ / $RuO_2$ /Al contact structure was tested on $n^+$-p shal-

low junction diodes of 0.35 μm junction depth. The diodes exhibit reverse leakage currents that remain unchanged after 30 min heat treatment at 600°C, but were all shorted after annealing at 650°C (Figure 1). This failure is attributed to localized breakdown of $RuO_2$ barrier undetected by BS. Problems of adhesion between Al and $RuO_2$ can be observed, and result in a slight degradation of the surface morphologies of the contact areas. Mo-O films also act as excellent diffusion barriers between Al and Si [7]. Figure 2 shows the histograms of the reverse current distribution of 40 $n^+$-p diodes with the <Si> /$Mo_{80}O_{20}$ /Al contacts measured before and after annealing at 600°C for 20 min. (The resistivity of the $Mo_{80}O_{20}$ layer is ~100 μΩ-cm.) No junction shorting is observed. Heat treatment is found to affect the surface morphologies little. Although BS detects a small outdiffusion tail of Mo in the annealed <Si> /$Mo_{80}O_{20}$ /Al sample, this movement of Mo remains very limited up to 40 min annealing at 600°C. Other Mo-O films containing at least 15 atomic percent of oxygen are also found to be good barriers against Al-Si diffusion for short time (~15 min) annealing at 600°C.

Clearly, both $RuO_2$ and Mo-O films are effective diffusion barriers between Si and Al even beyond the eutectic temperature of Al-Si (577°C). Work is underway to investigate the interfacial reactions between the barrier layers and Al.

The authors gratefully acknowledge the financial support from the Army Research Office under contract number DAAG29-85-K-0192, and Intel Coporation.

## FIGURE CAPTIONS

Figure 1. Electrical characteristics of a typical diode with the <Si> / $TiSi_2$ / $RuO_2$ /Al metallization before and after annealing at 600 and 650°C for 30 min [from reference 8].

Figure 2. Histograms of reverse diode leakage currents distributions with <Si> /$Mo_{80}O_{20}$ /Al contacts before and after annealing at 600°C for 20 min.

## REFERENCES

1) Present address: Optoelectronics Division, Hewlett-Packard Co., San Jose, CA 95131.

2) Permanent address: Shanghai Institute of Metallurgy, Academy of Sciences of China, Shanghai, China.

3) See, for example, H.P. Kattelus and M-A. Nicolet, in *Diffusion Phenomena in Thin Films*, edited by D. Gupta and P. S. Ho (Noyes, New Jersy), in press.

4) D.B. Rogers, R.D. Shannon, A.W. Sleight, and J. L. Gillson, Inorg. Chem. **8**, 841 (1969).

5) F.A. Shunk, *Constitution of Binary Alloys, Second Supplement* (McGraw-Hill, New York), 1969.

6) E. Kolawa, F.C.T. So, E.T-S. Pan, and M-A. Nicolet, submitted to J. Appl. Phys.

7) F.C.T. So, *Ph.D. thesis*, California Institute of Technology, 1987.

8) E. Kolawa, F.C.T. So, E.T-S. Pan, and M-A. Nicolet, Appl. Phys. Lett. **50**(13), 854 (1987).

9) R.P. Elliott *Constitution of Binary Alloys, First Supplement* (McGraw-Hill, New York), 1965.

10) *Binary Alloy Phase Diagrams*, edited by T.B. Massalski (ASM, Metals Park), 1986.

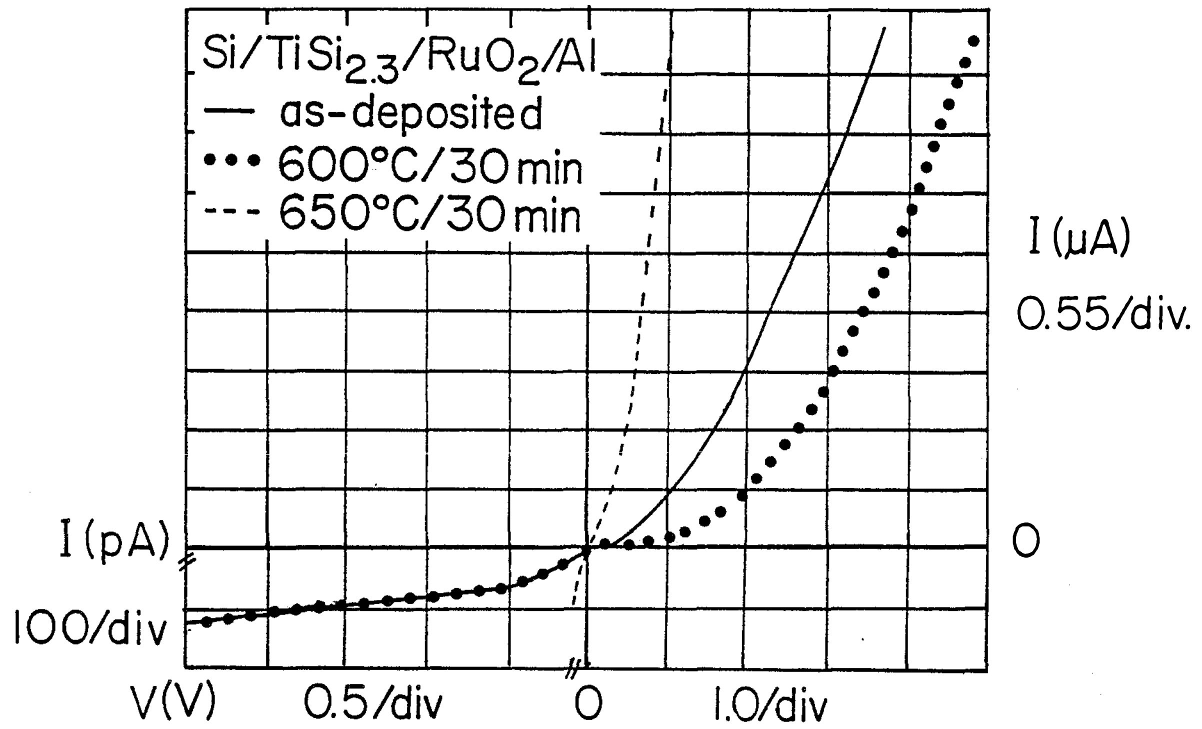


Figure 1

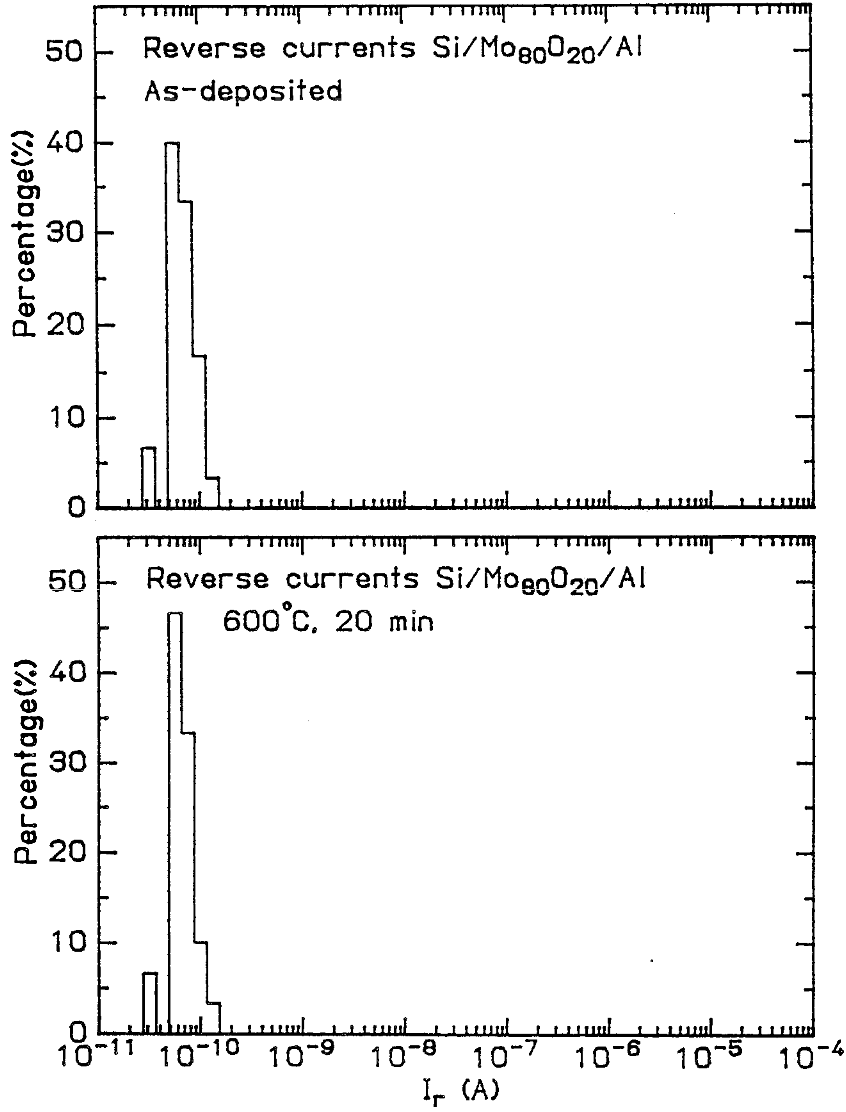


Figure 2